

Variational Bayesian Bow tie Neural Networks with Shrinkage

Alisa Sheinkman* and Sara Wade*

June 18, 2025

Abstract

Despite the dominant role of deep models in machine learning, limitations persist, including overconfident predictions, susceptibility to adversarial attacks, and underestimation of variability in predictions. The Bayesian paradigm provides a natural framework to overcome such issues and has become the gold standard for uncertainty estimation with deep models, also providing improved accuracy and a framework for tuning critical hyperparameters. However, exact Bayesian inference is challenging, typically involving variational algorithms that impose strong independence and distributional assumptions. Moreover, existing methods are sensitive to the architectural choice of the network. We address these issues by focusing on a stochastic relaxation of the standard feed-forward rectified neural network and using sparsity-promoting priors on the weights of the neural network for increased robustness to architectural design. Thanks to Polya-Gamma data augmentation tricks, which render a conditionally linear and Gaussian model, we derive a fast, approximate variational inference algorithm that avoids distributional assumptions and independence across layers. Suitable strategies to further improve scalability and account for multimodality are considered.

Keywords: Bayesian neural networks, variational inference, uncertainty quantification, shrinkage priors.

1 Introduction

Neural networks (NNs) are effective deep models that play a dominant role in machine learning and have achieved remarkable success across various domains including medicine and biological sciences (Jumper et al., 2021; Yu et al., 2021), natural language processing (Mikolov et al., 2013; Touvron et al., 2023), computer vision and image analysis (Dosovitskiy et al., 2020), data privacy and security (Yang et al., 2019) and beyond. However, modern machine learning applications often lack reliable, if any, uncertainty estimates (Guo et al., 2017; Gal, 2016; Ashukha et al., 2020). Classical deep models are easily fooled and are susceptible to adversarial attacks (Szegedy et al., 2014; Nguyen et al., 2015; Zong et al., 2024), and even when the adversarial attacks fail, the saliency interpretations of deep neural networks (DNNs) are rather brittle (Carbone et al., 2022). When data variations leading to out-of-distribution (OOD) shifts occur, neural networks often fail to generalize well (Hein et al., 2019; Zhang et al., 2024; Ashukha et al., 2020). Moreover, standard neural networks usually lack intuitive interpretation and explainability and so are regarded as black boxes (Lipton, 2018). To address these challenges, Bayesian neural networks (BNNs) have emerged as a compelling extension of conventional neural networks (for a review, see e.g. (Jospin et al., 2022; Arbel et al., 2023)). While finite (non-Bayesian) deep ensembles of independent neural networks have been shown to improve prediction and uncertainty estimates (Lakshminarayanan et al., 2017), the Bayesian approach creates infinite ensembles of deep neural networks. The advantage of this approach is that it controls the model complexity and builds regularization into the model by marginalizing the parameters. Indeed, BNNs have become the gold standard for uncertainty estimation in the context of data-driven decision-making and in safety-critical applications, where robustness and calibration are crucial (McAllister et al., 2017; Carbone et al., 2020; Gruver et al., 2023; Yang et al., 2024; Klarner et al., 2023).

A core problem of Bayesian machine learning lies in performing inference; in practice, the posterior distribution of the model’s parameters given observations is not available in closed form, and direct sampling

*School of Mathematics and Maxwell Institute for Mathematical Sciences, University of Edinburgh, a.sheinkman@sms.ed.ac.uk, sara.wade@ed.ac.uk

from the posterior is computationally expensive, meaning one has to employ approximate Bayesian inference. Markov chain Monte Carlo (MCMC) is a gold standard solution since it produces draws, which are asymptotically exact samples from the posterior, but for large data sets or complex models with multimodal posteriors, it can be prohibitively slow. Variational inference (VI [Jordan et al., 1999](#); [Blei et al., 2017](#)) instead utilizes optimization rather than sampling making it a more computationally effective method suitable for high-dimensional, large-scale problems. VI approximates the posterior with the closest (most commonly, in terms of the Kullback–Leibler divergence) member of some tractable variational family of distributions taken as close as possible to the true posterior.

In this work, we focus on advancing approximate inference for BNNs. Specifically, we improve the bow tie neural network of ([Smith et al., 2021](#)) by introducing sparsity-inducing priors, constructing a fast, approximate variational inference algorithm, and exploring further strategies to improve computational gains and performance in terms of both accuracy and uncertainty estimation. Below, we review related research and provide an outline of the paper and its contributions.

Related work. Sparsity-inducing priors are known for their ability to improve robustness to overparametrization in Bayesian modeling; they also lead to better calibrated uncertainty and, in certain settings, may recover the sparse structure of the target function (e.g. [Castillo et al., 2015](#); [Song and Liang, 2023](#); [Song, 2020](#)). Such priors generally fall within two classes: 1) the two-group discrete mixture priors with a point mass at zero (referred to as spike-and-slab priors) ([George and McCulloch, 1993](#); [Mitchell and Beauchamp, 1988](#)) or 2) shrinkage priors, which employ a single distribution to approximate the spike-and-slab shape, yet are more computationally attractive, as they avoid exploring the space of all possible models. Both types of priors have become widely used in Bayesian deep modeling, due to their high-dimensionality and overparametrization, and are further supported by theoretical guarantees (([Polson and Ročková, 2018](#); [Sun et al., 2022](#)) for BNNs with spike-and-slab priors and ([Castillo and Egels, 2024](#); [Lee and Lee, 2022](#)) for BNNs with heavy-tailed shrinkage priors).

To scale with the size of the data and model complexity, various variational algorithms and methods have been proposed for sparse BNNs (for an overview, see [Zhang et al., 2018](#)). Specifically, variational inference techniques for BNNs with spike-and-slab priors include ([Blundell et al., 2015](#); [Bai et al., 2020b,a](#); [Jantre et al., 2024](#)). Within the class of shrinkage priors, horseshoe priors ([Carvalho et al., 2009](#); [Piironen and Vehtari, 2017a](#)) on the BNN weights combined with variational approximations have been shown to provide competitive empirical results ([Louizos et al., 2017](#); [Ghosh et al., 2018, 2019](#)). Dropout regularization in neural networks has also been shown to be closely connected to sparse BNNs with suitable variational approximations ([Kingma et al., 2015](#); [Hron et al., 2018](#); [Louizos et al., 2017](#); [Liu et al., 2019](#); [Nalisnick et al., 2019](#)). In a slightly different direction, ([Li et al., 2024](#)) consider BNNs with Gaussian priors and introduce a variational inference methodology which enforces sparsity in the weights during the training. Finally, we mention the adaptive variational Bayes method of ([Ohn and Lin, 2024](#)), which was successfully applied to Bayesian deep learning scenarios; the framework operates on a collection of models, considers "sieve" priors ([Arbel et al., 2013](#)) to combine several variational approximations.

Contributions and outline. ([Smith et al., 2021](#)) introduced a bow tie neural network, where a stochastic relaxation of the rectified linear unit (ReLU) activation function leads to a model amenable to the Poly-Gamma (PG) data augmentation trick ([Polson et al., 2013](#)) and results in conditionally linear and Gaussian stochastic activations. In this paper, we improve bow tie neural networks in several ways. First, to improve robustness with increasing width and depth of the networks, we place sparsity-inducing global-local normal-generalized inverse Gaussians (N-GIG) priors ([Polson and Scott, 2012](#)) on the weights of the network. [Section 2](#) describes the bow tie model with shrinkage priors and implementation of PG data augmentation. Second, while ([Smith et al., 2021](#)) focus on MCMC, in [Section 3](#) we propose a (block) structured mean-field family for the approximate variational posterior, which is flexible and doesn't require parametric assumptions on the distributional form of each component as well as on independence across layers. For the chosen family, fast coordinate ascent variation inference (CAVI) ([Bishop, 2016](#)) can be performed, with all variational updates available in the closed form. Third, to improve the scalability of the algorithm, we consider two strategies: a stochastic variant that employs subsampling to cope with large data and a post-process node selection algorithm to obtain a sparse posterior that eases the storage and computational burden of predictions. Fourth, we propose improving accuracy and uncertainty estimation by considering ensembles of

variational approximations obtained by running several parallel variational algorithms with different random starting points. In this way, our approach accounts for the multimodality of the posterior distributions arising in Bayesian deep models. [Sections 3.1](#) and [3.2](#) derive the inference algorithm and in [Section 3.3](#) a stochastic variant ([Hoffman et al., 2013](#)) of the algorithm is developed. Further, we derive a variable selection procedure in [Section 3.4](#) for faster prediction ([Section 3.5](#)) and propose ensembles in [Section 3.6](#). We evaluate our method¹ on a range of classical regression tasks as well as synthetic regression tasks and demonstrate its competitiveness compared to alternative, well-known Bayesian algorithms in [Section 4](#).

2 Bayesian Augmented Bow Tie Neural Network with Shrinkage

2.1 Bow tie Neural Networks

We begin by describing the class of recently proposed *bow tie networks* ([Smith et al., 2021](#)), which are deep generative models that generalize feed-forward rectified linear neural networks with stochastic activations. Let $\mathbf{x}_n \in \mathbb{R}^{D_0}$ be the inputs, $\mathbf{y}_n \in \mathbb{R}^{D_{L+1}}$ be the outputs and $\mathbf{a}_n = \{\mathbf{a}_{n,l}\}_{l=1}^L$ with $\mathbf{a}_{n,l} \in \mathbb{R}^{D_l}$ be the latent activations at each of the L intermediate layers. For notational purposes, assume $\mathbf{a}_{n,0} = \mathbf{x}_n$. The model assumes:

$$\mathbf{y}_n | \mathbf{a}_n, \mathbf{x}_n, \boldsymbol{\theta} \sim \mathcal{N}(\mathbf{y}_n | \mathbf{z}_{n,L+1}, \boldsymbol{\Sigma}_{L+1}) \quad \text{for } n = 1, \dots, N,$$

where

$$\mathbf{a}_{n,l} | \mathbf{z}_{n,l}, \boldsymbol{\theta} \sim \mathcal{N}(f(\mathbf{z}_{n,l}), \boldsymbol{\Sigma}_l), \quad \text{with } \mathbf{z}_{n,l} = \mathbf{W}_l \mathbf{a}_{n,l-1} + \mathbf{b}_l \quad \text{for } l = 1, \dots, L+1. \quad (1)$$

Here $f(\mathbf{z})$ is a nonlinear activation function applied elementwise and the parameters $\boldsymbol{\theta} = (\mathbf{W}_l, \mathbf{b}_l, \boldsymbol{\Sigma}_l)_{l=1}^{L+1}$ consist of the weights $\mathbf{W}_l \in \mathbb{R}^{D_l \times D_{l-1}}$, biases $\mathbf{b}_l \in \mathbb{R}^{D_l}$ and covariance matrices $\boldsymbol{\Sigma}_l \in \mathbb{R}^{D_l \times D_l}$.

Note that [Equation \(1\)](#) is a stochastic relaxation of the standard feed-forward NN, which is recovered in the limiting case when $\boldsymbol{\Sigma}_l \rightarrow \mathbf{0}$ for $l = 1, \dots, L$. Instead of relying on local gradient-based algorithms, ([Smith et al., 2021](#)) introduces another relaxation of the model and employs a *Polya-Gamma data augmentation trick* ([Polson et al., 2013](#)) to render the model conditionally linear with Gaussian activations. Specifically, consider the ReLU activation function $f(z) = \max(0, z)$. It can alternatively be written as a product of z and a binary function γ , i.e. $f(z) = \gamma z$ where $\gamma = \mathbf{1}(z > 0)$. In this way, γ determines whether the node is activated ($\gamma = 1$) or not ($\gamma = 0$). The additional stochastic relaxation assumes that γ is not deterministic, but a binary random variable whose success probability depends on z . Specifically, the dependence is constructed through the logistic function $\sigma(x) = \exp(x)/(1 + \exp(x))$ and a temperature parameter $T \geq 0$:

$$\begin{aligned} \mathbf{a}_{n,l} | \mathbf{z}_{n,l}, \gamma_{n,l}, \boldsymbol{\theta} &\sim \mathcal{N}(\gamma_{n,l} \odot \mathbf{z}_{n,l}, \boldsymbol{\Sigma}_l), \\ \gamma_{n,l,d} &\stackrel{\text{ind}}{\sim} \text{Bern}(\sigma(z_{n,l,d}/T)) \quad \text{for } T > 0, \end{aligned}$$

where \odot represents the elementwise product. Thus, the nodes are turned off or on stochastically depending on their input. Note that in the limit as the temperature $T \rightarrow 0$, we have that $\gamma_{n,l,d} = \mathbf{1}(z_{n,l,d} > 0)$ and $\mathbf{a}_{n,l} | \mathbf{z}_{n,l}, \gamma_{n,l}, \boldsymbol{\theta} \sim \mathcal{N}(\mathbf{1}(\mathbf{z}_{n,l} > 0) \odot \mathbf{z}_{n,l}, \boldsymbol{\Sigma}_l)$.

For $T > 0$, after marginalizing the binary activations, the stochastic activations \mathbf{a}_n are distributed as a mixture of two normals:

$$\mathbf{a}_{n,l,d} | z_{n,l,d}, \boldsymbol{\theta} \sim \sigma(z_{n,l,d}/T) \mathcal{N}(z_{n,l,d}, \eta_{l,d}^2) + (1 - \sigma(z_{n,l,d}/T)) \mathcal{N}(0, \eta_{l,d}^2), \quad (2)$$

where the variance $\eta_{l,d}^2$ is the (d, d) th element of $\boldsymbol{\Sigma}_l$, and

$$\begin{aligned} \mathbb{E}[\mathbf{a}_{n,l,d} | z_{n,l,d}, \boldsymbol{\theta}] &= \mathbb{E}[\mathbb{E}[\mathbf{a}_{n,l,d} | z_{n,l,d}, \gamma_{n,l,d}, \boldsymbol{\theta}]] = \mathbb{E}[\gamma_{n,l,d} z_{n,l,d}] \\ &= \sigma(z_{n,l,d}/T) z_{n,l,d}, \end{aligned} \quad (3)$$

$$\mathbb{V}(\mathbf{a}_{n,l,d} | z_{n,l,d}, \boldsymbol{\theta}) = \mathbb{E}[\mathbb{V}(\mathbf{a}_{n,l,d} | z_{n,l,d}, \gamma_{n,l,d}, \boldsymbol{\theta})] + \mathbb{V}(\mathbb{E}[\mathbf{a}_{n,l,d} | z_{n,l,d}, \gamma_{n,l,d}, \boldsymbol{\theta}])$$

¹We provide a Python implementation of our model on [GitHub](#).

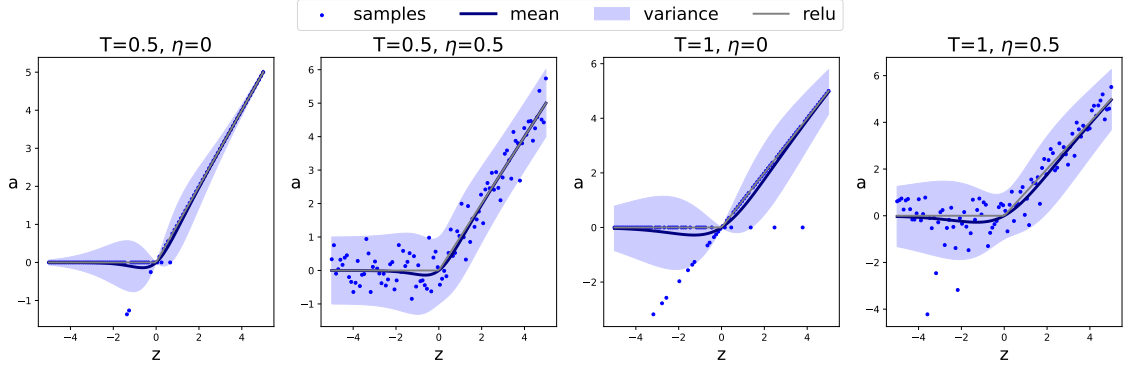


Figure 1: Conditional distribution of a given the input z for various settings of the temperature T and noise η , with the conditional mean in Equation (3) (solid line), conditional variance in Equation (4) (shaded region) and samples from the conditional distribution in Equation (2) (points).

$$\begin{aligned}
&= \mathbb{E}[\eta_{l,d}^2] + \mathbb{V}(\gamma_{n,l,d} z_{n,l,d}) \\
&= \eta_{l,d}^2 + z_{n,l,d}^2 \sigma(z_{n,l,d}/T) (1 - \sigma(z_{n,l,d}/T)).
\end{aligned} \tag{4}$$

The conditional distribution of $a_{n,l,d}$ is displayed in Figure 1, for different combinations of the temperature parameter T and variance $\eta_{l,d}^2$. The ReLU activation is recovered in the case of $T = 0$ and $\eta_{l,d}^2 = 0$, while other choices of T and $\eta_{l,d}^2$ generalize the ReLU. The stochastic activations have smoother conditional mean functions for non-zero values of T , with potential bimodality (density resembles a bow tie, hence the name) for larger T relative to η . This may be relevant in settings with multimodal predictive distributions, although our experiments focus on small temperature values for more similarity to the ReLU.

2.2 Shrinkage Priors

Prior elicitation in Bayesian neural networks is challenging, as understanding how the high-dimensional weights map to the functions implemented by the network is not trivial. Standard Gaussian priors are often a default choice, also due to their link with ℓ_2 regularization in maximum a posteriori (MAP) inference; indeed, such priors were used in (Smith et al., 2021). For an overview and discussion on priors in Bayesian neural networks, see (Fortuin, 2022).

We take an alternative approach to the Gaussian priors of (Smith et al., 2021) in order to sparsify our model. Sparsity-inducing priors have been shown to provide improvement in the predictive performance of deep models and can provide a data-driven approach to selecting the width and depth, easing the difficult task of specifying the network architecture. In this work, we focus on a class of continuous shrinkage priors, namely, global-local normal scale-mixtures with generalized inverse Gaussian shrinkage priors on the scale parameters, referred to as *global-local normal-generalized inverse Gaussian priors* (Griffin and Brown, 2021). Global-local scale-mixtures aim to shrink less important weights whilst leaving large ones, which is achieved through a global parameter controlling the overall shrinkage, with the local parameters allowing deviations at the level of individual nodes (Polson and Scott, 2012; Bhadra et al., 2019). This choice of priors is also motivated by the theoretical guarantees for high-dimensional regression (Song and Liang, 2023; Griffin and Brown, 2010; Polson et al., 2013), for a survey on global-local shrinkage methods we refer to (Griffin and Brown, 2021).

The N-GIG priors on the weights have the following hierarchical structure:

$$\mathbb{P}(\mathbf{W}_l | \psi_l, \tau_l) = \prod_{d=1}^{D_l} \prod_{d'=1}^{D_{l-1}} \mathcal{N}(W_{l,d,d'} | 0, \tau_l \psi_{l,d,d'}), \tag{5}$$

$$\mathbb{P}(\psi_l) = \prod_{d=1}^{D_l} \prod_{d'=1}^{D_{l-1}} \text{GIG}(\psi_{l,d,d'} | \nu_{\text{loc},l}, \delta_{\text{loc},l}, \lambda_{\text{loc},l}), \tag{6}$$

$$\mathbb{P}(\tau_l) = \text{GIG}(\tau_l \mid \nu_{\text{glob}}, \delta_{\text{glob}}, \lambda_{\text{glob}}), \quad (7)$$

where τ_l is the global shrinkage parameter for layer l and $\psi_{l,d,d'}$ is the local shrinkage parameter for each weight. The generalized inverse Gaussian (GIG) prior is given by:

$$\text{GIG}(\psi \mid \nu, \delta, \lambda) \propto \psi^{\nu-1} \exp\left(-\frac{1}{2}(\delta^2/\psi + \lambda^2\psi)\right),$$

with parameters ν , δ , and λ ; for a proper prior, $\nu > 0$ if $\delta = 0$ or $\nu < 0$ if $\lambda = 0$. In Equation (6), we allow the GIG parameters for the local scale parameters $\psi_{l,d,d'}$ to vary across layers to adjust local shrinkage for wider layers. Furthermore, to encourage more shrinkage for larger depth and width, we scale the global parameters τ_l with respect to L and the local parameters $\psi_{l,d,d'}$ with respect to D_l (details of our approach are provided Appendix D.1).

When the global shrinkage parameter τ_l is fixed, examples of the marginal distribution for $w_{l,d,d'}$ include Laplace (Park and Casella, 2008), Student-t (ST) (Tipping, 2001), Normal-Gamma (NG) (Caron and Doucet, 2008; Griffin and Brown, 2010), Normal inverse Gaussian (NIG) (Caron and Doucet, 2008). Each example has a different tail behavior, inducing different forms of shrinkage (see Table 1 for an overview and Figure 2 (a) for a visualization). Note that if the prior is polynomial-tailed, then for large signals the amount of shrinkage is mitigated even given small τ_l (Polson and Scott, 2012). The global shrinkage parameter τ_l leads to a non-separable penalty for the weights within the same layer, i.e. after integrating out τ_l , the weights within the same layer are dependent. This is illustrated in the top row of Figure 2 (b), which shows how the conditional prior density of one weight varies given different values of another weight within the same layer, for two choices of inverse Gamma (IG) and Gamma mixing priors. Instead, across layers the weights are independent, as illustrated by the contour plots for the joint density in the bottom row of Figure 2 (b). The bottom row of Figure 2 (b) also highlights how the variance depends on the width of the layer, with more hidden units and smaller variance for the second layer compared to the first.

The opposite effects of varying width and depth in deep neural networks are studied in (Vladimirova et al., 2021); while depth accentuates a model’s non-Gaussianity, the width makes models increasingly Gaussian. Indeed, infinitely wide BNNs are closely related to Gaussian processes (GPs), typically relying on appropriately scaled i.i.d. Gaussian weights (Neal, 2012; Lee et al., 2018; Matthews et al., 2018) and relaxing these assumptions, e.g. through ordering, constraints, heavy tails, or bottlenecks, results in non-Gaussian limits, such as stable processes (Peluchetti et al., 2020), deep GPs (Agrawal et al., 2020) or more exotic processes (Sell and Singh, 2023; Chada et al., 2022). The sparsity-promoting priors in Equations (5) to (7) provide a framework for the data to inform on the width and depth of the network.

2.3 Poly-Gamma Data Augmentation

As in (Smith et al., 2021), we employ *Poly-Gamma data augmentation* (Polson et al., 2013) to render the model conditionally linear and Gaussian. First, recall the definition of the Poly-Gamma distribution with parameters $b > 0$ and $c \in \mathbb{R}$, denoted $\text{PG}(b, c)$. The random variable $X \sim \text{PG}(b, c)$ if

$$X \stackrel{D}{=} \frac{1}{2\pi^2} \sum_{k=1}^{\infty} \frac{g_k}{(k - 1/2)^2 + c^2/4\pi^2}, \quad \text{where } g_k \stackrel{iid}{\sim} \text{Gam}(b, 1).$$

Table 1: Examples with the class of N-GIG priors.

Marginal for $w_{l,d,d'}$ when τ_l is fixed				
	Student-T	Laplace	NG	NIG
Mixing distribution	Inverse Gamma (IG)	Gamma	Gamma	Inverse Gaussian (IGauss)
Parameters	$\nu < 0, \delta > 0, \lambda = 0$	$\nu = 1, \delta = 0, \lambda$	$\nu, \delta = 0, \lambda$	$\nu = \frac{1}{2}, \delta, \lambda$
Tail behavior	polynomial-tailed	exponential-tailed	exponential-tailed	exponential-tailed

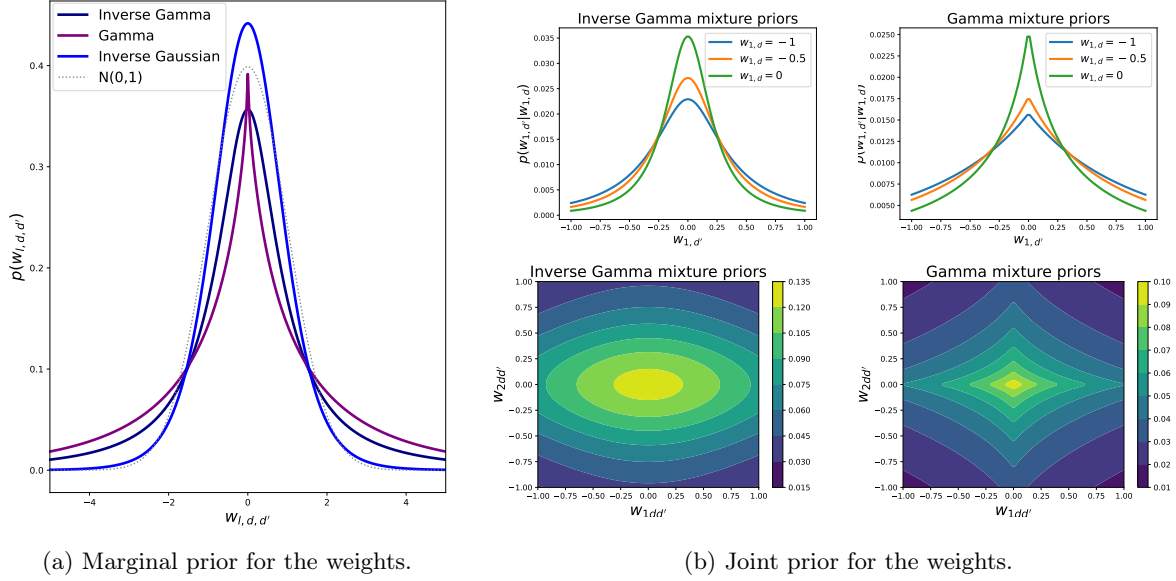


Figure 2: Illustration of the prior on the weights. (a) the marginal density of the weights for different choices within the GIG family. (b) the conditional prior of the weights within the same layer (top) and joint prior of the weights across layers (bottom) for two choices of IG (left) and Gamma (right) mixing priors.

The key identity that we use is:

$$\frac{\exp(z)^a}{(1 + \exp(z))^b} = 2^{-b} \exp(\kappa z) \int_0^\infty \exp\left(-\frac{\omega z^2}{2}\right) p(\omega) d\omega, \quad (8)$$

where $\kappa = a - b/2$ and $p(\omega) = PG(\omega|b, 0)$. The integral is a Gaussian kernel, thus if $z = \mathbf{w}^T \mathbf{x}$, conditioned on the latent variable ω , \mathbf{w} has a Gaussian distribution and conditioned on \mathbf{w} , ω has a PG distribution. While to sample from the PG distribution, one can use the alternating series method of (Devroye, 2006), all finite moments of the PG random variables are available in closed form, and that becomes useful for expectation-maximization or variational Bayes algorithms. Specifically, for $c > 0$

$$\mathbb{E}[\omega] = \frac{b \exp(c) - 1}{2c \exp(c)}. \quad (9)$$

Moreover, the PG distribution is closed under convolution with the same scale parameter; if $\omega_1 \sim PG(b_1, c)$ and $\omega_2 \sim PG(b_2, c)$, then $\omega_1 + \omega_2 \sim PG(b_1 + b_2, c)$.

2.4 Augmented Model

The model in Section 2.1 augmented with stochastic activations $\mathbf{a} = (\mathbf{a}_{n,l})$ and binary activations $\boldsymbol{\gamma} = (\boldsymbol{\gamma}_{n,l})$ is:

$$p(\mathbf{y}, \mathbf{a}, \boldsymbol{\gamma} | \boldsymbol{\theta}) = \prod_{n=1}^N N(\mathbf{y}_n | \mathbf{z}_{n,L+1}, \boldsymbol{\Sigma}_{L+1}) \prod_{n=1}^N \prod_{l=1}^L N(\mathbf{a}_{n,l} | \boldsymbol{\gamma}_{n,l} \odot \mathbf{z}_{n,l}, \boldsymbol{\Sigma}_l) \\ \times \prod_{d=1}^{D_l} \frac{\exp(z_{n,l,d}/T)^{\gamma_{n,l,d}}}{1 + \exp(z_{n,l,d}/T)}.$$

Then using the Equation (8), the last term can be written as:

$$\frac{\exp(z_{n,l,d}/T)^{\gamma_{n,l,d}}}{1 + \exp(z_{n,l,d}/T)} = 2^{-1} \exp\left(\frac{\kappa_{n,l,d} z_{n,l,d}}{T}\right) \int_0^\infty \exp\left(-\frac{\omega_{n,l,d} z_{n,l,d}^2}{2T^2}\right) p(\omega_{n,l,d}) d\omega_{n,l,d},$$

where $\omega_{n,l,d} \sim \text{PG}(1, 0)$ and $\kappa_{n,l,d} = \gamma_{n,l,d} - 1/2$. Thus, introducing the additional augmented variables $\boldsymbol{\omega} = (\omega_{n,l,d})$, we arrive at the augmented model:

$$p(\mathbf{y}, \mathbf{a}, \boldsymbol{\gamma}, \boldsymbol{\omega} | \boldsymbol{\theta}) \propto \prod_{n=1}^N \text{N}(\mathbf{y}_n | \mathbf{z}_{n,L+1}, \boldsymbol{\Sigma}_{L+1}) \prod_{n=1}^N \prod_{l=1}^L \text{N}(\mathbf{a}_{n,l} | \boldsymbol{\gamma}_{n,l} \odot \mathbf{z}_{n,l}, \boldsymbol{\Sigma}_l) \\ \times \prod_{d=1}^{D_l} \exp\left(\frac{\kappa_{n,l,d} z_{n,l,d}}{T}\right) \exp\left(-\frac{\omega_{n,l,d} z_{n,l,d}^2}{2T^2}\right) p(\omega_{n,l,d}).$$

The covariance matrices are assumed to be diagonal $\boldsymbol{\Sigma}_l = \text{diag}(\eta_{l,1}^2, \dots, \eta_{l,D_l}^2)$, with variances denoted by $\boldsymbol{\eta}_l = (\eta_{l,1}^2, \dots, \eta_{l,D_l}^2)$. Additionally, we assume conjugate priors for the variances $\eta_{l,d}^2 \stackrel{iid}{\sim} \text{IG}(\alpha_0^h, \beta_0^h)$ for $l = 1, \dots, L$ and $\eta_{L+1,d}^2 \stackrel{iid}{\sim} \text{IG}(\alpha_0, \beta_0)$ and for the biases $b_{l,d} \stackrel{iid}{\sim} \text{N}(0, s_0^2)$. Here, we consider different prior parameters α_0^h, β_0^h for the variance terms associated to the hidden layers in comparison to the parameters α_0, β_0 for the final layer. In particular, α_0, β_0 are chosen to reflect prior knowledge in the noise, while α_0^h, β_0^h are chosen so that the prior concentrates on small values and realizations of the stochastic activation function are more similar to the ReLU.

A graphical model of the bow tie BNN with stochastic relaxation and shrinkage priors is displayed in [Figure 3](#), and the posterior distribution over both the model parameters and latent variables is:

$$p(\mathbf{a}, \boldsymbol{\gamma}, \boldsymbol{\omega}, \mathbf{W}, \mathbf{b}, \boldsymbol{\eta}, \boldsymbol{\psi}, \boldsymbol{\tau}) \propto \prod_{n=1}^N \text{N}(\mathbf{y}_n | \mathbf{z}_{n,L+1}, \boldsymbol{\Sigma}_{L+1}) \prod_{n=1}^N \prod_{l=1}^L \text{N}(\mathbf{a}_{n,l} | \boldsymbol{\gamma}_{n,l} \odot \mathbf{z}_{n,l}, \boldsymbol{\Sigma}_l) \\ \times \prod_{d=1}^{D_l} \exp\left(\frac{\kappa_{n,l,d} z_{n,l,d}}{T}\right) \exp\left(-\frac{\omega_{n,l,d} z_{n,l,d}^2}{2T^2}\right) p(\omega_{n,l,d}) \\ \times \prod_{d=1}^{D_{L+1}} \text{IG}(\eta_{L+1,d}^2 | \alpha_0, \beta_0) \times \prod_{l=1}^L \prod_{d=1}^{D_l} \text{IG}(\eta_{l,d}^2 | \alpha_0^h, \beta_0^h) \times \prod_{n=1}^N \prod_{l=1}^L \prod_{d=1}^{D_l} \text{Bern}\left(\gamma_{n,l,d} | \sigma\left(\frac{z_{n,l,d}}{T}\right)\right) \\ \times \prod_{l=1}^L \left(\prod_{d=1}^{D_l} \left(\text{N}(b_{l,d} | 0, s_0^2) \times \prod_{d'=1}^{D_{l-1}} \text{N}(W_{l,d,d'} | 0, \tau_l \psi_{l,d,d'}) \right) \right) \\ \times \prod_{l=1}^L \left(\text{GIG}(\tau_l | \nu_{\text{glob}}, \delta_{\text{glob}}, \lambda_{\text{glob}}) \prod_{d=1}^{D_l} \prod_{d'=1}^{D_{l-1}} \text{GIG}(\psi_{l,d,d'} | \nu_{\text{loc},l}, \delta_{\text{loc},l}, \lambda_{\text{loc},l}) \right).$$

3 Inference

3.1 Variational Bayes

While Markov chain Monte Carlo is considered the gold-standard tool for approximating posterior distributions in Bayesian modeling due to its asymptotic guarantees, MCMC algorithms can be prohibitively slow when the model dimension and sample size are large. Instead, we focus on variational inference, an alternative fast, approximate Bayesian inference method that has gained popularity in the literature ([Ormerod and Wand, 2010](#); [Zhang et al., 2018](#)), due to both the explosion in the amount of data collected and the use of highly parametrized models for increased flexibility. VI has been shown to yield reasonably accurate approximations in several problems as well as desirable frequentist properties. Namely, consistency and asymptotic normality of the variational posterior expectation are established in ([Wang and Blei, 2019](#)), and theoretical guarantees for optimal contraction rates of variational posteriors under certain assumptions appear in several recent works ([Zhang and Gao, 2020](#); [Alquier and Ridgway, 2020](#); [Bhattacharya et al., 2023](#); [Yang et al., 2020](#); [Ray and Szabó, 2022](#)). We refer readers interested in the caveats of VI to ([Yao et al., 2018](#); [Barber et al., 2011](#); [Hron et al., 2018](#)).

Consider fitting a model parameterized by $\boldsymbol{\theta}$ to the observed data \mathcal{D} . In variational inference, the true posterior $p(\boldsymbol{\theta} | \mathcal{D})$ is approximated by a density $q(\boldsymbol{\theta})$ taken from a family of distributions \mathcal{F} that minimizes

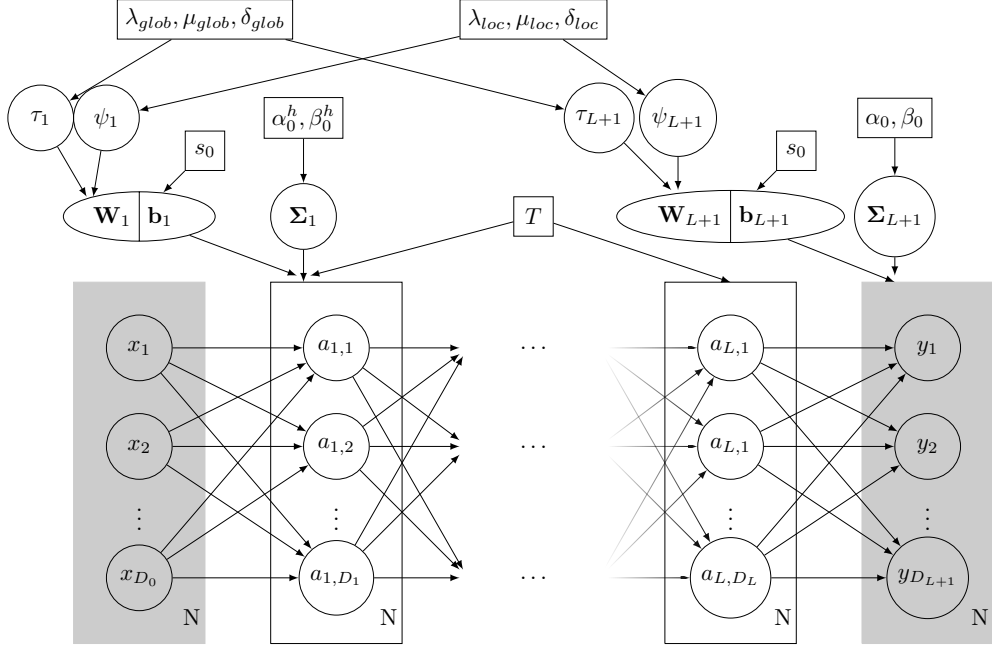


Figure 3: Directed Acyclic Graph of the model.

the Kullback-Leibler divergence between the approximate and true posterior, or equivalently maximizes the *evidence lower bound* (ELBO)

$$\text{ELBO} = \mathbb{E}_{q(\boldsymbol{\theta})} \left[\log \left(\frac{p(\boldsymbol{\theta}, \mathcal{D})}{q(\boldsymbol{\theta})} \right) \right]. \quad (10)$$

A common choice for \mathcal{F} is the nonparametric, mean-field family on a partition $\{\boldsymbol{\theta}_1, \dots, \boldsymbol{\theta}_J\}$ of $\boldsymbol{\theta}$, assuming that the variational posterior factorizes over (blocks) of latent variables: $q(\boldsymbol{\theta}) = \prod_{j=1}^J q_j(\boldsymbol{\theta}_j)$, where $J \leq \dim(\boldsymbol{\theta})$. Without any further parametric assumptions, it has been shown (Hinton and van Camp, 1993; MacKay, 1995; Jordan et al., 1999) that the optimal choice for each product component q_j is

$$q_j(\boldsymbol{\theta}_j) \propto \exp \left[\mathbb{E}_{-j} \log (p(\boldsymbol{\theta}, \mathcal{D})) \right], \quad (11)$$

where the above expectation is taken with respect to $\prod_{j' \neq j} q_{j'}(\boldsymbol{\theta}_{j'})$. The process of sweeping through the components of the partition and updating one at a time via Equation (11) is known as *coordinate ascent variational inference* (CAVI). (Wand et al., 2011) studies CAVI’s performance and improvement techniques in the case of elaborate distributions. Limitations of the mean-field assumption can be found in (Wand et al., 2011; Neville et al., 2014; Coker et al., 2022).

We specify the mean-field family for the approximate variational posterior:

$$q(\mathbf{a}, \boldsymbol{\gamma}, \boldsymbol{\omega}, \mathbf{W}, \mathbf{b}, \boldsymbol{\eta}, \boldsymbol{\psi}, \boldsymbol{\tau}) = q(\mathbf{a})q(\boldsymbol{\gamma})q(\boldsymbol{\omega})q(\mathbf{W}, \mathbf{b})q(\boldsymbol{\eta})q(\boldsymbol{\psi})q(\boldsymbol{\tau}). \quad (12)$$

Note that the assumption on the family above could be referred to as the *structured mean-field assumption*. Importantly, unlike existing variational algorithms for BNNs, we do not make any assumptions on independence of parameters between layers. The calculation of each component of the variational posterior is given in the Appendix A, where using Equation (11) we obtain the following update steps.

Global shrinkage parameters: the parameters $\boldsymbol{\tau}$ are independent across layers (and can be updated in parallel) with a GIG variational posterior:

$$q(\boldsymbol{\tau}) = \prod_{l=1}^{L+1} \text{GIG} \left(\tau_l \mid \hat{\nu}_{\text{glob}, l}, \hat{\delta}_{\text{glob}, l}, \lambda_{\text{glob}} \right), \quad (13)$$

where for $l = 1, \dots, L+1$,

$$\hat{\nu}_{\text{glob},l} = \nu_{\text{glob}} - \frac{D_l D_{l-1}}{2} \quad \text{and} \quad \hat{\delta}_{\text{glob},l} = \sqrt{\delta_{\text{glob}}^2 + \sum_d^{D_l} \sum_{d'}^{D_{l-1}} \mathbb{E} \left[\frac{1}{\psi_{l,d,d'}} \right] \mathbb{E} [W_{l,d,d'}^2]}.$$

Local shrinkage parameters: the parameters ψ are independent across and within layers (and can be updated in parallel) with a GIG variational posterior:

$$q(\psi) = \prod_l^{L+1} \prod_d^{D_l} \prod_{d'}^{D_{l-1}} \text{GIG} \left(\psi_{l,d,d'} \mid \hat{\nu}_{\text{loc},l,d,d'}, \hat{\delta}_{\text{loc},l,d,d'}, \lambda_{\text{loc},l} \right), \quad (14)$$

where for $l = 1, \dots, L+1$, $d = 1, \dots, D_l$, $d' = 1, \dots, D_{l-1}$,

$$\hat{\nu}_{\text{loc},l,d,d'} = \nu_{\text{loc},l} - \frac{1}{2} \quad \text{and} \quad \hat{\delta}_{\text{loc},l,d,d'} = \sqrt{\mathbb{E} \left[\frac{1}{\tau_l} \right] \mathbb{E} [W_{l,d,d'}^2] + \delta_{\text{loc},l}^2}.$$

Covariance matrix: the diagonal elements of the covariance matrix η_l are independent across and within layers (and can be updated in parallel) with an inverse-Gamma variational posterior:

$$q(\eta) = \prod_l^{L+1} \prod_d^{D_l} \text{IG}(\eta_{l,d}^2 \mid \alpha_{l,d}, \beta_{l,d}), \quad (15)$$

where for the hidden layers $l = 1, \dots, L$, the updated variational parameters for $d = 1, \dots, D_l$ are given by

$$\begin{aligned} \alpha_{l,d} &= \alpha_0^h + \frac{N}{2}, \\ \beta_{l,d} &= \beta_0^h + \frac{1}{2} \sum_n^N \left(\mathbb{E} [\mathbf{a}_{n,l,d}] - \mathbb{E} [\gamma_{n,l,d}] \mathbb{E} [\widetilde{\mathbf{W}}_{l,d}] \mathbb{E} [\tilde{\mathbf{a}}_{n,l-1}] \right)^2 + \mathbb{E} [a_{n,l,d}^2] - \mathbb{E} [\mathbf{a}_{n,l,d}]^2 \\ &\quad + \frac{1}{2} \sum_n^N \text{Tr} \left(\mathbb{E} [\widetilde{\mathbf{W}}_{l,d}^T \widetilde{\mathbf{W}}_{l,d}] \mathbb{E} [\tilde{\mathbf{a}}_{n,l-1} \tilde{\mathbf{a}}_{n,l-1}^T] \right) - \mathbb{E} [\gamma_{n,l,d}]^2 \text{Tr} \left(\mathbb{E} [\widetilde{\mathbf{W}}_{l,d}^T] \mathbb{E} [\widetilde{\mathbf{W}}_{l,d}] \mathbb{E} [\tilde{\mathbf{a}}_{n,l-1}] \mathbb{E} [\tilde{\mathbf{a}}_{n,l-1}^T] \right). \end{aligned}$$

And for the final layer, the updated variational parameters for $d = 1, \dots, D_{L+1}$ are given by

$$\begin{aligned} \alpha_{L+1,d} &= \alpha_0 + \frac{N}{2}, \\ \beta_{L+1,d} &= \beta_0 + \frac{1}{2} \sum_n^N \left(y_{n,d} - \mathbb{E} [\widetilde{\mathbf{W}}_{L+1,d}] \mathbb{E} [\tilde{\mathbf{a}}_{n,L}] \right)^2 \\ &\quad + \frac{1}{2} \sum_n^N \text{Tr} \left(\mathbb{E} [\widetilde{\mathbf{W}}_{L+1,d}^T \widetilde{\mathbf{W}}_{L+1,d}] \mathbb{E} [\tilde{\mathbf{a}}_{n,L} \tilde{\mathbf{a}}_{n,L}^T] \right) - \text{Tr} \left(\mathbb{E} [\widetilde{\mathbf{W}}_{L+1,d}]^T \mathbb{E} [\widetilde{\mathbf{W}}_{L+1,d}] \mathbb{E} [\tilde{\mathbf{a}}_{n,L}] \mathbb{E} [\tilde{\mathbf{a}}_{n,L}^T] \right). \end{aligned}$$

Note that in the above, $\mathbf{W}_{l,d}$ represents the d -th row of the weight matrix \mathbf{W}_l . Additionally, for $l = 1, \dots, L+1$ we introduce the notation $\widetilde{\mathbf{W}}_{l,d} = (b_{l,d}, \mathbf{W}_{l,d})$ and $\widetilde{\mathbf{W}} = (\mathbf{b}, \mathbf{W})$, and let the vector $\tilde{\mathbf{a}}_{n,l}$ represent the stochastic activation augmented with an entry of one, i.e. $\tilde{\mathbf{a}}_{n,l} = (1, \mathbf{a}_{n,l}^T)^T$.

Weights and biases: the weights and biases are independent across layers and within layers, independent across the D_l regression problems, with a Gaussian variational posterior:

$$q(\mathbf{b}, \mathbf{W}) = \prod_l^{L+1} \prod_d^{D_l} \text{N} \left(\widetilde{\mathbf{W}}_{l,d} \mid \mathbf{m}_{l,d}, \mathbf{B}_{l,d} \right), \quad (16)$$

where for the hidden layers $l = 1, \dots, L$, the updated variational parameters for $d = 1, \dots, D_l$ are given by

$$\begin{aligned}\mathbf{B}_{l,d}^{-1} &= \mathbf{D}_{l,d}^{-1} + \sum_n \left(\frac{1}{T^2} \mathbb{E}[\omega_{n,l,d}] + \mathbb{E}[(\eta_{l,d})^{-2}] \mathbb{E}[\gamma_{n,l,d}] \right) \mathbb{E}[\tilde{\mathbf{a}}_{n,l-1} \tilde{\mathbf{a}}_{n,l-1}^T], \\ \mathbf{m}_{l,d}^T &= \mathbf{B}_{l,d} \left(\sum_n \mathbb{E}[(\eta_{l,d})^{-2}] \mathbb{E}[\gamma_{n,l,d}] \mathbb{E}[\mathbf{a}_{n,l,d} \tilde{\mathbf{a}}_{n,l-1}] + \frac{1}{T} \mathbb{E}[\tilde{\mathbf{a}}_{n,l-1}] \left(\mathbb{E}[\gamma_{n,l,d}] - \frac{1}{2} \right) \right),\end{aligned}$$

and for the final layer, the updated variational parameters for $d = 1, \dots, D_{L+1}$ are given by

$$\begin{aligned}\mathbf{B}_{L+1,d}^{-1} &= \mathbf{D}_{L+1,d}^{-1} + \mathbb{E}[(\eta_{L+1,d})^{-2}] \sum_n \mathbb{E}[\tilde{\mathbf{a}}_{n,L} \tilde{\mathbf{a}}_{n,L}^T], \\ \mathbf{m}_{L+1,d}^T &= \mathbf{B}_{L+1,d} \mathbb{E}[(\eta_{L+1,d})^{-2}] \left(\sum_n y_n \mathbb{E}[\tilde{\mathbf{a}}_{n,L}] \right),\end{aligned}$$

where for $l = 1, \dots, L+1$ and $d = 1, \dots, D_l$,

$$\mathbf{D}_{l,d}^{-1} = \text{diag} \left(s_0^{-2}, \mathbb{E}[\tau_l^{-1}] \mathbb{E}[\psi_{l,d,1}^{-1}], \dots, \mathbb{E}[\tau_l^{-1}] \mathbb{E}[\psi_{l,d,D_{l-1}}^{-1}] \right).$$

Polya-Gamma augmented variables: ω are independent across observations $n = 1, \dots, N$, layers $l = 1, \dots, L$, and width $d = 1, \dots, D_l$, with a Polya-Gamma variational posterior:

$$q(\omega) = \prod_n \prod_l \prod_d \text{PG}(\omega_{n,l,d} \mid 1, A_{n,l,d}), \quad (17)$$

with updated variational parameters:

$$A_{n,l,d} = \frac{1}{T} \sqrt{\left(\text{Tr} \left(\mathbb{E}[\tilde{\mathbf{W}}_{l,d}^T \tilde{\mathbf{W}}_{l,d}] \mathbb{E}[\tilde{\mathbf{a}}_{n,l-1} \tilde{\mathbf{a}}_{n,l-1}^T] \right) \right)}.$$

Note that simulating from or evaluating the density of the PG is not necessary, and the CAVI updates of the other parameters only require computing the expectation of ω with respect to the variational posterior in Equation (17), which is straightforward to compute (Equation (9)).

Binary activations: γ are independent across observations $n = 1, \dots, N$, layers $l = 1, \dots, L$, and width $d = 1, \dots, D_l$, with a Bernoulli variational posterior:

$$q(\gamma) = \prod_n \prod_l \prod_d \text{Bern}(\gamma_{n,l,d} \mid \rho_{n,l,d}), \quad (18)$$

with

$$\rho_{n,l,d} = \sigma \left(-\frac{\mathbb{E}[\eta_{l,d}^{-2}]}{2} \text{Tr} \left(\mathbb{E}[\tilde{\mathbf{W}}_{l,d}^T \tilde{\mathbf{W}}_{l,d}] \mathbb{E}[\tilde{\mathbf{a}}_{n,l-1} \tilde{\mathbf{a}}_{n,l-1}^T] \right) + \mathbb{E}[\eta_{l,d}^{-2}] \mathbb{E}[\tilde{\mathbf{W}}_{l,d}] \mathbb{E}[\tilde{\mathbf{a}}_{n,l-1} \mathbf{a}_{n,l,d}] + \frac{1}{T} \mathbb{E}[\tilde{\mathbf{W}}_{l,d}] \mathbb{E}[\tilde{\mathbf{a}}_{n,l-1}] \right).$$

The parameters $\rho_{n,l,d}$ represent the posterior probability that the node is active and are illustrated for the toy example of Section 4.1 in Figure 4.

Stochastic activations: \mathbf{a} are independent across observations $n = 1, \dots, N$ and conditionally Gaussian given the previous layer with variational posterior:

$$q(\mathbf{a}) = \prod_{n=1}^N \prod_{l=1}^L \text{N}(\mathbf{a}_{n,l} \mid \mathbf{t}_{n,l} + \mathbf{M}_{n,l} \mathbf{a}_{n,l-1}, \mathbf{S}_{n,l}), \quad (19)$$

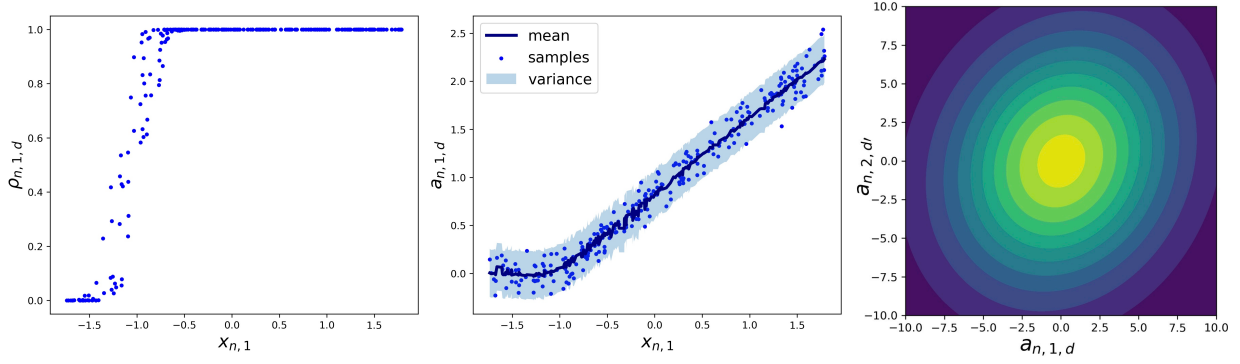


Figure 4: An illustration of the variational posterior of the binary and stochastic activations. The variational posterior of $\gamma_{n,1,d}$ (on the left) and $a_{n,1,d}$ (in the middle), both as a function of $x_{n,1}$ across all observations, along with the joint distribution of $(a_{n,1,d}, a_{n,2,d'})$ (on the right) in the case of the toy example of Section 4 for particular values of d, d', n .

where denote $\mathbf{a}_{n,0} := \mathbf{x}_n, \mathbf{S}_{n,L} := \mathbf{S}_L$ and the updated variational parameters for $n = 1, \dots, N$ and $l = 1, \dots, L-1$ are

$$\begin{aligned} \mathbf{S}_{n,l}^{-1} &= \hat{\Sigma}_l^{-1} - \mathbf{M}_{n,l+1}^T \mathbf{S}_{n,l+1}^{-1} \mathbf{M}_{n,l+1} + \sum_{d=1}^{D_{l+1}} \left(\mathbb{E} \left[\frac{1}{\eta_{l+1,d}^2} \right] \mathbb{E} [\gamma_{n,l+1,d}] + \frac{1}{T^2} \mathbb{E} [\omega_{n,l+1,d}] \right) \mathbb{E} [\mathbf{W}_{l+1,d}^T \mathbf{W}_{l+1,d}], \\ \mathbf{t}_{n,l} &= \mathbf{S}_{n,l} \left(\mathbf{M}_{n,l+1}^T \mathbf{S}_{n,l+1}^{-1} \mathbf{t}_{n,l+1} + \hat{\Sigma}_l^{-1} \mathbb{E} [\gamma_{n,l}] \odot \mathbb{E} [\mathbf{b}_l] + \frac{1}{T} \sum_{d=1}^{D_{l+1}} \mathbb{E} [\mathbf{W}_{l+1,d}^T] \left(\mathbb{E} [\gamma_{n,l+1,d}] - \frac{1}{2} \right) - \right. \\ &\quad \left. - \sum_{d=1}^{D_{l+1}} \left(\mathbb{E} \left[\frac{1}{\eta_{l+1,d}^2} \right] \mathbb{E} [\gamma_{n,l+1,d}] + \frac{1}{T^2} \mathbb{E} [\omega_{n,l+1,d}] \right) \mathbb{E} [\mathbf{W}_{l+1,d} b_{l+1,d}] \right), \\ \mathbf{M}_{n,l} &= \mathbf{S}_{n,l} \hat{\Sigma}_l^{-1} \mathbb{E} [\gamma_{n,l}] \mathbf{1}_{D_{l-1}}^T \odot \mathbb{E} [\mathbf{W}_l], \\ \hat{\Sigma}_l^{-1} &= \text{diag} \left(\mathbb{E} [\eta_{l,1}^{-2}], \dots, \mathbb{E} [\eta_{l,D_l}^{-2}] \right). \end{aligned}$$

And for the final layer with $n = 1, \dots, N$ and $l = L$,

$$\begin{aligned} \mathbf{S}_L^{-1} &= \hat{\Sigma}_L^{-1} + \sum_{d=1}^{D_{L+1}} \mathbb{E} \left[\frac{1}{\eta_{L+1,d}^2} \right] \mathbb{E} [\mathbf{W}_{L+1,d}^T \mathbf{W}_{L+1,d}], \\ \mathbf{t}_{n,L} &= \mathbf{S}_L \left(\left(\sum_{d=1}^{D_{L+1}} \mathbb{E} \left[\frac{1}{\eta_{L+1,d}^2} \right] (-\mathbb{E} [\mathbf{W}_{L+1,d}^T b_{L+1,d}] + \mathbb{E} [\mathbf{W}_{L+1,d}^T] y_{n,d}) \right) + \hat{\Sigma}_L^{-1} \mathbb{E} [\gamma_{n,L}] \odot \mathbb{E} [\mathbf{b}_L] \right), \\ \mathbf{M}_{n,L} &= \mathbf{S}_L \hat{\Sigma}_L^{-1} \mathbb{E} [\gamma_{n,L}] \mathbf{1}_{D_{L-1}}^T \odot \mathbb{E} [\mathbf{W}_L], \\ \hat{\Sigma}_L^{-1} &= \text{diag} \left(\mathbb{E} [\eta_{L,1}^{-2}], \dots, \mathbb{E} [\eta_{L,D_L}^{-2}] \right). \end{aligned}$$

Figure 4 illustrates on the toy example of Section 4.1 how the variational posterior of the stochastic activations (middle) resembles a smoothed, noisy ReLU. Due the independence assumption between the stochastic and binary activations, the potentially bimodal bow tie distribution (Equation (2)) is approximated with a unimodal Gaussian in the variational framework, which may better approximate the true posterior when the temperature is not too large relative to the noise (see Figure 1). In addition, the proposed approximation has the advantage of avoiding explicit assumptions of independence between layers, enabling it to capture dependencies between stochastic activations across layers, as illustrated for the toy example in Figure 4 (right).

The corresponding optimization objective, i.e. the ELBO in Equation (10), is available in closed form and provided in the Appendix B.

Algorithm 1 VI with EM

Require: Initialize hyperparameters**while** ELBO has not converged **do** **for** $l = 1, \dots, L$ **do** update $\nu_{\text{glob},l}$ and $\delta_{\text{glob},l}$ {parameters of τ_l } update $\nu_{\text{loc},l,d,d'}$ and $\delta_{\text{loc},l,d,d'}$ {parameters of $\psi_{l,d,d'}$ for $d = 1 \dots D_l, d' = 1 \dots D_{l-1}$ } update $\alpha_{l,d}$ and $\beta_{l,d}$ {parameters of $\eta_{l,d}$ for $d = 1 \dots D_l$ } update $A_{n,l,d}$ {parameter of $\omega_{n,l,d}$ for $d = 1 \dots D_l, n = 1 \dots N$ } **end for** update $\nu_{\text{glob},L+1}$ and $\delta_{\text{glob},L+1}$ {parameters of τ_{L+1} } update $\nu_{\text{loc},L+1,d,d'}$ and $\delta_{\text{loc},L+1,d,d'}$ {parameters of $\psi_{L+1,d,d'}$ for $d = 1 \dots D_y, d' = 1 \dots D_L$ } update $\alpha_{L+1,d}$ and $\beta_{L+1,d}$ for $d = 1 \dots D_y$ **for** $l = 1, \dots, L$ **do** update $\mathbf{S}_{n,l}$, $\mathbf{M}_{n,l}$ and $\mathbf{t}_{n,l}$ {parameters of $\mathbf{a}_{n,l}$ for $n = 1 \dots N$ } **end for** **for** $l = 1, \dots, L$ **do** update $\mathbf{B}_{l,d}$ and $\mathbf{m}_{l,d}$ {parameters of $(b_{l,d}, \mathbf{W}_{l,d})$ for $d = 1 \dots D_l$ } update $\rho_{n,l,d}$ {parameter of $\gamma_{n,l,d}$ for $d = 1 \dots D_l, n = 1 \dots N$ } **end for** update $\mathbf{B}_{L+1,d}$ and $\mathbf{m}_{L+1,d}$ {parameters of $(b_{L+1,d}, \mathbf{W}_{L+1,d})$ for $d = 1 \dots D_y$ } update h_{glob} {EM for global hyperparameter}**end while**

3.2 VI with EM

The hyperparameters can play a crucial role in Bayesian neural networks. When dealing with the sparsity-inducing priors setting an excessively large scale parameter weakens the shrinkage effects, whilst choosing a scale parameter that is too small may wipe out the effects of the important hidden nodes. Manually picking suitable values is challenging, and instead, we seek a more efficient strategy, utilizing the similarity between the variational and *expectation-maximization (EM) algorithms*. Specifically, we investigate the hybrid scheme combining VI with an EM step (Osborne et al., 2022) so that the steps of the CAVI algorithm proceed with the EM update to set the hyperparameter for global shrinkage variable τ . Due to weak identifiability, we do not jointly update global and local hyperparameters. Let h_{glob} represent δ_{glob} or λ_{glob} and consider the ELBO treated as a function of h_{glob} , then the optimal values as approximate MAP estimates are:

$$h_{\text{glob}} = \arg \max \mathbb{E}_{\text{glob}}[\text{ELBO}],$$

where

$$\begin{aligned} \mathbb{E}_{\text{glob}}[\text{ELBO}] &= \mathbb{E} \left[\sum_{l=1}^{L+1} \log(\text{GIG}(\tau_l \mid \nu_{\text{glob}}, \delta_{\text{glob}}, \lambda_{\text{glob}})) \right] \\ &= (L+1) (\nu_{\text{glob}} (\log(\lambda_{\text{glob}}) - \log(\delta_{\text{glob}})) - \log(2K_{\nu_{\text{glob}}}(\lambda_{\text{glob}}\delta_{\text{glob}}))) \\ &\quad + \sum_{l=1}^{L+1} (\nu_{\text{glob}} - 1) \mathbb{E}[\log \tau_l] - \frac{1}{2} \left(\delta_{\text{glob}}^2 \mathbb{E} \left[\frac{1}{\tau_l} \right] + \lambda_{\text{glob}}^2 \mathbb{E}[\tau_l] \right). \end{aligned}$$

In the case of the IG priors, one's aim is to set optimal δ_{glob} , in the case of the Gamma and IGauss priors, the parameters of interest are λ_{glob} . We provide specific examples of the shrinkage parameters and the corresponding optimal values in [Appendix E.2](#).

The resulting algorithm (described in [Algorithm 1](#)) scales linearly with the number of hidden layers and the number of samples but cubically with the number of hidden units; the computational complexities corresponding to individual factors of the variational family are provided in [Appendix A](#). In the following subsections, we discuss two strategies to improve scalability. First, to handle large N , CAVI can be combined with subsampling through stochastic VI (Hoffman et al., 2013), and second, a post-processing node selection algorithm is proposed to obtain a sparse variational posterior for faster predictive inference.

3.3 Stochastic Variational Inference

At each iteration, CAVI has to cycle through the entire data set, which can be computationally expensive and inefficient for large sample sizes. An alternative to coordinate ascent is gradient-based optimization, which extends the algorithm by employing stochastic variational inference (SVI [Hoffman et al., 2013](#)) and subsampling. Forst, recall that the variational posterior of the latent variables $\mathbf{a}, \gamma, \omega$ factorizes across data points, that is

$$q(\mathbf{a})q(\gamma)q(\omega) = \prod_{n=1}^N q(\mathbf{a}_n)q(\gamma_n)q(\omega_n).$$

To highlight the need for stochastic VI, we observe that for each layer $l = 1, \dots, L$ the ordinary coordinate ascent needs to iterate through N local variational parameters corresponding to variables $\mathbf{a}_{n,l}, \gamma_{n,l}$ and $\omega_{n,l}$ with $\gamma_{n,l}$ and $\omega_{n,l}$ both having D_l variational parameters to update, and $\mathbf{a}_{n,l}$ having of order D_l^2 variational parameters. For large N , this can be computationally burdensome. To overcome this, stochastic VI uses the coordinate ascent variational updates obtained in [Section 3.1](#) to set the local parameters for a subset of points, and the intermediate global parameters are obtained by following the noisy natural gradient of ELBO ([Hoffman et al., 2013](#)).

At each iteration t , the SVI algorithm first uniformly samples a collection of indices $S(t)$ without replacement, where the computational gains are obtained as long as $|S(t)| \ll N$. For each index $s \in S(t)$, the local variational parameters are optimized in a coordinate ascent manner with updates in [Equations \(17\) to \(19\)](#), and the convergence is monitored with noisy estimates of the local ELBO, that is

$$\mathbb{E}[\log p(\mathbf{y}, \mathbf{a}, \gamma, \omega | \mathbf{W}, \mathbf{b}, \Sigma)] - \mathbb{E}[\log q(\mathbf{a})] - \mathbb{E}[\log q(\gamma)] - \mathbb{E}[\log q(\omega)],$$

the estimate of which is provided [Appendix C](#). Next, the global parameters, \mathbf{W}, \mathbf{b} and η , are updated via a linear combination of previous values and intermediate updates

$$(1 - \ell_t)\text{parameter}^{(t-1)} + \ell_t \times \text{intermediate parameter}^{(t)}, \quad (20)$$

where ℓ_t is the learning rate and the intermediate parameters are obtained via [Equations \(15\) and \(16\)](#) but with the sufficient statistics, which involve sums over N , replaced with the scaled sums over $S(t)$. Additional details and the step-by-step algorithm are provided in [Appendix C](#). The convergence of the stochastic gradient descent depends on the choice of the step sizes ℓ_t in the Robbins-Monro sequence ([Robbins and Monro, 1951](#)), and we follow ([Hoffman et al., 2013](#)), who set

$$\ell_t = (1 + t)^{-k}, \quad k \in (0.5, 1], \quad (21)$$

where k is the forgetting rate. We monitor the convergence of the algorithm by obtaining noisy estimates of the ELBO (provided in [Appendix C](#)) where the sums over $n = 1, \dots, N$ are replaced with the scaled sums over $n \in S$.

3.4 Inferring the Network Structure

The choice of the network architecture has significant practical implications on the generalization of the model, and so sparsity-promoting priors for the network weights have emerged as a promising approach for increased robustness to the choice of architecture. In this article, we focus on a class of continuous shrinkage priors, which results in more tractable computations, yet also implies non-zero posterior means and does not lead to automatic network architecture selection. To address this, we consider a post-processing node selection algorithm to obtain a sparse variational posterior, which both aids interpretability and improves scalability of predictive inference (discussed in [Section 3.5](#))

In Bayesian linear regression with shrinkage priors, several post-processing methods have been proposed to yield a sparse solution (see e.g. ([Piironen et al., 2020](#); [Li and Pati, 2017](#); [Griffin, 2024](#))). The method known as decoupling shrinkage and selection (DSS) ([Hahn and Carvalho, 2015](#)) obtains sparse estimates of the weights by minimizing the sum of the predictive loss function with a parsimony-inducing penalty. An alternative approach is the the penalized credible regions (PenCR) method ([Zhang et al., 2021](#)), which

identifies the "sparsest" solution in posterior credible regions corresponding to different levels; it is shown to perform well in the case of global-local shrinkage priors and under certain assumptions, PenCR produces the same results as DSS. Similarly, we propose to make use of credible intervals to select nodes. Following (Li and Lin, 2010), we implement an automatic *credible interval criterion* which selects a node as long as its credible interval doesn't cover zero. Specifically, recall that the variational posterior of the weights is $W_{l,d,d'} \sim N(m_{l,d,d'}^W, B_{l,d,d'}^W)$ for $l = 1, \dots, L, d = 1, \dots, D_l, d' = 1, \dots, D_{l-1}$, where $\mathbf{m}_{l,d}^W$ and $\mathbf{B}_{l,d}^W$ denote the subsets of the mean $\mathbf{m}_{l,d}$ and covariance matrix $\mathbf{B}_{l,d}$ corresponding to the weights. Then, we obtain sparse weights $\widehat{W}_{l,d,d'}$ with sparse variational distribution $\widehat{q}(b_{l,d}, \widehat{\mathbf{W}}_{l,d})$ for some $l \in \mathcal{L} \subseteq \{1, \dots, L+1\}$, $d \in \mathcal{D}_l \subseteq \{1, \dots, D_l\}, d' \in \mathcal{D}_{l-1} \subseteq \{1, \dots, D_{l-1}\}$, defined by setting:

$$\widehat{W}_{l,d,d'} \sim \begin{cases} N\left(m_{l,d,d'}^W, \left(B_{l,d}^W\right)_{d'd'}\right) & \text{if } \max(Q(W_{l,d,d'} > 0), Q(W_{l,d,d'} < 0)) \geq \kappa, \\ \delta_0 & \text{otherwise,} \end{cases}$$

where $Q(W_{l,d,d'} < 0) = 1 - Q(W_{l,d,d'} > 0) = \Phi(-m_{l,d,d'}^W / \sqrt{(B_{l,d}^W)_{d'd'}})$. The threshold κ is chosen to control the *Bayesian false discovery rate*, which is calculated as

$$\widehat{\text{FDR}}(\kappa) = \frac{\sum_{l,d,d'} (1 - \mathcal{Q}_{l,d,d'}) \mathbf{1}(\mathcal{Q}_{l,d,d'} > \kappa)}{\sum_{l,d,d'} \mathbf{1}(\mathcal{Q}_{l,d,d'} > \kappa)},$$

with $\mathcal{Q}_{l,d,d'} = \max(Q(W_{l,d,d'} > 0), Q(W_{l,d,d'} < 0))$. Specifically, for a specified error rate α , κ is set to satisfy $\widehat{\text{FDR}}(\kappa) < \alpha$. Algorithm 2 describes the node selection procedure which begins with ordering $\mathcal{Q}_{l,d,d'}$ in the descending order and going down through the thresholds to assign κ to the smallest $\mathcal{Q}_{l,d,d'}$ such that its false discovery rate doesn't exceed α .

Once we sweep through $\mathcal{Q}_{l,d,d'}$, we do a backwards pass to remove the nodes with no connections. If the node has no outgoing connections, then all the incoming connections need to be removed, and conversely, if the node has no incoming connections, then all the outgoing connections can be removed. An example of the network resulting after applying the Algorithm 2 is illustrated by the Figure 7.

3.5 Predictions

For a new \mathbf{x}_* , the predictive distribution of \mathbf{y}_* given the data is approximated as:

$$\begin{aligned} p(\mathbf{y}_* | \mathbf{x}_*, \mathcal{D}) &= \int p(\mathbf{y}_* | \mathbf{x}_*, \boldsymbol{\theta}, \mathcal{D}) p(\boldsymbol{\theta} | \mathcal{D}, \mathbf{x}_*) d\boldsymbol{\theta} \\ &= \int p(\mathbf{y}_* | \mathbf{a}_*, \mathbf{W}, \mathbf{b}, \boldsymbol{\eta}) p(\mathbf{a}_*, \mathbf{W}, \mathbf{b}, \boldsymbol{\eta} | \mathcal{D}, \mathbf{x}_*) d\mathbf{a}_* d\mathbf{W} d\mathbf{b} d\boldsymbol{\eta} \\ &\approx \int p(\mathbf{y}_* | \mathbf{a}_*, \mathbf{W}, \mathbf{b}, \boldsymbol{\eta}) q(\mathbf{a}_*) q(\mathbf{W}, \mathbf{b}) q(\boldsymbol{\eta}) d\mathbf{a}_* d\mathbf{W} d\mathbf{b} d\boldsymbol{\eta} \\ &= \int N(\mathbf{y}_* | \mathbf{W}_{L+1} \mathbf{a}_{*,L} + \mathbf{b}_{L+1}, \boldsymbol{\Sigma}_{L+1}) q(\mathbf{a}_{*,L}) q(\mathbf{W}_{L+1}, \mathbf{b}_{L+1}) q(\boldsymbol{\eta}_{L+1}) d\mathbf{a}_{*,L} d\mathbf{W}_{L+1} d\mathbf{b}_{L+1} d\boldsymbol{\eta}_{L+1}. \end{aligned} \tag{22}$$

Equation (22) requires first computing the approximate variational predictive distributions $q(\mathbf{a}_*)$, $q(\boldsymbol{\gamma}_*)$ and $q(\boldsymbol{\omega}_*)$, which are updated in a similar way to Section 3.1.

Specifically, the stochastic activations are conditionally Gaussian given the previous layer with variational predictive distribution:

$$q(\mathbf{a}_*) = \prod_{l=1}^L N(\mathbf{a}_{*,l} | \mathbf{t}_{*,l} + \mathbf{M}_{*,l} \mathbf{a}_{*,l-1}, \mathbf{S}_{*,l}),$$

where $\mathbf{a}_{*,0} = \mathbf{x}_*$. For the final layer, we have:

$$\mathbf{S}_{*,L}^{-1} = \hat{\boldsymbol{\Sigma}}_L^{-1}; \quad \mathbf{t}_{*,L} = \mathbb{E}[\boldsymbol{\gamma}_{*,L}] \odot \mathbb{E}[\mathbf{b}_L]; \quad \mathbf{M}_{*,L} = \mathbb{E}[\boldsymbol{\gamma}_{*,L}] \mathbf{1}_{D_{L-1}}^T \odot \mathbb{E}[\mathbf{W}_L].$$

Algorithm 2 Node selection algorithm

Require: $\mathcal{I} = \{\mathcal{Q}_{l,d,d'} \mid l = 1 \dots L, d = 1 \dots D_{l+1}, d' = 1 \dots D_l\}$.

$\hat{\kappa} = \max(\mathcal{I})$

$\mathcal{I} = \mathcal{I} \setminus \hat{\kappa}$

if $\widehat{\text{FDR}}(\max(\mathcal{I})) < \alpha$ **then**

$\hat{\kappa} = \max(\mathcal{I})$

$\mathcal{I} = \mathcal{I} \setminus \hat{\kappa}$

else

break

end if

for $l = 1 \dots L, d = 1 \dots D_{l+1}, d' = 1 \dots D_l$ **do**

if $\mathcal{Q}_{l,d,d'} \geq \hat{\kappa}$ **then**

$\widehat{W}_{l,d,d'} \sim N\left(m_{l,d,d'}^W, \left(B_{l,d}^W\right)_{d'd'}\right)$

else

$\widehat{W}_{l,d,d'} = 0$ a.s.

end if

end for

for $l = L + 1, \dots, 2, d = 1, \dots, D_l$, **do**

if $\widehat{W}_{l,d} = 0$ a.s. **then**

$\widehat{W}_{l-1,d',d} = 0$ a.s. $\forall d' = 1, \dots, D_{l-1}$

else

if $\widehat{W}_{l-1,d',d} = 0$ a.s. $\forall d' = 1, \dots, D_{l-1}$ **then**

$\widehat{W}_{l,d} = 0$ a.s.

end if

end if

end for

Ensure: $\widehat{q}(b_{l,d}, \widehat{\mathbf{W}}_{l,d}), l \in \mathcal{L}, d \in \mathcal{D}_l, d' \in \mathcal{D}_{l-1}$.

For all other layers $l = 1, \dots, L - 1$, we have:

$$\begin{aligned} \mathbf{S}_{*,l}^{-1} &= \hat{\Sigma}_l^{-1} - \mathbf{M}_{*,l+1}^T \mathbf{S}_{*,l+1}^{-1} \mathbf{M}_{*,l+1} + \sum_{d=1}^{D_{l+1}} \left(\mathbb{E} \left[\frac{1}{\eta_{l+1,d}^2} \right] \mathbb{E} [\gamma_{*,l,d}] + \frac{1}{T^2} \mathbb{E} [\omega_{*,l+1,d}] \right) \mathbb{E} [\mathbf{W}_{l+1,d}^T \mathbf{W}_{l+1,d}], \\ \mathbf{t}_{*,l} &= \mathbf{S}_{*,l} \left(\mathbf{M}_{*,l+1}^T \mathbf{S}_{*,l+1}^{-1} \mathbf{t}_{*,l+1} + \hat{\Sigma}_l^{-1} \mathbb{E} [\gamma_{*,l}] \odot \mathbb{E} [\mathbf{b}_l] - \sum_{d=1}^{D_{l+1}} \mathbb{E} \left[\frac{1}{\eta_{l+1,d}^2} \right] \mathbb{E} [\gamma_{*,l,d}] \mathbb{E} [\mathbf{W}_{l+1,d}^T b_{l+1,d}] \right. \\ &\quad \left. + \frac{1}{T} \sum_{d=1}^{D_{l+1}} \mathbb{E} [\mathbf{W}_{l+1,d}^T] \left(\mathbb{E} [\gamma_{*,l+1,d}] - \frac{1}{2} \right) - \frac{1}{T^2} \sum_{d=1}^{D_{l+1}} \mathbb{E} [\omega_{*,l+1,d}] \mathbb{E} [\mathbf{W}_{l+1,d} b_{l+1,d}] \right), \\ \mathbf{M}_{*,l} &= \mathbf{S}_{*,l} \hat{\Sigma}_l^{-1} \mathbb{E} [\gamma_{*,l}] \mathbf{1}_{D_{l-1}}^T \odot \mathbb{E} [\mathbf{W}_l]. \end{aligned}$$

The binary activations are independent across layers $l = 1, \dots, L$ and width $d = 1, \dots, D_l$, with a Bernoulli variational predictive distribution:

$$q(\gamma_*) = \prod_l \prod_d \text{Bern}(\gamma_{*,l,d} \mid \rho_{*,l,d}), \quad (23)$$

with

$$\rho_{*,l,d} = \sigma \left(-\frac{\mathbb{E} [\eta_{l,d}^{-2}]}{2} \text{Tr} \left(\mathbb{E} [\widetilde{\mathbf{W}}_{l,d}^T \widetilde{\mathbf{W}}_{l,d}] \mathbb{E} [\widetilde{\mathbf{a}}_{*,l-1} \widetilde{\mathbf{a}}_{*,l-1}^T] \right) + \mathbb{E} [\eta_{l,d}^{-2}] \mathbb{E} [\widetilde{\mathbf{W}}_{l,d}] \mathbb{E} [\widetilde{\mathbf{a}}_{*,l-1} a_{*,l,d}] + \frac{1}{T} \mathbb{E} [\widetilde{\mathbf{W}}_{l,d}] \mathbb{E} [\widetilde{\mathbf{a}}_{*,l-1}] \right).$$

Finally, the Polya-Gamma augmented variables are independent across layers $l = 1, \dots, L$ and width $d = 1, \dots, D_l$, with a Polya-Gamma variational predictive distribution:

$$q(\omega_*) = \prod_l \prod_d^{D_l} \text{PG}(\omega_{*,l,d} \mid 1, A_{*,l,d}), \quad (24)$$

with updated variational parameters:

$$A_{*,l,d} = \frac{1}{T} \sqrt{\left(\text{Tr} \left(\mathbb{E} \left[\widetilde{\mathbf{W}}_{l,d}^T \widetilde{\mathbf{W}}_{l,d} \right] \mathbb{E} \left[\widetilde{\mathbf{a}}_{*,l-1} \widetilde{\mathbf{a}}_{*,l-1}^T \right] \right) \right)}.$$

Thus, before computing predictions, we first iterate to update the variational predictive distributions of \mathbf{a}_* , γ_* , and ω_* . The corresponding ELBO (derived in the [Appendix B.2](#)) is monitored for convergence. While a closed-form expression for the integral in [Equation \(22\)](#) is unavailable, generating samples from the variational predictive is straightforward;

$$\mathbf{y}_*^{(j)} \sim \text{N} \left(\mathbf{y}_* \mid \mathbf{W}_{L+1}^{(j)} \mathbf{a}_{*,L}^{(j)} + \mathbf{b}_{L+1}^{(j)}, \boldsymbol{\Sigma}_{L+1}^{(j)} \right), \quad (25)$$

for $j = 1, \dots, J$, where $(\mathbf{W}_{L+1}^{(j)}, \mathbf{b}_{L+1}^{(j)}) \sim q(\mathbf{W}_{L+1}, \mathbf{b}_{L+1})$, $\eta_{L+1}^{(j)} \sim q(\eta_{L+1})$, and $\mathbf{a}_{*,l}^{(j)} \mid \mathbf{a}_{*,l-1}^{(j)} \sim q(\mathbf{a}_{*,l} \mid \mathbf{a}_{*,l-1})$ for $l = 1, \dots, L$, are iid draws from the variational posterior. These samples can be used to obtain a Monte Carlo approximation to investigate potential non-normality in the predictive distribution in [Equation \(22\)](#) and to compute credible intervals based on the highest posterior density region.

We can also compute the expectation and variance of \mathbf{y}_* in closed form. Specifically, the expectation of \mathbf{y}_* under the variational predictive distribution is:

$$\mathbb{E}[\mathbf{y}_* \mid \mathbf{x}_*, \mathcal{D}] \approx \mathbb{E}_{q_{L+1}}[\mathbf{W}_{L+1}] \mathbb{E}_{q_{*,L}}[\mathbf{a}_{*,L}] + \mathbb{E}_{q_{L+1}}[\mathbf{b}_{L+1}], \quad (26)$$

where recursively

$$\mathbb{E}_{q_{*,L}}[\mathbf{a}_{*,L}] = \mathbb{E}_{q_{*,L-1}} \left[\mathbb{E}_{q(\mathbf{a}_{*,L} \mid \mathbf{a}_{*,L-1})}[\mathbf{a}_{*,L}] \right] = \mathbf{t}_{*,L} + \mathbf{M}_{*,L} \mathbb{E}_{q_{*,L-1}}[\mathbf{a}_{*,L-1}].$$

Similarly, the variational variance of \mathbf{y}_* is

$$\text{Var}[y_{*,d} \mid \mathbf{x}_*, \mathcal{D}] \approx \text{Var}_{q_{L+1}}[\mathbf{W}_{L+1,d} \mathbf{a}_{*,L} + \mathbf{b}_{L+1,d}] + \mathbb{E}_{q_{L+1}}[\eta_{L+1,d}^2],$$

where the first term represents the signal variance and is computed as

$$\begin{aligned} \text{Var}_{q_{L+1}}[\mathbf{W}_{L+1,d} \mathbf{a}_{*,L} + \mathbf{b}_{L+1,d}] &= \mathbb{E}_{q_{L+1}}[(\mathbf{W}_{L+1,d} \mathbf{a}_{*,L} + \mathbf{b}_{L+1,d})^2] - (\mathbb{E}_{q_{L+1}}[\mathbf{W}_{L+1,d}] \mathbb{E}_{q_L}[\mathbf{a}_{*,L}] + \mathbb{E}_{q_{L+1}}[\mathbf{b}_{L+1,d}])^2 \\ &= \text{Tr} \left(\mathbb{E}_{q_{L+1}}[\mathbf{W}_{L+1,d}^T \mathbf{W}_{L+1,d}] \mathbb{E}_{q_L}[\mathbf{a}_{*,L} \mathbf{a}_{*,L}^T] - \mathbb{E}_{q_{L+1}}[\mathbf{W}_{L+1,d}]^T \mathbb{E}_{q_{L+1}}[\mathbf{W}_{L+1,d}] \mathbb{E}_{q_L}[\mathbf{a}_{*,L}] \mathbb{E}_{q_L}[\mathbf{a}_{*,L}]^T \right) \\ &\quad + \text{Var}_{q_{L+1}}(\mathbf{b}_{L+1,d}) + 2\text{Cov}_{q_{L+1}}(\mathbf{W}_{L+1,d}, \mathbf{b}_{L+1,d}) \mathbb{E}_{q_L}[\mathbf{a}_{*,L}], \end{aligned}$$

which requires the recursive computation:

$$\mathbb{E}_{q_L}[\mathbf{a}_{*,L} \mathbf{a}_{*,L}^T] = \mathbf{S}_{*,L} + \mathbf{t}_{*,L} \mathbf{t}_{*,L}^T + 2\mathbf{M}_{*,L} \mathbb{E}_{q_{L-1}}[\mathbf{a}_{*,L-1}] \mathbf{t}_{*,L}^T + \mathbf{M}_{*,L} \mathbb{E}_{q_{L-1}}[\mathbf{a}_{*,L-1} \mathbf{a}_{*,L-1}^T] \mathbf{M}_{*,L}^T.$$

Sparse prediction Observe that the variational algorithm used for prediction scales linearly with the number of hidden layers and the number of samples but cubically with the number of hidden units, this motivates the node-selection method proposed in [Section 3.4](#). To save on both computation and storage, the variational predictive distribution can be computed based on the sparse variational posterior ([Section 3.4](#)). For a new data point \mathbf{x}_* , we obtain expectation and variance of \mathbf{y}_* by first computing the sparse versions of variational predictive distributions $\hat{q}(\mathbf{a}_*)$, $\hat{q}(\gamma_*)$ and $\hat{q}(\omega_*)$ as in [Equations \(19\)](#), [\(23\)](#) and [\(24\)](#) by plugging $\hat{q}(b_{l,d}, \widetilde{\mathbf{W}}_{l,d})$ instead of the $q(b_{l,d}, \mathbf{W}_{l,d})$, which only requires updates for the subset of nodes with nonzero weights.

3.6 Ensembles of Variational Approximations

While the variational algorithm described in [Section 3.1](#) increases the ELBO at each epoch, the ELBO is a non-convex function of the variational parameters and only convergence to a local optimum is guaranteed. Due to identifiability issues, the posterior distribution of a Bayesian neural network is highly multimodal, and exploring this posterior is notoriously challenging ([Papamarkou et al., 2022](#)). A single variational approximation tends to concentrate around one mode and can understate posterior uncertainty. Several approaches have been proposed to overcome such issues. Recently, ([Ohn and Lin, 2024](#)) introduced adaptive variational inference, which achieves optimal posterior contraction rate and model selection consistency by considering several variational approximations obtained in different models. Similarly, ([Yao et al., 2022](#)) introduced an approach which uses parallel runs of inference algorithms to cover as many modes of the posterior distribution as possible and then combines these using Bayesian stacking. While the idea of combining the outputs of several neural networks is not novel ([Hansen and Salamon, 1990](#); [Levin et al., 1990](#)), we note that deep non-Bayesian ensembles recently received quite a lot of attention ([Lakshminarayanan et al., 2017](#)) and several alternatives and modifications enabling uncertainty quantification were proposed ([Wilson and Izmailov, 2020](#); [D' Angelo and Fortuin, 2021](#); [Pearce et al., 2020](#); [Wenzel et al., 2020b](#)). Observing non-optimality of conventional deep ensembles combining point estimates ([Wu and Williamson, 2024](#)), in our approach, we adopt the ideas of ([Ohn and Lin, 2024](#); [Yao et al., 2022](#)) and consider ensembles of posterior approximations in a similar but simpler fashion. Specifically, we consider an ensemble of variational approximations, obtained by running in parallel the variational algorithm multiple times with different random starting points and combining those with respect to the optimization objective. In this case, letting $k = 1, \dots, K$ index the different variational approximations, we compute the weight w_k associated with each approximation in accordance with the tempered ELBO:

$$w_k \propto \exp(\zeta \text{ELBO}_k),$$

where ζ is a tempering parameter, setting which to be in the interval $(0, 0.1]$ allows for avoiding a strong dominance of a single particular model. We can interpret this as a Bayesian model averaging (BMA) across the K different models/approximations. While in a classical BMA setting, the weights would be proportional to the marginal likelihood for each model, the use of the ELBO is motivated as it provides a lower bound to the marginal likelihood and can be computed in closed form. Next, we compute predictions by taking a weighted average of the predictive distributions of each model (given in [Equation \(26\)](#)), that is

$$\mathbb{E}[\mathbf{y}_* | \mathbf{x}_*, \mathcal{D}] \approx \sum_{k=1}^K w_k \mathbb{E}_{q_k}[\mathbf{y}_* | \mathbf{x}_*, \mathcal{D}],$$

where each expectation is taken with respect to q_k (the k th variational approximation). Similarly, we can compute the variance as

$$\text{Var}(\mathbf{y}_* | \mathbf{x}_*, \mathcal{D}) \approx \sum_{k=1}^K w_k \text{Var}_{q_k}(\mathbf{y}_* | \mathbf{x}_*, \mathcal{D}) + \sum_{k=1}^K w_k (\mathbb{E}_{q_k}[\mathbf{y}_* | \mathbf{x}_*, \mathcal{D}])^2 - \left(\sum_{k=1}^K w_k \mathbb{E}_{q_k}[\mathbf{y}_* | \mathbf{x}_*, \mathcal{D}] \right)^2.$$

The following approach has the potential to improve both predictive accuracy and uncertainty quantification. Once again, we can investigate the variational predictive distribution (beyond the mean and variance) by first sampling a model with probability (w_1, \dots, w_K) and then given that selected model k , generating a sample \mathbf{y}_* from the k th variational predictive distribution (as described in [Equation \(25\)](#)).

4 Experiments

We evaluate the variational bow tie neural network (VBNN) on several datasets. First, we consider a simple nonlinear synthetic example to compare with a ground truth. We then validate VBNN on the diabetes dataset, first considered in ([Efron et al., 2004](#)) to demonstrate the least angle regression (LARS) algorithm for variable selection, and subsequently, used in different proposals for sparsity-promoting priors algorithms (e.g. ([Park and Casella, 2008](#); [Li and Lin, 2010](#))). Lastly, we consider a range of popular regression datasets from the UCI Machine Learning Repository ([M. et al., 2007](#)).

Table 2: List of the models considered to evaluate the performance of our method.

Model	Description
mfVI	BNN with Automatic Differentiation VI with mean-field family
HMC	BNN with Hamiltonian Monte Carlo with No-U-Turn sampler
BBB	Bayes by Backprob
HSBNN	BNN with Horseshoe priors inferred with Black Box VI
VBNN	Our model inferred with CAVI
GVBNN	VBNN with Gaussian priors inferred with CAVI
SVBNN	Our model inferred with SVI

The importance of suitable initialization choice in NNs is well known (Wenzel et al., 2020a; Daniely et al., 2016; He et al., 2015), and we design two possible random initialization schemes of the VBNN, which are described in Appendix D.1 and used in all experiments. Convergence of the ELBO is monitored during the training and prediction stages, where if three consecutive measurements of ELBO for training differ by less than the specified threshold, the phase is stopped and the model moves to the prediction stage, where we proceed similarly. In most experiments, the thresholds during the training and prediction stages are set, respectively, to $1e-5$ and $1e-4$.

We compare the performance of VBNN to various frameworks (summarized in Table 2), namely, to BNNs inferred with automatic differentiation VI with the mean-field variational family (mfVI) (Kucukelbir et al., 2017) and Hamiltonian Monte Carlo with the No-U-Turn sampler (HMC) (Hoffman et al., 2014) implemented in Numpyro (Phan et al., 2019), Bayes by Backprop (BBB) (Blundell et al., 2015) implemented with Pytorch, and BNNs with Horseshoe priors (HSBNN) of (Ghosh et al., 2019) which considers a structured variational family and learns the variational parameters by obtaining gradient estimators. We also consider the variational bow tie neural network with Gaussian priors (GVBNN), in contrast to shrinkage priors. As CAVI may be expensive for large data, in Section 4.3 we additionally consider VBNN inferred with SVI (SVBNN). Further comparisons between the performance of VBNN and SVBNN are provided in Appendix D.6.

For all the datasets, we evaluate the performance over 10 random splits, where we use 90% of the data for the training and 10% for testing the model. We record the root mean squared error (RMSE), the predictive negative log-likelihood of the test data (NLL) and the empirical coverage (EC) (see Appendix D for additional implementation details). The empirical coverage reports the fraction of observations contained within the $(1 - \alpha) * 100\%$ credible intervals (CIs), which are computed based on the Gaussian approximation. In the ideal setting, the computed EC should equal the CI level. More specifically, let \mathbf{y}_i^* be the true target for test points $i = 1, \dots, N^*$ and $q_{\alpha/2}$ and $q_{1-\alpha/2}$ be the quantiles based on the model’s Gaussian approximation for some $\alpha \in [0.5, 1]$, then

$$EC(\alpha) = \frac{1}{N^*} \sum_{i=1}^{N^*} \mathbf{1}(\mathbf{y}_i^* \in [q_{\alpha/2}, q_{1-\alpha/2}]).$$

If $EC(\alpha) > 1 - \alpha$ then the CIs are too wide; a worse scenario occurs when $EC(\alpha) < 1 - \alpha$ as it means that the CIs are too narrow and the model is overconfident in its predictions.

4.1 Simulated Example

We construct a synthetic dataset generated by first uniformly sampling a two-dimensional input vector $\mathbf{x}_n = (x_{n,1}, x_{n,2})$, with $x_{n,d} \sim \text{Unif}([-2, 2])$, and assume only the first feature influences the output: $y_n = f(x_{n,1}) + \epsilon_n = 0.1x_{n,1}^2 + 10 \sin(x_{n,1}) + \epsilon_n$, where $\epsilon_n \sim \text{N}(0, 0.5)$. Then, the dataset consisting of $N = 300$ observations is used to investigate the performance of VBNN compared to the GVBNN, mfVI, HMC, BBB and HSBNN baselines as we increase the number of hidden layers, setting $L = 1, 2$ or 4 , whilst keeping the number of hidden units in each layer fixed to $D_H = 20$. In general, for this simple non-linear example, the performance tends to deteriorate with increasing architecture complexity (larger depth). While HMC performs consistently well across all depths, the cost associated with the sampling approach is high. VBNN is competitive to HSBNN and outperforms mfVI, GVBNN and BBB in terms of accuracy (see Figure 5). Further, except for HMC, the empirical coverage of VBNN is the most robust to the choice of depth; for the

largest choice of $L = 4$, mfVI, BBB, GVBNN and even HSBNN provide overly wide CIs while VBNN more closely reaches the desired coverage (see Figure 6).

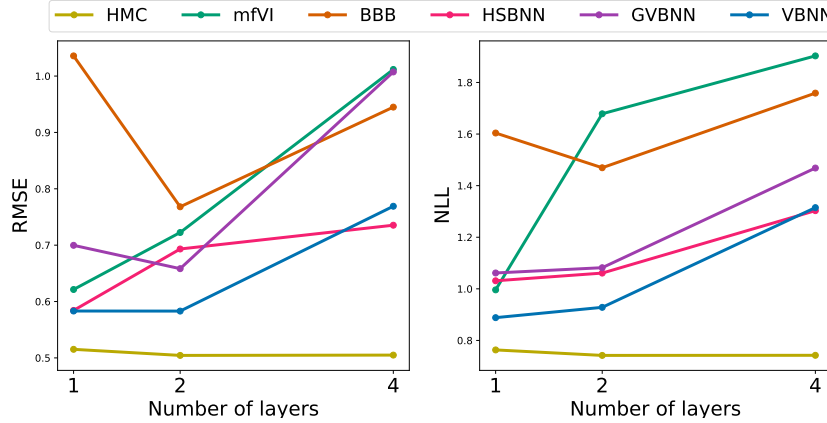


Figure 5: Simulated example. Performance in terms of the RMSE and NLL as the depth increases for different models and algorithms. HMC can be seen as a gold standard. VBNN is competitive with HSBNN and is more robust to the choice of depth and overparameterization than GVBNN, mfVI, BBB.

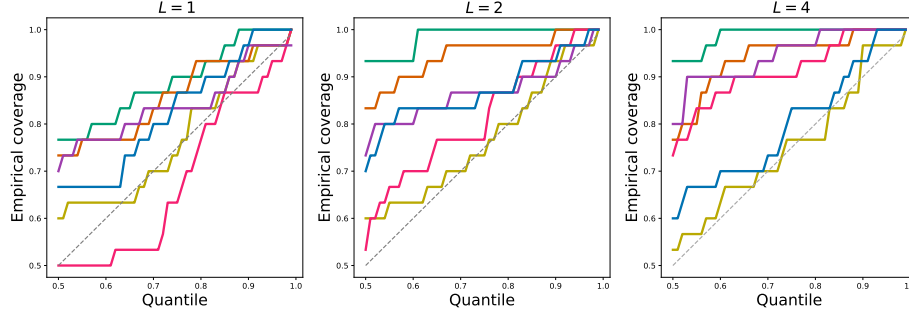
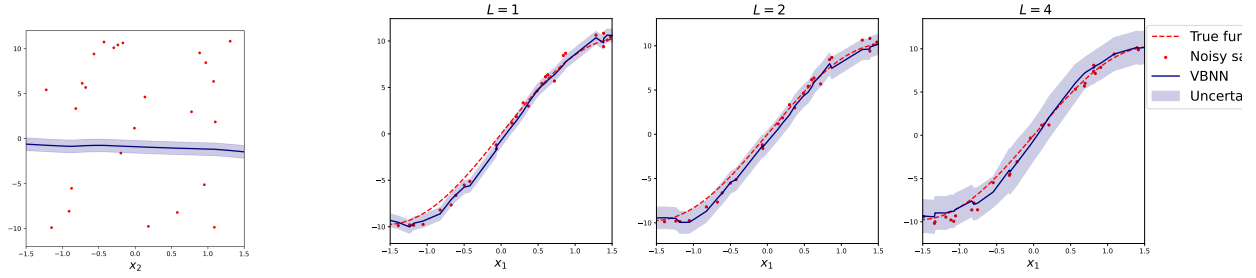


Figure 6: Simulated example. Empirical coverage (which is the fraction of observations contained within the CIs of level $1 - \alpha$) as a function of CI level for the simulated dataset for three different settings of the network’s depth. The dashed gray line depicts the ideal scenario with empirical coverage equal to CI level, while above and below the gray line indicate coverage greater or less than CI level, i.e. CIs are too wide or too small, respectively.

For each depth, Figure 7 illustrates the predictive means and uncertainties computed for the observations as well as DAGs of networks’ structures obtained after the post-process node selection algorithm described in Section 3.4, where the Bayesian false discovery rate is constrained by setting the error rate to $\alpha = 0.01$. The sparsity-promoting prior combined with the node selection algorithm can effectively prune the overparametrized neural networks; for example, the sparse one-layer neural network contains only 11 hidden nodes with 33 total edges/weights from the initial $D_H = 20$ with 60 total edges/weights. Moreover, the estimated regression function and credible intervals both from the variational predictive and the sparse variation predictive distribution, recover the true function well. In this way, VBNN provides an effective tool to reduce predictive computational complexity and storage as well as ease interpretation. Note that the predictions show no relation with the coordinate x_2 (Figure 7a), recovering the true function, but some of the connections from x_2 are still present in the sparse network (Figure 7c), due to identifiability issues, although with overall low weight.



(a) The predictive mean as a function of depth the second coordinate for $L = 1$. (b) The predictive mean and uncertainty quantification for the observations for different depths $L = 1, 2, 4$. (c) The architecture of the network for the bound on the FDR $\alpha = 0.01$ for depths $L = 1, 2, 4$ (left to right).

Figure 7: Simulated example. Predictive means and pointwise CIs computed for the observations as a function of the second coordinate (a) and first coordinate for different depths (b). The architecture of the network is visualized in (c) for the bound on the FDR $\alpha = 0.01$ for different settings of the network’s depth of $L = 1, 2, 4$ (left to right).

4.2 Diabetes Example

The `diabetes` data consists of $n = 442$ entries obtained for $p = 10$ input variables and a quantitative response measuring disease progression. The predictors are age, sex, body mass index, average blood pressure and six blood serum measurements and the goal is to determine which of these are relevant for forecasting diabetes progression. We fit a neural network with one hidden layer $L = 1$ and $D_H = 20$ and perform the node selection algorithm with the FDR bounded by $\alpha = 0.01$. Figure 8 illustrates the shrinkage and node selection algorithm and compares the coefficients of the Lasso linear model (Tibshirani, 1996) to the original and the sparsified weights of our model. Lasso regression produces sparse coefficients by minimising the residual sum of squares with an added penalty term; the penalty parameter crucially determines the level of sparsity and is tuned with cross-validation (LassoCV). Predictors with considerable effect obtained by both models coincide, whilst some of the variables the Lasso model excludes (e.g. age) are still present in the VBNN’s estimates. Compared with Lasso, VBNN has the advantage of learning potential nonlinear relationships between disease progression and the predictors, which is explored in Figure 9, illustrating the predictive means and uncertainty of the observations of VBNN for four of the predictors (with all other predictors are fixed to their mean). While the uncertainty is wide, the results suggest potential nonlinear relationships, e.g. with lamotrigine and age, the latter of which is not selected in Lasso. Moreover, Figure 9 highlights how predictions obtained from the sparse version of the variational predictive distribution almost overlap, thus providing a reasonable, cheaper approximation. However, we note that the predictive performance is similar to LassoCV, with the most competitive methods being VBNN, HMC and BBB (see Table 3 and supplementary Figure 12 in Appendix D.3).

Table 3: RMSE, NLL and empirical coverage for diabetes dataset.

	RMSE	NLL	Coverage
LassoCV	54.2 ± 6.5	$5.4 \pm .13$	$.96 \pm .03$
mfVI	57.2 ± 7.4	9.3 ± 1.7	$.47 \pm .1$
HMC	54.5 ± 7.8	$5.4 \pm .16$	$.96 \pm .04$
BBB	54.9 ± 7.3	$5.49 \pm .18$	$.94 \pm .04$
HSBNN	56.8 ± 7.4	6.8 ± 1.6	$.67 \pm .15$
GVBNB	55.65 ± 7.8	$5.5 \pm .14$	$.96 \pm .04$
VBNN	54.5 ± 7.2	$5.4 \pm .15$	$.96 \pm .04$

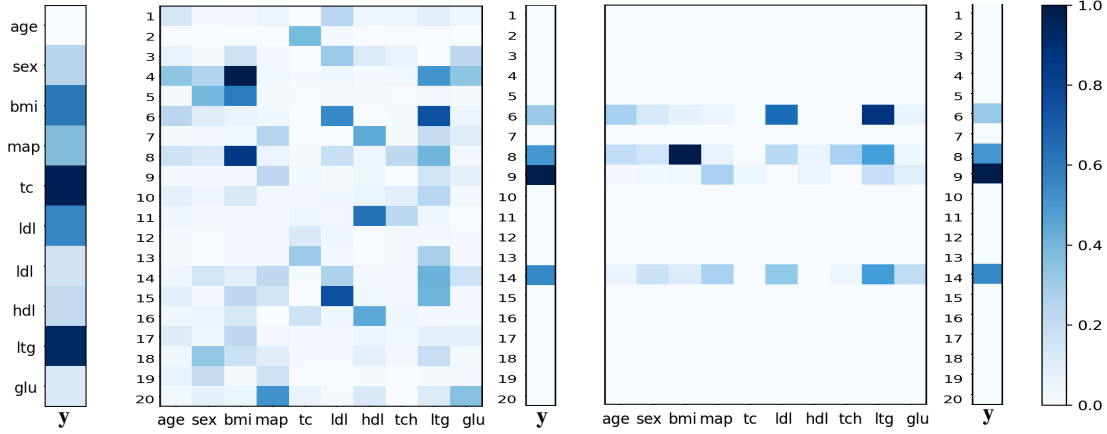


Figure 8: Diabetes example. Coefficients of LassoCV regression (on the left), posterior means of the weights of the neural network (in the middle) and posterior means of the sparse weights obtained for $\alpha = 0.01$ (on the right). For illustrative purposes, absolute values of the coefficients and weights are shown with max-min scaling.

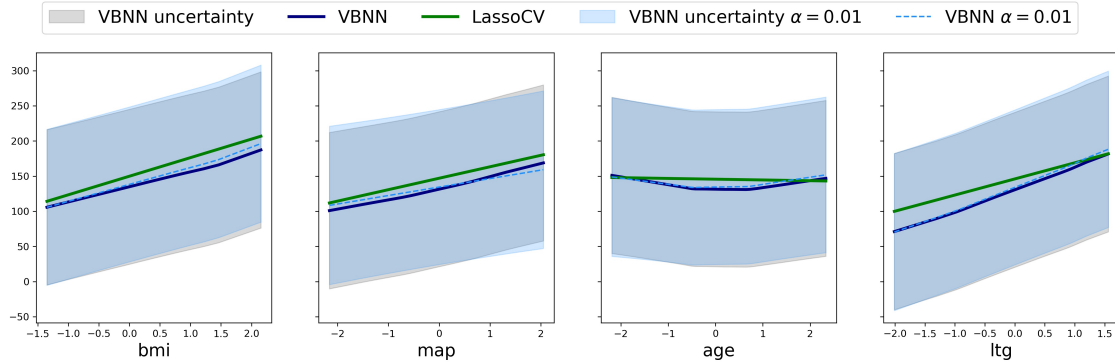


Figure 9: Diabetes example. Slices of the predictive mean and pointwise credible intervals for observations as a function of four predictors obtained by VBNN with and without node selection and by Lasso with cross-validation.

4.3 UCI Regression Datasets

Lastly, we consider publicly available datasets from the UCI Machine Learning Repository (M. et al., 2007): Boston housing (Harrison and Rubinfeld, 1978), Energy (Tsanas and Xifara, 2012), Yacht dynamics (J. et al., 2013), Concrete compressive strength (Yeh, 2007) and Concrete slump test (Yeh, 2009) (see Appendix D.4 for the description of the datasets). For all of the UCI regression tasks, we fit a neural network with one hidden layer and $D_H = 50$ hidden units. Figure 10 compares RMSE, NLL and empirical coverage of

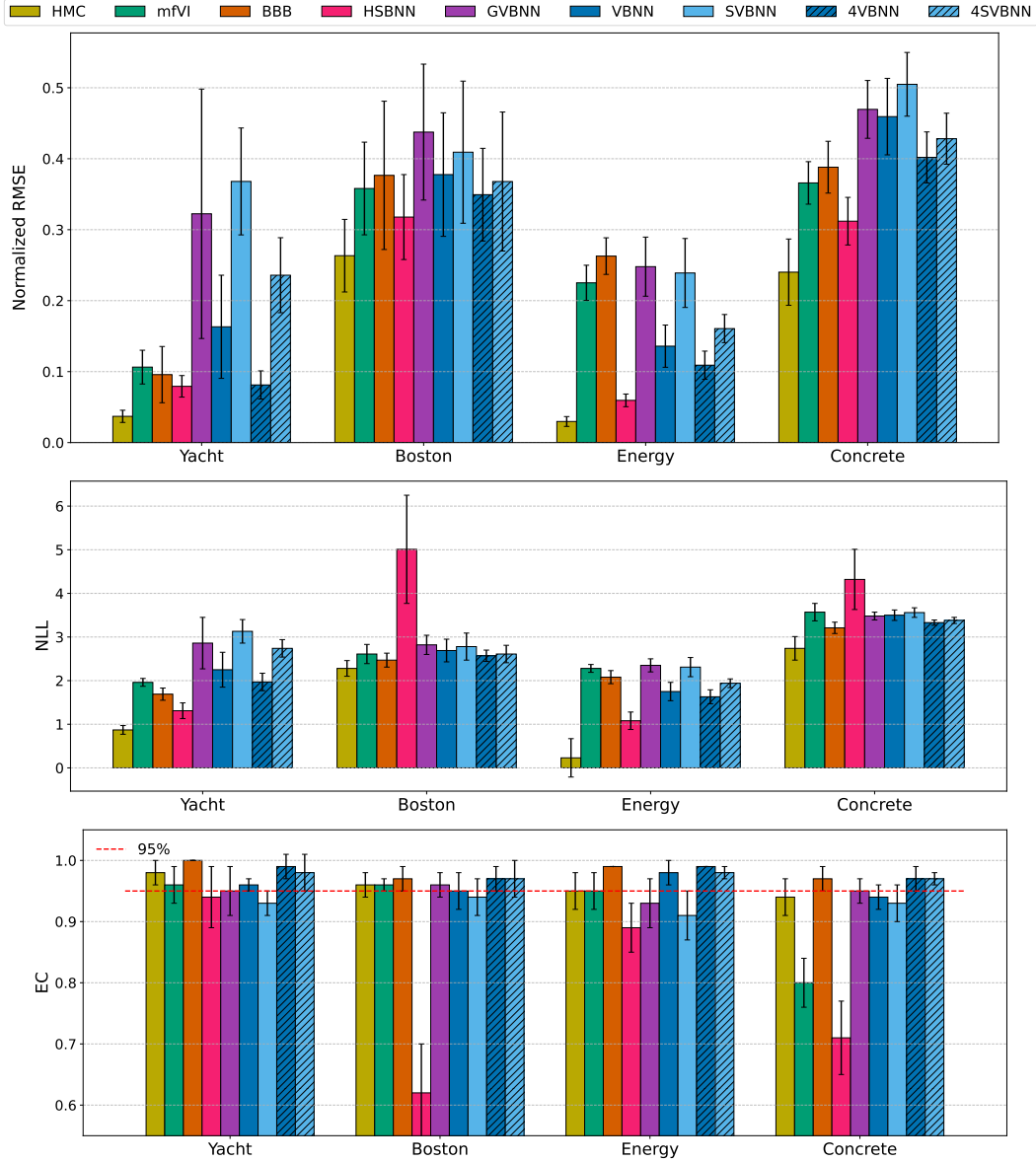


Figure 10: RMSE (normalized w.r.t. to the standard deviation of the target), NLL and empirical coverage for UCI datasets. When illustrating the coverage, the dashed red line depicts the ideal scenario with empirical coverage equal to 95% CI level.

the observations across the methods (see also Table 4 in Appendix D.5), where we additionally consider ensembles of four variational approximations with VBNN and SVBNN (denoted as 4VBNN and 4SVBNN, respectively). Overall, HMC outperforms all the considered methods, but at a much higher cost. VBNN provides an improvement compared to GVBNN, further motivating the choice of sparsity-inducing priors, and while SVBNN offers considerable computational savings, the quality of the approximation deteriorates compared to VBNN. Overall, VBNN has consistently well-calibrated uncertainty quantification and empirical coverage for the observations compared with other variational approaches, and ensembles of VBNNs are competitive with other approaches in terms of the RMSE and NLL. Further, we consider slump dataset and implement ensembles of 4 parallel runs of all of the considered methods (4mfVI, 4BBB, 4HSBNN, 4GVBNN, 4VBNN, 4SVBNN) and compare the results to approximations obtained in a single run (mfVI, BBB, HSBNN, GVBNN, VBNN, SVBNN). We do not consider HMC in this experiment due to its computational costs.

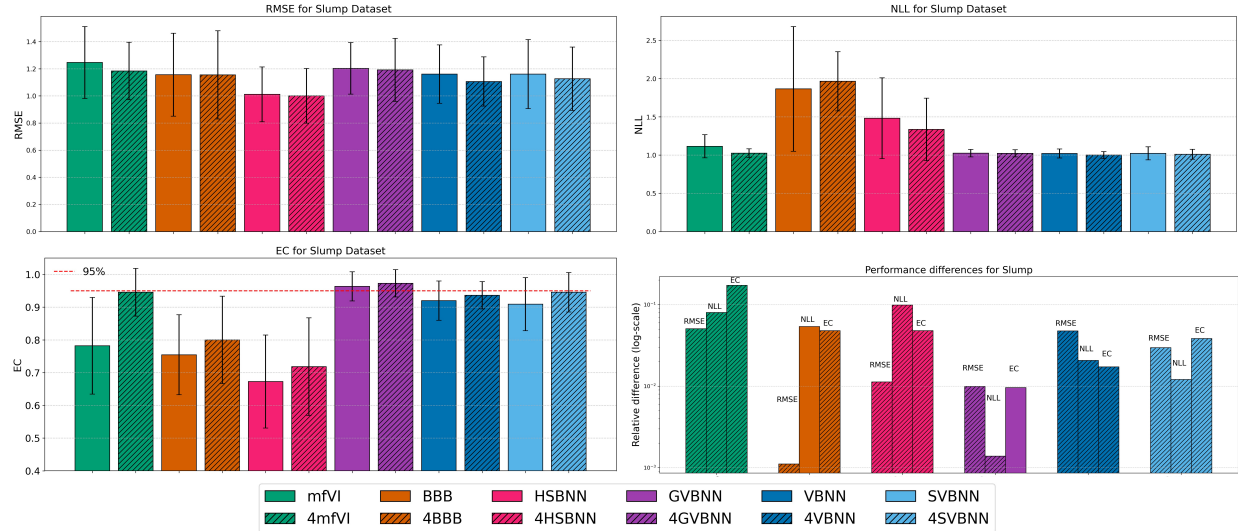


Figure 11: Slump dataset. Performance in terms of the RMSE, NLL and EC for single models (plain colored) and ensembles (color with hatches) obtained from four parallel runs. RMSE and NLL are scaled with respect to the best model (top row). The relative performance (bottom right) is illustrated on the log-scale, and color reflects if ensembles improved the metric (i.e. bar with hatches illustrates the scale of improvements obtained with ensembles, conversely, bar without the hatches illustrates the scale at which single run outperformed ensembles).

Figure 11 compares RMSE, NLL, EC of the 12 methods and additionally illustrates relative differences among approaches, where for RMSE and NLL, we consider absolute relative differences between ensembles and single runs, and for empirical coverage of the observations, we illustrate the absolute deviation from the 95% CI. Overall, ensembles improve uncertainty quantification, and in most cases also RMSE and NLL (the only exception being NLL for BBB). While BBB and HSBNN have the lowest RMSE (although with high variability), the NLL and empirical coverage suggest overconfidence, even with ensembles. In contrast, VBNN has an improved balance between accuracy and uncertainty quantification, which is further enhanced by ensembles.

5 Discussion

In this paper, we presented a variational bow tie neural network (VBNN) that is amendable to Polya-gamma data augmentation so that the variational inference can be performed via the CAVI algorithm. While the idea of the stochastic relaxation described in Section 2.1 was introduced in (Smith et al., 2021), the novelty of our model is in the employment of the variational inference techniques as well as sparsity-inducing priors. Namely, we implement continuous global-local shrinkage priors and propose a post-process technique for node selection. Additionally, we consider an improvement of the classical CAVI algorithm by adding EM steps for critical hyperparameters. In this way, we enrich the class of models which are handled within the structured mean-field paradigm. We provide all the necessary computations, techniques, and illustrative experiments demonstrating the utility of the model. Addressing the scalability with respect to the number of data points, we extend the CAVI algorithm to SVI (Hoffman et al., 2013) which benefits from exploiting natural gradients and subsampling. In the future, we could improve the algorithm by employing an adaptive learning rate which is based on realisations of a noisy estimate of the natural gradient of ELBO with respect to global variational parameters and moving averages (Ranganath et al., 2013; Schaul et al., 2013). Alternatively, instead of changing the learning rate, one could adapt the mini-batch size based on the estimated gradient noise covariance and the magnitude of the gradient (Balles et al., 2017). To address scalability with respect to the network’s width, future work will explore incorporating node selection within the CAVI algorithm when training.

The variational bow tie neural network is also amenable to other prior choices. For example, horseshoe priors can be implemented through the introduction of auxiliary variables to replace each half-Cauchy random variable with the hierarchical formulation based on Inverse-Gamma variables (Wand et al., 2011; Louizos et al., 2017; Ghosh et al., 2018). Additionally, the regularized version of horseshoe priors ("ponyshoe") could be considered, which is known to perform better than the classical horseshoe, especially when the larger coefficients are weakly identified by the data (Piironen and Vehtari, 2017b,a; Ghosh et al., 2019). Finally, an extension to other output types, such as classification tasks, can be developed through additional Polya-gamma augmentation techniques (Durante and Rigon, 2019).

References

- Devanshu Agrawal, Theodore Papamarkou, and Jacob Hinkle. 2020. Wide neural networks with bottlenecks are deep Gaussian processes. *Journal of Machine Learning Research* 21, 175 (2020).
- Pierre Alquier and James Ridgway. 2020. Concentration of tempered posteriors and of their variational approximations. *The Annals of Statistics* 48, 3 (2020), 1475–1497.
- Julyan Arbel, Chislaine Gayraud, and Rousseau Judith. 2013. Bayesian Optimal Adaptive Estimation Using a Sieve Prior. *Scandinavian Journal of Statistics* 40, 3 (2013), 549–570.
- Julyan Arbel, Konstantinos Pitas, Mariia Vladimirova, and Vincent Fortuin. 2023. A primer on Bayesian neural networks: review and debates. arXiv:2309.16314
- Arsenii Ashukha, Alexander Lyzhov, Dmitry Molchanov, and Dmitry Vetrov. 2020. Pitfalls of In-Domain Uncertainty Estimation and Ensembling in Deep Learning. In *International Conference on Learning Representations*.
- Jincheng Bai, Qifan Song, and Guang Cheng. 2020a. Adaptive Variational Bayesian Inference for Sparse Deep Neural Network. <https://doi.org/10.48550/arXiv.1910.04355> arXiv:1910.04355
- Jincheng Bai, Qifan Song, and Guang Cheng. 2020b. Efficient variational inference for sparse deep learning with theoretical guarantee. *Advances in Neural Information Processing Systems* 33 (2020), 466–476.
- Lukas Balles, Javier Romero, and Philipp Hennig. 2017. Coupling Adaptive Batch Sizes with Learning Rates. In *Conference on Uncertainty in Artificial Intelligence*. Curran Associates, Inc., 675–684.
- David Barber, A Taylan Cemgil, and Silvia Chiappa. 2011. *Bayesian time series models*. Cambridge University Press.
- Anindya Bhadra, Jyotishka Datta, Nicholas G Polson, and Brandon Willard. 2019. Lasso meets horseshoe. *Statist. Sci.* 34, 3 (2019), 405–427.
- Anirban Bhattacharya, Debdeep Pati, and Yun Yang. 2023. On the Convergence of Coordinate Ascent Variational Inference. arXiv:2306.01122
- Christopher M Bishop. 2016. *Pattern Recognition and Machine Learning*. Springer New York.
- David M Blei, Alp Kucukelbir, and Jon D McAuliffe. 2017. Variational inference: A review for statisticians. *J. Amer. Statist. Assoc.* 112, 518 (2017), 859–877.
- Charles Blundell, Julien Cornebise, Koray Kavukcuoglu, and Daan Wierstra. 2015. Weight uncertainty in neural network. In *International Conference on Machine Learning*. PMLR, 1613–1622.
- Ginevra Carbone, Luca Bortolussi, and Guido Sanguinetti. 2022. Resilience of Bayesian Layer-Wise Explanations under Adversarial Attacks. In *2022 International Joint Conference on Neural Networks*. 1–8. <https://doi.org/10.1109/IJCNN55064.2022.9892788>
- Ginevra Carbone, Matthew Wicker, Luca Laurenti, Andrea Patane, Luca Bortolussi, and Guido Sanguinetti. 2020. Robustness of Bayesian neural networks to gradient-based attacks. In *Advances in Neural Information Processing Systems*, Vol. 33. 15602–15613.

- François Caron and Arnaud Doucet. 2008. Sparse Bayesian nonparametric regression. In *Proceedings of the 25th International Conference on Machine Learning (Helsinki, Finland) (ICML '08)*. Association for Computing Machinery, 88–95. <https://doi.org/10.1145/1390156.1390168>
- Carlos M. Carvalho, Nicholas G. Polson, and James G. Scott. 2009. Handling Sparsity via the Horseshoe. In *Proceedings of the Twelfth International Conference on Artificial Intelligence and Statistics (Proceedings of Machine Learning Research, Vol. 5)*, David van Dyk and Max Welling (Eds.). PMLR, Hilton Clearwater Beach Resort, Clearwater Beach, Florida USA, 73–80.
- Ismaël Castillo and Paul Egels. 2024. Posterior and variational inference for deep neural networks with heavy-tailed weights. arXiv:2406.03369
- Ismaël Castillo, Johannes Schmidt-Hieber, and Aad Van der Vaart. 2015. Bayesian linear regression with sparse priors. *The Annals of Statistics* (2015), 1986–2018.
- Neil K Chada, Ajay Jasra, Kody JH Law, and Sumeetpal S Singh. 2022. Multilevel Bayesian Deep Neural Networks. *Computing Research Repository* (2022).
- Beau Coker, Wessel P Bruinsma, David R Burt, Weiwei Pan, and Finale Doshi-Velez. 2022. Wide mean-field bayesian neural networks ignore the data. In *International Conference on Artificial Intelligence and Statistics*. PMLR, 5276–5333.
- Amit Daniely, Roy Frostig, and Yoram Singer. 2016. Toward Deeper Understanding of Neural Networks: The Power of Initialization and a Dual View on Expressivity. In *Advances in Neural Information Processing Systems*, Vol. 29. Curran Associates, Inc.
- Luc Devroye. 2006. Nonuniform random variate generation. *Handbooks in operations research and management science* 13 (2006), 83–121.
- Alexey Dosovitskiy, Lucas Beyer, Alexander Kolesnikov, Dirk Weissenborn, Xiaohua Zhai, Thomas Unterthiner, Mostafa Dehghani, Matthias Minderer, Georg Heigold, Sylvain Gelly, et al. 2020. An Image is Worth 16x16 Words: Transformers for Image Recognition at Scale. In *International Conference on Learning Representations*.
- Francesco D' Angelo and Vincent Fortuin. 2021. Repulsive Deep Ensembles are Bayesian. In *Advances in Neural Information Processing Systems*, M. Ranzato, A. Beygelzimer, Y. Dauphin, P.S. Liang, and J. Wortman Vaughan (Eds.), Vol. 34. Curran Associates, Inc., 3451–3465.
- Daniele Durante and Tommaso Rigon. 2019. Conditionally conjugate mean-field variational Bayes for logistic models. *Statist. Sci.* 34, 3 (2019), 472 – 485. <https://doi.org/10.1214/19-STS712>
- Bradley Efron, Trevor Hastie, Iain Johnstone, and Robert Tibshirani. 2004. Least Angle Regression. *Annals of Statistics* (2004), 407–451.
- Vincent Fortuin. 2022. Priors in bayesian deep learning: A review. *International Statistical Review* 90, 3 (2022), 563–591.
- Yarin Gal. 2016. *Uncertainty in Deep Learning*. Ph.D. Dissertation. University of Cambridge.
- Edward I George and Robert E McCulloch. 1993. Variable selection via Gibbs sampling. *J. Amer. Statist. Assoc.* 88, 423 (1993), 881–889.
- Soumya Ghosh, Jiayu Yao, and Finale Doshi-Velez. 2018. Structured variational learning of Bayesian neural networks with horseshoe priors. In *International Conference on Machine Learning*. PMLR, 1744–1753.
- Soumya Ghosh, Jiayu Yao, and Finale Doshi-Velez. 2019. Model Selection in Bayesian Neural Networks via Horseshoe Priors. *Journal of Machine Learning Research* 20, 182 (2019).
- Jim E Griffin. 2024. Expressing and visualizing model uncertainty in Bayesian variable selection using Cartesian credible sets. <https://doi.org/10.48550/arXiv.2402.12323> arXiv:2402.12323

- Jim E Griffin and Philip J Brown. 2010. Inference with normal-gamma prior distributions in regression problems. *Bayesian Analysis* 5, 1 (2010), 171–188.
- Jim E Griffin and Philip J Brown. 2021. Bayesian global-local shrinkage methods for regularisation in the high dimension linear model. *Chemometrics and Intelligent Laboratory Systems* 210 (2021).
- Nate Gruver, Samuel Stanton, Nathan Frey, Tim GJ Rudner, Isidro Hotzel, Julien Lafrance-Vanasse, Arvind Rajpal, Kyunghyun Cho, and Andrew Gordon Wilson. 2023. Protein design with guided discrete diffusion. In *Proceedings of the 37th International Conference on Neural Information Processing Systems*. 12489–12517.
- Chuan Guo, Geoff Pleiss, Yu Sun, and Kilian Q. Weinberger. 2017. On Calibration of Modern Neural Networks. In *Proceedings of the 34th International Conference on Machine Learning (Proceedings of Machine Learning Research, Vol. 70)*, Doina Precup and Yee Whye Teh (Eds.). PMLR, 1321–1330.
- P Richard Hahn and Carlson M Carvalho. 2015. Decoupling Shrinkage and Selection in Bayesian Linear Models: A Posterior Summary Perspective. , 435–448 pages.
- L.K. Hansen and P. Salamon. 1990. Neural network ensembles. *IEEE Transactions on Pattern Analysis and Machine Intelligence* 12 (1990), 993–1001. <https://doi.org/10.1109/34.58871>
- David Harrison and Daniel L Rubinfeld. 1978. Hedonic housing prices and the demand for clean air. *Journal of Environmental Economics and Management* 1 (1978), 81–102. [https://doi.org/10.1016/0095-0696\(78\)90006-2](https://doi.org/10.1016/0095-0696(78)90006-2)
- Kaiming He, Xiangyu Zhang, Shaoqing Ren, and Jian Sun. 2015. Delving Deep into Rectifiers: Surpassing Human-Level Performance on ImageNet Classification. In *Proceedings of the 2015 IEEE International Conference on Computer Vision (ICCV)*. 1026–1034.
- Matthias Hein, Maksym Andriushchenko, and Julian Bitterwolf. 2019. Why ReLU Networks Yield High-Confidence Predictions Far Away From the Training Data and How to Mitigate the Problem. In *2019 IEEE/CVF Conference on Computer Vision and Pattern Recognition (CVPR)*. IEEE, 41–50.
- Geoffrey E. Hinton and Drew van Camp. 1993. Keeping the neural networks simple by minimizing the description length of the weights. In *Proceedings of the Sixth Annual Conference on Computational Learning Theory (Santa Cruz, California, USA) (COLT '93)*. Association for Computing Machinery, New York, NY, USA, 5–13. <https://doi.org/10.1145/168304.168306>
- Matthew D Hoffman, David M Blei, Chong Wang, and John Paisley. 2013. Stochastic variational inference. *Journal of Machine Learning Research* (2013).
- Matthew D Hoffman, Andrew Gelman, et al. 2014. The No-U-Turn sampler: adaptively setting path lengths in Hamiltonian Monte Carlo. *Journal of Machine Learning Research*. 15, 1 (2014), 1593–1623.
- Jiri Hron, Alex Matthews, and Zoubin Ghahramani. 2018. Variational Bayesian dropout: pitfalls and fixes. In *Proceedings of the 35th International Conference on Machine Learning (Proceedings of Machine Learning Research, Vol. 80)*. PMLR, 2019–2028.
- Gerritsma J., Onnink R., and Versluis A. 2013. Yacht Hydrodynamics. <https://archive.ics.uci.edu/dataset/243/yacht+hydrodynamics>
- Sanket Jantre, Shrijita Bhattacharya, and Tapabrata Maiti. 2024. Spike-and-slab shrinkage priors for structurally sparse Bayesian neural networks. *IEEE Transactions on Neural Networks and Learning Systems* (2024).
- Antoran Javier. 2019. Bayesian Neural Networks. <https://github.com/JavierAntoran/Bayesian-Neural-Networks>

- Michael I. Jordan, Zoubin Ghahramani, Tommi S. Jaakkola, and Lawrence K. Saul. 1999. An Introduction to Variational Methods for Graphical Models. *Machine Learning* 37, 2 (1999), 183–233. <https://doi.org/10.1023/A:1007665907178>
- Laurent Valentin Jospin, Hamid Laga, Farid Boussaid, Wray Buntine, and Mohammed Bannamoun. 2022. Hands-on Bayesian neural networks — A tutorial for deep learning users. *IEEE Computational Intelligence Magazine* 17, 2 (2022), 29–48.
- John Jumper, Richard Evans, Alexander Pritzel, Tim Green, Michael Figurnov, Olaf Ronneberger, Kathryn Tunyasuvunakool, Russ Bates, Augustin Židek, Anna Potapenko, et al. 2021. Highly accurate protein structure prediction with AlphaFold. *Nature* 596, 7873 (2021), 583–589.
- Durk P Kingma, Tim Salimans, and Max Welling. 2015. Variational Dropout and the Local Reparameterization Trick. In *Advances in Neural Information Processing Systems*, C. Cortes, N. Lawrence, D. Lee, M. Sugiyama, and R. Garnett (Eds.), Vol. 28. Curran Associates, Inc.
- Leo Klarner, Tim G. J. Rudner, Michael Reutlinger, Torsten Schindler, Garrett M Morris, Charlotte Deane, and Yee Whye Teh. 2023. Drug Discovery under Covariate Shift with Domain-Informed Prior Distributions over Functions. In *Proceedings of the 40th International Conference on Machine Learning (Proceedings of Machine Learning Research, Vol. 202)*, Andreas Krause, Emma Brunskill, Kyunghyun Cho, Barbara Engelhardt, Sivan Sabato, and Jonathan Scarlett (Eds.). PMLR, 17176–17197.
- Alp Kucukelbir, Dustin Tran, Rajesh Ranganath, Andrew Gelman, and David M Blei. 2017. Automatic differentiation variational inference. *Journal of Machine Learning Research* 18, 14 (2017), 1–45.
- Balaji Lakshminarayanan, Alexander Pritzel, and Charles Blundell. 2017. Simple and Scalable Predictive Uncertainty Estimation using Deep Ensembles. In *Advances in Neural Information Processing Systems*, I. Guyon, U. Von Luxburg, S. Bengio, H. Wallach, R. Fergus, S. Vishwanathan, and R. Garnett (Eds.), Vol. 30. Curran Associates, Inc.
- Jaehoon Lee, Yasaman Bahri, Roman Novak, Samuel S Schoenholz, Jeffrey Pennington, and Jascha Sohl-Dickstein. 2018. Deep Neural Networks as Gaussian Processes. In *International Conference on Learning Representations*.
- Kyeongwon Lee and Jaeyong Lee. 2022. Asymptotic properties for bayesian neural network in besov space. *Advances in Neural Information Processing Systems* 35 (2022), 5641–5653.
- E. Levin, N. Tishby, and S.A. Solla. 1990. A statistical approach to learning and generalization in layered neural networks. *Proc. IEEE* 78 (1990), 1568–1574. <https://doi.org/10.1109/5.58339>
- Hanning Li and Debdeep Pati. 2017. Variable selection using shrinkage priors. *Computational Statistics & Data Analysis* 107, C (2017), 107–119.
- Junbo Li, Zichen Miao, Qiang Qiu, and Ruqi Zhang. 2024. Training Bayesian Neural Networks with Sparse Subspace Variational Inference. In *The Twelfth International Conference on Learning Representations*.
- Qing Li and Nan Lin. 2010. The Bayesian elastic net. *Bayesian Analysis* 5, 1 (2010), 151 – 170. <https://doi.org/10.1214/10-BA506>
- Zachary C Lipton. 2018. The mythos of model interpretability: In machine learning, the concept of interpretability is both important and slippery. *Queue* 16, 3 (2018), 31–57.
- Yuhang Liu, Wenyong Dong, Lei Zhang, Dong Gong, and Qinfeng Shi. 2019. Variational bayesian dropout with a hierarchical prior. In *Proceedings of the IEEE/CVF Conference on Computer Vision and Pattern Recognition*. 7124–7133.
- Christos Louizos, Karen Ullrich, and Max Welling. 2017. Bayesian compression for deep learning. In *Proceedings of the 31st International Conference on Neural Information Processing Systems (NIPS’17)*. Curran Associates Inc., Red Hook, NY, USA, 3290–3300.

- Kelly M., Longjohn R., and Nottingham K. 2007. The UCI Machine Learning Repository. <https://archive.ics.uci.edu>
- David JC MacKay. 1995. Probable networks and plausible predictions—a review of practical Bayesian methods for supervised neural networks. *Network: Computation in Neural Systems* 6, 3 (1995), 469.
- Alexander G de G Matthews, Jiri Hron, Mark Rowland, Richard E Turner, and Zoubin Ghahramani. 2018. Gaussian Process Behaviour in Wide Deep Neural Networks. In *International Conference on Learning Representations*.
- Rowan McAllister, Yarin Gal, Alex Kendall, Mark Van Der Wilk, Amar Shah, Roberto Cipolla, and Adrian Weller. 2017. Concrete problems for autonomous vehicle safety: advantages of Bayesian deep learning. In *Proceedings of the 26th International Joint Conference on Artificial Intelligence*. 4745–4753.
- Tomas Mikolov, Ilya Sutskever, Kai Chen, Greg S Corrado, and Jeff Dean. 2013. Distributed Representations of Words and Phrases and their Compositionality. In *Advances in Neural Information Processing Systems*, C.J. Burges, L. Bottou, M. Welling, Z. Ghahramani, and K.Q. Weinberger (Eds.), Vol. 26. Curran Associates, Inc.
- Toby J Mitchell and John J Beauchamp. 1988. Bayesian variable selection in linear regression. *J. Amer. Statist. Assoc.* 83, 404 (1988), 1023–1032.
- Eric Nalisnick, José Miguel Hernández-Lobato, and Padhraic Smyth. 2019. Dropout as a structured shrinkage prior. In *International Conference on Machine Learning*. PMLR, 4712–4722.
- Radford M Neal. 2012. *Bayesian learning for neural networks*. Vol. 118. Springer Science & Business Media.
- Sarah E. Neville, John T. Ormerod, and Matthew P Wand. 2014. Mean field variational Bayes for continuous sparse signal shrinkage: Pitfalls and remedies. *Electronic Journal of Statistics* 8, 1 (2014). <https://doi.org/10.1214/14-ejs910>
- Anh Nguyen, Jason Yosinski, and Jeff Clune. 2015. Deep neural networks are easily fooled: High confidence predictions for unrecognizable images. In *2015 IEEE Conference on Computer Vision and Pattern Recognition (CVPR)*. IEEE Computer Society, 427–436.
- Ilsang Ohn and Lizhen Lin. 2024. Adaptive variational Bayes: Optimality, computation and applications. *The Annals of Statistics* 52, 1 (2024), 335–363.
- John T. Ormerod and Matthew P Wand. 2010. Explaining variational approximations. *The American Statistician* 64, 2 (2010).
- Nathan Osborne, Christine B Peterson, and Marina Vannucci. 2022. Latent network estimation and variable selection for compositional data via variational EM. *Journal of Computational and Graphical Statistics* 31, 1 (2022), 163–175.
- Theodore Papamarkou, Jacob Hinkle, M. Todd Young, and David Womble. 2022. Challenges in Markov chain Monte Carlo for Bayesian neural networks. *Statist. Sci.* 37, 3 (2022), 425 – 442. <https://doi.org/10.1214/21-STS840>
- Trevor Park and George Casella. 2008. The Bayesian Lasso. *J. Amer. Statist. Assoc.* 103, 482 (2008), 681–686.
- Tim Pearce, Felix Leibfried, and Alexandra Brintrup. 2020. Uncertainty in neural networks: Approximately bayesian ensembling. In *International Conference on Artificial Intelligence and Statistics*. PMLR, 234–244.
- Stefano Peluchetti, Stefano Favaro, and Sandra Fortini. 2020. Stable behaviour of infinitely wide deep neural networks. In *Proceedings of the Twenty Third International Conference on Artificial Intelligence and Statistics*, Vol. 108. 1137–1146.

- Du Phan, Neeraj Pradhan, and Martin Jankowiak. 2019. Composable Effects for Flexible and Accelerated Probabilistic Programming in NumPyro. [arXiv:1912.11554](https://arxiv.org/abs/1912.11554)
- Juho Piironen, Markus Paasiniemi, and Aki Vehtari. 2020. Projective inference in high-dimensional problems: Prediction and feature selection. *Electronic Journal of Statistics* 14, 1 (2020), 2155 – 2197. <https://doi.org/10.1214/20-EJS1711>
- Juho Piironen and Aki Vehtari. 2017a. On the Hyperprior Choice for the Global Shrinkage Parameter in the Horseshoe Prior. In *Proceedings of the 20th International Conference on Artificial Intelligence and Statistics (Proceedings of Machine Learning Research, Vol. 54)*, Aarti Singh and Jerry Zhu (Eds.). PMLR, 905–913.
- Juho Piironen and Aki Vehtari. 2017b. Sparsity information and regularization in the horseshoe and other shrinkage priors. *Electronic Journal of Statistics* 11, 2 (2017), 5018.
- Nicholas G Polson and Veronika Ročková. 2018. Posterior concentration for sparse deep learning. *Advances in Neural Information Processing Systems* 31 (2018).
- Nicholas G Polson and James G Scott. 2012. Shrink globally, act locally: Sparse Bayesian regularization and prediction. *Bayesian statistics* 9, 501-538 (2012), 105.
- Nicholas G Polson, James G Scott, and Jesse Windle. 2013. Bayesian inference for logistic models using Pólya–Gamma latent variables. *J. Amer. Statist. Assoc.* 108, 504 (2013), 1339–1349.
- Rajesh Ranganath, Chong Wang, Blei David, and Eric Xing. 2013. An Adaptive Learning Rate for Stochastic Variational Inference. In *Proceedings of the 30th International Conference on Machine Learning (Proceedings of Machine Learning Research)*, Sanjoy Dasgupta and David McAllester (Eds.). PMLR, Atlanta, Georgia, USA, 298–306.
- Kolyan Ray and Botond Szabó. 2022. Variational Bayes for High-Dimensional Linear Regression With Sparse Priors. *J. Amer. Statist. Assoc.* 117, 539 (2022), 1270–1281. <https://doi.org/10.1080/01621459.2020.1847121>
- Herbert Robbins and Sutton Monro. 1951. A Stochastic Approximation Method. *The Annals of Mathematical Statistics* 22, 3 (1951), 400 – 407. <https://doi.org/10.1214/aoms/1177729586>
- Christian Schäfer and Nicolas Chopin. 2013. Sequential Monte Carlo on large binary sampling spaces. *Statistics and Computing* 23 (2013), 163–184.
- Tom Schaul, Sixin Zhang, and Yann LeCun. 2013. No more pesky learning rates. In *International conference on machine learning*. PMLR, 343–351.
- Torben Sell and Sumeetpal Sidhu Singh. 2023. Trace-class Gaussian priors for Bayesian learning of neural networks with MCMC. *Journal of the Royal Statistical Society Series B: Statistical Methodology* 85, 1 (2023), 46–66.
- Jimmy TH Smith, Dieterich Lawson, and Scott W Linderman. 2021. Bayesian Inference in Augmented Bow Tie Networks. *Proceedings of Bayesian Deep Learning Workshop* (2021).
- Qifan Song. 2020. Bayesian shrinkage towards sharp minimaxity. *Electronic Journal of Statistics* 14 (2020), 2714–2741.
- Qifan Song and Faming Liang. 2023. Nearly optimal Bayesian shrinkage for high-dimensional regression. *Science China Mathematics* 66, 2 (2023), 409–442.
- Yan Sun, Qifan Song, and Faming Liang. 2022. Learning sparse deep neural networks with a spike-and-slab prior. *Statistics & Probability Letters* 180 (2022).
- Christian Szegedy, Wojciech Zaremba, Ilya Sutskever, Joan Bruna, Dumitru Erhan, Ian Goodfellow, and Rob Fergus. 2014. Intriguing properties of neural networks. In *2nd International Conference on Learning Representations*. ICLR.

- Robert Tibshirani. 1996. Regression Shrinkage and Selection via the Lasso. *Journal of the Royal Statistical Society. Series B (Methodological)* 58, 1 (1996), 267–288.
- Michael E. Tipping. 2001. Sparse bayesian learning and the relevance vector machine. *Journal of Machine Learning Research* 1 (Jan. 2001), 211–244. <https://doi.org/10.1162/15324430152748236>
- Hugo Touvron, Thibaut Lavril, Gautier Izacard, Xavier Martinet, Marie-Anne Lachaux, Timothée Lacroix, Baptiste Rozière, Naman Goyal, Eric Hambro, Faisal Azhar, Aurelien Rodriguez, Armand Joulin, Edouard Grave, and Guillaume Lample. 2023. LLaMA: Open and Efficient Foundation Language Models. arXiv:2302.13971
- Athanasios Tsanas and Angeliki Xifara. 2012. Energy Efficiency. <https://archive.ics.uci.edu/dataset/242/energy+efficiency>
- Mariia Vladimirova, Julyan Arbel, and Stéphane Girard. 2021. Dependence between Bayesian neural network units. In *BDL 2021-Workshop. Bayesian Deep Learning NeurIPS*. 1–9.
- Matthew P Wand, John T Ormerod, Simone A Padoan, and Rudolf Frühwirth. 2011. Mean Field Variational Bayes for Elaborate Distributions. *Bayesian Analysis* 6, 4 (2011), 1–48.
- Yixin Wang and David M Blei. 2019. Frequentist consistency of variational Bayes. *J. Amer. Statist. Assoc.* 114, 527 (2019), 1147–1161.
- Florian Wenzel, Kevin Roth, Bastiaan Veeling, Jakub Swiatkowski, Linh Tran, Stephan Mandt, Jasper Snoek, Tim Salimans, Rodolphe Jenatton, and Sebastian Nowozin. 2020a. How Good is the Bayes Posterior in Deep Neural Networks Really?. In *International Conference on Machine Learning*. PMLR, 10248–10259.
- Florian Wenzel, Jasper Snoek, Dustin Tran, and Rodolphe Jenatton. 2020b. Hyperparameter ensembles for robustness and uncertainty quantification. *Advances in Neural Information Processing Systems* 33 (2020), 6514–6527.
- Andrew G Wilson and Pavel Izmailov. 2020. Bayesian deep learning and a probabilistic perspective of generalization. *Advances in Neural Information Processing Systems* 33 (2020), 4697–4708.
- Luhuan Wu and Sinead A Williamson. 2024. Posterior uncertainty quantification in neural networks using data augmentation. In *International Conference on Artificial Intelligence and Statistics*. PMLR, 3376–3384.
- Qiang Yang, Yang Liu, Tianjian Chen, and Yongxin Tong. 2019. Federated Machine Learning: Concept and Applications. *ACM Trans. Intell. Syst. Technol.* 10, 2 (jan 2019).
- Yuchen Yang, Bo Hui, Haolin Yuan, Neil Gong, and Yinzhi Cao. 2024. SneakyPrompt: Jailbreaking Text-to-image Generative Models. In *2024 IEEE Symposium on Security and Privacy (SP)*. IEEE Computer Society, 123–123.
- Yun Yang, Debdeep Pati, and Anirban Bhattacharya. 2020. α -variational inference with statistical guarantees. *The Annals of Statistics* 48, 2 (2020), 886–905.
- Yuling Yao, Aki Vehtari, and Andrew Gelman. 2022. Stacking for non-mixing Bayesian computations: The curse and blessing of multimodal posteriors. *Journal of Machine Learning Research* 23, 1 (2022), 3426–3471.
- Yuling Yao, Aki Vehtari, Daniel Simpson, and Andrew Gelman. 2018. Yes, but Did It Work?: Evaluating Variational Inference. In *Proceedings of the 35th International Conference on Machine Learning (Proceedings of Machine Learning Research, Vol. 80)*, Jennifer Dy and Andreas Krause (Eds.). PMLR, 5581–5590.
- I-Cheng Yeh. 2007. Concrete Compressive Strength. <https://archive.ics.uci.edu/dataset/165/concrete+compressive+strength>

- I-Cheng Yeh. 2009. Concrete Slump Test. <https://archive.ics.uci.edu/dataset/182/concrete+slump+test>
- Hang Yu, Laurence T. Yang, Qingchen Zhang, David Armstrong, and M. Jamal Deen. 2021. Convolutional neural networks for medical image analysis: State-of-the-art, comparisons, improvement and perspectives. *Neurocomputing* 444 (2021), 92–110.
- Cheng Zhang, Judith B  tepage, Hedvig Kjellstr  m, and Stephan Mandt. 2018. Advances in variational inference. *IEEE Transactions on Pattern Analysis and Machine Intelligence* 41, 8 (2018), 2008–2026.
- Fengshuo Zhang and Chao Gao. 2020. Convergence rates of variational posterior distributions. *The Annals of Statistics* 48, 4 (2020), 2180–2207.
- Tianren Zhang, Chujie Zhao, Guanyu Chen, Yizhou Jiang, and Feng Chen. 2024. Feature Contamination: Neural Networks Learn Uncorrelated Features and Fail to Generalize. In *Proceedings of The 41st International Conference on Machine Learning*.
- Yan Dora Zhang, Weichang Yu, and Howard D Bondell. 2021. Variable Selection with Shrinkage Priors via Sparse Posterior Summaries. In *Handbook of Bayesian Variable Selection*. Chapman and Hall/CRC, 179–198.
- Yongshuo Zong, Tingyang Yu, Ruchika Chavhan, Bingchen Zhao, and Timothy Hospedales. 2024. Fool Your Vision and Language Model with Embarrassingly Simple Permutations. In *Proceedings of the 41st International Conference on Machine Learning (Proceedings of Machine Learning Research, Vol. 235)*. PMLR, 62892–62913.

A Derivations of the Variational Posterior

Global shrinkage parameters. Using Equation (11), the variational posterior for the global shrinkage parameters is:

$$\begin{aligned}
q(\boldsymbol{\tau}) &\propto \exp \left(\mathbb{E} \left[\log \prod_{l=1}^{L+1} \prod_d^{D_l} \prod_{d'}^{D_{l-1}} N(W_{l,d,d'} | 0, \tau_l \psi_{l,d,d'}) \right] + \log \prod_{l=1}^{L+1} \text{GIG}(\tau_l | \nu_{\text{glob}}, \delta_{\text{glob}}, \lambda_{\text{glob}}) \right) \\
&\propto \prod_{l=1}^{L+1} \prod_d^{D_l} \prod_{d'}^{D_{l-1}} \exp \mathbb{E} \left[\log \left(\frac{1}{\sqrt{\tau_l \psi_{l,d,d'}}} \exp \left(-\frac{W_{l,d,d'}^2}{2\tau_l \psi_{l,d,d'}} \right) \right) \right] \times \prod_{l=1}^{L+1} \tau_l^{\nu_{\text{glob}}-1} \exp \left(-\frac{1}{2} \left(\frac{\delta_{\text{glob}}^2}{\tau_l} + \lambda_{\text{glob}}^2 \tau_l \right) \right) \\
&\propto \prod_{l=1}^{L+1} \tau_l^{\nu_{\text{glob}}-1} \exp \left(-\frac{\delta_{\text{glob}}^2}{2\tau_l} - \frac{\lambda_{\text{glob}}^2 \tau_l}{2} \right) \prod_d^{D_l} \prod_{d'}^{D_{l-1}} \tau_l^{-\frac{1}{2}} \exp \left(-\frac{\mathbb{E} \left[\frac{1}{\psi_{l,d,d'}} \right] \mathbb{E} [W_{l,d,d'}^2]}{2\tau_l} \right) \\
&\propto \prod_{l=1}^{L+1} \tau_l^{\nu_{\text{glob}} - \frac{D_l D_{l-1}}{2} - 1} \exp \left(-\frac{1}{2} \left(\frac{1}{\tau_l} \left(\sum_d^{D_l} \sum_{d'}^{D_{l-1}} \mathbb{E} \left[\frac{1}{\psi_{l,d,d'}} \right] \mathbb{E} [W_{l,d,d'}^2] + \delta_{\text{glob}}^2 \right) + \lambda_{\text{glob}}^2 \tau_l \right) \right) \\
&\propto \prod_{l=1}^{L+1} \text{GIG}(\tau_l | \hat{\nu}_{\text{glob},l}, \hat{\delta}_{\text{glob},l}, \lambda_{\text{glob}}),
\end{aligned}$$

where for $l = 1, \dots, L+1$

$$\begin{aligned}
\hat{\nu}_{\text{glob},l} &= \nu_{\text{glob}} - \frac{D_l D_{l-1}}{2}, \\
\hat{\delta}_{\text{glob},l} &= \sqrt{\delta_{\text{glob}}^2 + \sum_d^{D_l} \sum_{d'}^{D_{l-1}} \mathbb{E} \left[\frac{1}{\psi_{l,d,d'}} \right] \mathbb{E} [w_{l,d,d'}^2]}.
\end{aligned}$$

Assuming hidden layers of the dimension D , the computational complexity of updating the global shrinkage variable is $\mathcal{O}(LD \max(D_0, D, D_{L+1}))$.

Local shrinkage parameters. Similarly, the variational posterior for the local shrinkage parameters is:

$$\begin{aligned}
q(\boldsymbol{\psi}) &\propto \prod_l^{L+1} \exp \left(\mathbb{E} \left[\log \prod_d^{D_l} \prod_{d'}^{D_{l-1}} \mathcal{N}(W_{l,d,d'} | 0, \tau_l \psi_{l,d,d'}) \right] + \log \prod_{d=1}^{D_l} \prod_{d'}^{D_{l-1}} \text{GIG}(\psi_{l,d,d'} | \nu_{\text{loc},l}, \delta_{\text{loc},l}, \lambda_{\text{loc},l}) \right) \\
&\propto \prod_l^{L+1} \prod_d^{D_l} \prod_{d'}^{D_{l-1}} \exp \left(\frac{1}{2} \log \psi_{l,d,d'} - \frac{\mathbb{E} \left[\frac{1}{\tau_l} \right] \mathbb{E} \left[\frac{1}{\psi_{l,d,d'}} \right] \mathbb{E} [W_{l,d,d'}^2]}{2} \right) \psi_{l,d,d'}^{\nu_{\text{loc},l}-1} \exp \left(-\frac{1}{2} \left(\frac{\delta_{\text{loc},l}^2}{\psi_{l,d,d'}} + \lambda_{\text{loc},l}^2 \psi_{l,d,d'} \right) \right) \\
&\propto \prod_l^{L+1} \prod_d^{D_l} \prod_{d'}^{D_{l-1}} \psi_{l,d,d'}^{\nu_{\text{loc},l}-\frac{1}{2}} \exp \left(-\frac{1}{2} \left(\frac{1}{\psi_{l,d,d'}} \left(\mathbb{E} \left[\frac{1}{\tau_l} \right] \mathbb{E} [W_{l,d,d'}^2] + \delta_{\text{loc},l}^2 \right) + \lambda_{\text{loc},l}^2 \psi_{l,d,d'} \right) \right) \\
&\propto \prod_l^{L+1} \prod_d^{D_l} \prod_{d'}^{D_{l-1}} \text{GIG}(\psi_{l,d,d'} | \hat{\nu}_{\text{loc},l,d,d'}, \hat{\delta}_{\text{loc},l,d,d'}, \lambda_{\text{loc},l}),
\end{aligned}$$

where for $l = 1, \dots, L+1$, $d = 1, \dots, D_l$, $d' = 1, \dots, D_{l-1}$

$$\begin{aligned}
\hat{\nu}_{\text{loc},l,d,d'} &= \nu_{\text{loc},l} - \frac{1}{2}, \\
\hat{\delta}_{\text{loc},l,d,d'} &= \sqrt{\mathbb{E} \left[\frac{1}{\tau_l} \right] \mathbb{E} [W_{l,d,d'}^2] + \delta_{\text{loc},l}^2}.
\end{aligned}$$

Similarly, given hidden layers of the dimension D , the computational complexity of updating the global shrinkage variable is $\mathcal{O}(LD \max(D_0, D, D_{L+1}))$.

Covariance matrix. Under the assumption of a diagonal covariance matrix, with parameters $\boldsymbol{\eta}_l = (\eta_{l,1}^2, \dots, \eta_{l,D_l}^2)$, the variational posterior is:

$$\begin{aligned}
q(\boldsymbol{\eta}) &\propto \exp \left(\mathbb{E} \left[\log \prod_n^N \mathcal{N}(\mathbf{y}_n | \mathbf{z}_{n,L+1}, \boldsymbol{\Sigma}_{L+1}) + \log \prod_n^N \prod_l^L \mathcal{N}(\mathbf{a}_{n,l} | \boldsymbol{\gamma}_{n,l} \odot \mathbf{z}_{n,l}, \boldsymbol{\Sigma}_l) \right] \right) \\
&\times \prod_l^L \prod_d^{D_l} \text{IG}(\eta_{l,d}^2 | \alpha_0^h, \beta_0^h) \prod_d^{D_{L+1}} \text{IG}(\eta_{l,d}^2 | \alpha_0, \beta_0) \\
&\propto \exp \left(-\frac{1}{2} \mathbb{E} \left[\sum_n^N \sum_d^{D_{L+1}} (\eta_{L+1,d})^{-2} (y_{n,d} - z_{n,L+1,d})^2 \right] \right) \prod_d^{D_{L+1}} \left((\eta_{L+1,d}^2)^{-\alpha_0-1-\frac{N}{2}} \exp \left(-\frac{\beta_0}{\eta_{L+1,d}^2} \right) \right) \\
&\times \prod_l^L \exp \left(-\frac{1}{2} \mathbb{E} \left[\sum_n^N \sum_d^{D_l} (\eta_{l,d})^{-2} (\mathbf{a}_{n,l,d} - \boldsymbol{\gamma}_{n,l,d} \odot \mathbf{z}_{n,l,d})^2 \right] \right) \times \prod_l^L \prod_d^{D_l} \left((\eta_{l,d}^2)^{-\alpha_0^h-1-\frac{N}{2}} \exp \left(-\frac{\beta_0^h}{\eta_{l,d}^2} \right) \right) \\
&\propto \prod_d^{D_{L+1}} \left((\eta_{L+1,d}^2)^{-\alpha_0-1-\frac{N}{2}} \right) \exp \left(-\frac{1}{\eta_{L+1,d}^2} \left(\beta_0 + \frac{1}{2} \sum_n^N \mathbb{E} [(y_{n,d} - z_{n,L+1,d})^2] \right) \right) \\
&\times \prod_l^L \prod_d^{D_l} (\eta_{l,d}^2)^{-\alpha_0^h-1-\frac{N}{2}} \exp \left(-\frac{1}{\eta_{l,d}^2} \left(\beta_0^h + \frac{1}{2} \sum_n^N \mathbb{E} [(\mathbf{a}_{n,l,d} - \boldsymbol{\gamma}_{n,l,d} \odot \mathbf{z}_{n,l,d})^2] \right) \right).
\end{aligned}$$

Thus, $q(\boldsymbol{\eta}) \propto \prod_l^{L+1} \prod_d^{D_l} \text{IG}(\alpha_{l,d}, \beta_{l,d})$, where

$$\begin{aligned}
\alpha_{l,d} &= \alpha_0^h + \frac{N}{2}, \quad d = 1, \dots, D_l, \quad l = 1, \dots, L, \\
\alpha_{L+1,d} &= \alpha_0 + \frac{N}{2}, \quad d = 1, \dots, D_{L+1},
\end{aligned}$$

$$\beta_{l,d} = \beta_0^h + \frac{1}{2} \sum_n^N \mathbb{E} \left[(a_{n,l,d} - \gamma_{n,l,d} \odot z_{n,l,d})^2 \right], \quad d = 1, \dots, D_l, \quad l = 1, \dots, L,$$

$$\beta_{L+1,d} = \beta_0 + \frac{1}{2} \sum_n^N \mathbb{E} \left[(y_{n,d} - z_{n,L+1,d})^2 \right], \quad d = 1, \dots, D_{L+1}.$$

For the parameters $\beta_{l,d}$, we must compute the sum of squares terms. For the last layer $l = L + 1$, this term, for each data point n , is given by:

$$\begin{aligned} \mathbb{E} \left[(y_{n,d} - z_{n,L+1,d})^2 \right] &= \sum_n^N (y_{n,d} - \mathbb{E}[\mathbf{W}_{L+1,d}] \mathbb{E}[\mathbf{a}_{n,L}] - \mathbb{E}[b_{L+1,d}])^2 \\ &+ \sum_n^N \mathbb{E}[b_{L+1,d}^2] - \mathbb{E}[b_{L+1,d}]^2 + 2\mathbb{E}[b_{L+1,d} \mathbf{W}_{L+1,d}] \mathbb{E}[\mathbf{a}_{n,L}] - 2\mathbb{E}[b_{L+1,d}] \mathbb{E}[\mathbf{W}_{L+1,d}] \mathbb{E}[\mathbf{a}_{n,L}] \\ &+ 2 \sum_n^N \text{Tr}(\mathbb{E}[\mathbf{W}_{L+1,d}^T \mathbf{W}_{L+1,d}] \mathbb{E}[\mathbf{a}_{n,L} \mathbf{a}_{n,L}^T]) - \text{Tr}(\mathbb{E}[\mathbf{W}_{L+1,d}^T] \mathbb{E}[\mathbf{W}_{L+1,d}] \mathbb{E}[\mathbf{a}_{n,L}] \mathbb{E}[\mathbf{a}_{n,L}^T]). \end{aligned}$$

Instead, for an intermediate layer $l = 1, \dots, L$, the sum of squares term, for each data point n , is given by:

$$\begin{aligned} \mathbb{E} \left[(a_{n,l,d} - \gamma_{n,l,d} \cdot z_{n,l,d})^2 \right] &= \sum_n^N (\mathbb{E}[a_{n,l,d}] - \mathbb{E}[\gamma_{n,l,d}] \mathbb{E}[b_{l,d}] - \mathbb{E}[\gamma_{n,l,d}] \mathbb{E}[\mathbf{W}_{l,d}] \mathbb{E}[\mathbf{a}_{n,l-1}])^2 \\ &+ \sum_n^N \mathbb{E}[a_{n,l,d}^2] - \mathbb{E}[a_{n,l,d}]^2 + \mathbb{E}[\gamma_{n,l,d}] \mathbb{E}[b_{l,d}^2] - \mathbb{E}[\gamma_{n,l,d}]^2 \mathbb{E}[b_{l,d}]^2 \\ &+ \sum_n^N \mathbb{E}[\gamma_{n,l,d}] \text{Tr}(\mathbb{E}[\mathbf{W}_{l,d}^T \mathbf{W}_{l,d}] \mathbb{E}[\mathbf{a}_{n,l-1} \mathbf{a}_{n,l-1}^T]) - \mathbb{E}[\gamma_{n,l,d}]^2 \text{Tr}(\mathbb{E}[\mathbf{W}_{l,d}^T] \mathbb{E}[\mathbf{W}_{l,d}] \mathbb{E}[\mathbf{a}_{n,l-1} \mathbf{a}_{n,l-1}^T]) \\ &+ 2 \sum_n^N \mathbb{E}[\gamma_{n,l,d}] \mathbb{E}[b_{l,d} \mathbf{W}_{l,d}] \mathbb{E}[\mathbf{a}_{n,l-1}] - \mathbb{E}[\gamma_{n,l,d}]^2 \mathbb{E}[b_{l,d}] \mathbb{E}[\mathbf{W}_{l,d}] \mathbb{E}[\mathbf{a}_{n,l-1}]. \end{aligned}$$

The complexity of obtaining variational update for $\boldsymbol{\eta}$ is then $\mathcal{O}(NL \max(D, D_0)^2 \max(D_{L+1}, D))$.

Weights and biases. The variational posterior for the weights and biases is:

$$\begin{aligned} q(\mathbf{b}, \mathbf{W}) &\propto \exp \left(\mathbb{E} \left[\log \prod_n^N \text{N}(y_n \mid \mathbf{W}_{L+1} \mathbf{a}_{n,L} + \mathbf{b}_{L+1}, \boldsymbol{\Sigma}_{L+1}) \prod_n^N \prod_l^L \text{N}(\mathbf{a}_{n,l} \mid \gamma_{n,l} \odot (\mathbf{W}_l \mathbf{a}_{n,l-1} + \mathbf{b}_l), \boldsymbol{\Sigma}_l) \right] \right) \\ &\times \exp \left(\mathbb{E} \left[\log \prod_n^N \prod_l^L \prod_d^{D_l} \exp \left(\frac{(\gamma_{n,l,d} - \frac{1}{2}) z_{n,l,d}}{T} \right) \exp \left(-\frac{\omega_{n,l,d} z_{n,l,d}^2}{2T^2} \right) \right] \right) \\ &\times \exp \left(\mathbb{E} \left[\log \prod_l^{L+1} \prod_d^{D_l} \prod_{d'}^{D_{l-1}} \text{N}(W_{l,d,d'} \mid 0, \tau_l \psi_{l,d,d'}) \right] \right) \prod_l^{L+1} \prod_d^{D_l} \text{N}(b_{l,d} \mid 0, s_0^2) \\ &\propto \prod_n^N \exp \left(\mathbb{E} \left[\log \frac{1}{\sqrt{|\boldsymbol{\Sigma}_{L+1}|}} \right] \right) \exp \left(\mathbb{E} \left[-\frac{1}{2} (\mathbf{y}_n - \mathbf{W}_{L+1} \mathbf{a}_{n,L} - \mathbf{b}_{L+1})^T (\boldsymbol{\Sigma}_{L+1})^{-1} (\mathbf{y}_n - \mathbf{W}_{L+1} \mathbf{a}_{n,L} - \mathbf{b}_{L+1}) \right] \right) \\ &\times \prod_l^L \prod_n^N \exp \left(\mathbb{E} \left[\log \frac{1}{\sqrt{|\boldsymbol{\Sigma}_l|}} \right] \right) \exp \left(\mathbb{E} \left[\left(-\frac{1}{2} (\mathbf{a}_{n,l} - \gamma_{n,l} \mathbf{W}_l \mathbf{a}_{n,l-1} - \gamma_{n,l} \mathbf{b}_l)^T (\boldsymbol{\Sigma}_l)^{-1} (\mathbf{a}_{n,l} - \gamma_{n,l} \mathbf{W}_l \mathbf{a}_{n,l-1} - \gamma_{n,l} \mathbf{b}_l) \right) \right] \right) \\ &\times \prod_l^L \prod_n^N \prod_d^{D_l} \exp \left(\mathbb{E} \left[\frac{(\gamma_{n,l,d} - \frac{1}{2}) (\mathbf{W}_{l,d} \mathbf{a}_{n,l-1} + b_{l,d})}{T} \right] \right) \exp \left(\mathbb{E} \left[-\frac{\omega_{n,l,d} (\mathbf{W}_{l,d} \mathbf{a}_{n,l-1} + b_{l,d})^2}{2T^2} \right] \right) \end{aligned}$$

$$\times \prod_l^{L+1} \prod_d^{D_l} \prod_{d'}^{D_{l-1}} \exp \left(-\frac{W_{l,d,d'}^2}{2} \mathbb{E} \left[\frac{1}{\tau_l} \right] \mathbb{E} \left[\frac{1}{\psi_{l,d,d'}} \right] \right) \prod_l^{L+1} \prod_d^{D_l} \exp \left(-\frac{b_{l,d}^2}{2s_0^2} \right).$$

Therefore, using also the fact that $\mathbf{\Sigma}_l$ is diagonal, we have that the variational posterior factorizes as $q(\mathbf{b}, \mathbf{W}) = \prod_l^{L+1} \prod_{d=1}^{D_l} q(b_{l,d}, \mathbf{W}_{l,d})$. We consider the terms $q(b_{l,d}, \mathbf{W}_{l,d})$ for the intermediate layers $l = 1, \dots, L$ and $q(b_{L+1,d}, \mathbf{W}_{L+1,d})$ for the last layer separately.

Starting with the last layer $L+1$, we first introduce the matrix

$$\mathbf{D}_{L+1,d}^{-1} = \text{diag} \left(s_0^{-2}, \mathbb{E} [\tau_{L+1}^{-1}] \mathbb{E} [\psi_{L+1,d,1}^{-1}], \dots, \mathbb{E} [\tau_{L+1}^{-1}] \mathbb{E} [\psi_{L+1,d,D_L}^{-1}] \right).$$

Then, for the variational posterior of the weights and biases for the d th dimension of the final layer, we only need to consider the relevant terms:

$$\begin{aligned} q(b_{L+1,d}, \mathbf{W}_{L+1,d}) &\propto \exp \left(-\frac{1}{2} \widetilde{\mathbf{W}}_{L+1,d} \mathbf{D}_{L+1,d}^{-1} \widetilde{\mathbf{W}}_{L+1,d}^T - \frac{1}{2} \mathbb{E} [(\eta_{L+1,d})^{-2}] \sum_n^N \mathbb{E} \left[(y_{n,d} - \widetilde{\mathbf{W}}_{L+1,d} \widetilde{\mathbf{a}}_{n,L})^2 \right] \right) \\ &\propto \exp \left(-\frac{1}{2} \widetilde{\mathbf{W}}_{L+1,d} \mathbf{D}_{L+1,d}^{-1} \widetilde{\mathbf{W}}_{L+1,d}^T - \frac{1}{2} \mathbb{E} [(\eta_{L+1,d})^{-2}] \left(\widetilde{\mathbf{W}}_{L+1,d} \left(\sum_n^N \mathbb{E} [\widetilde{\mathbf{a}}_{n,L} \widetilde{\mathbf{a}}_{n,L}^T] \right) \widetilde{\mathbf{W}}_{L+1,d}^T - 2 \widetilde{\mathbf{W}}_{L+1,d} \left(\sum_n^N y_n \mathbb{E} [\widetilde{\mathbf{a}}_{n,L}] \right) \right) \right) \\ &\propto \exp \left(-\frac{1}{2} \left(\widetilde{\mathbf{W}}_{L+1,d} \left(\mathbf{D}_{L+1,d}^{-1} + \mathbb{E} [(\eta_{L+1,d})^{-2}] \sum_n^N \mathbb{E} [\widetilde{\mathbf{a}}_{n,L} \widetilde{\mathbf{a}}_{n,L}^T] \right) \widetilde{\mathbf{W}}_{L+1,d}^T - 2 \mathbb{E} [(\eta_{L+1,d})^{-2}] \widetilde{\mathbf{W}}_{L+1,d} \left(\sum_n^N y_n \mathbb{E} [\widetilde{\mathbf{a}}_{n,L}] \right) \right) \right) \\ &\propto \exp \left(-\frac{1}{2} \left(\widetilde{\mathbf{W}}_{L+1,d} \mathbf{B}_{L+1,d}^{-1} \widetilde{\mathbf{W}}_{L+1,d}^T - 2 \widetilde{\mathbf{W}}_{L+1,d} \mathbf{B}_{L+1,d}^{-1} \mathbf{m}_{L+1,d}^T \right) \right), \end{aligned}$$

where

$$\begin{aligned} \mathbf{B}_{L+1,d}^{-1} &= \mathbf{D}_{L+1,d}^{-1} + \mathbb{E} [(\eta_{L+1,d})^{-2}] \sum_n^N \mathbb{E} [\widetilde{\mathbf{a}}_{n,L} \widetilde{\mathbf{a}}_{n,L}^T], \\ \mathbf{m}_{L+1,d}^T &= \mathbf{B}_{L+1,d} \mathbb{E} [(\eta_{L+1,d})^{-2}] \left(\sum_n^N y_n \mathbb{E} [\widetilde{\mathbf{a}}_{n,L}] \right). \end{aligned}$$

Thus, completing the square, we have that

$$q(b_{L+1,d}, \mathbf{W}_{L+1,d}) = \mathcal{N} \left(\widetilde{\mathbf{W}}_{L+1,d} \mid \mathbf{m}_{L+1,d}, \mathbf{B}_{L+1,d} \right).$$

Next, for the intermediate layers $l = 1, \dots, L$, we can similarly obtain the variational posterior of the weights and biases $q(b_{l,d}, \mathbf{W}_{l,d})$ for dimensions $d = 1, \dots, D_l$. We introduce the matrices

$$\mathbf{D}_{l,d}^{-1} = \text{diag} \left(s_0^{-2}, \mathbb{E} [\tau_l^{-1}] \mathbb{E} [\psi_{l,d,1}^{-1}], \dots, \mathbb{E} [\tau_l^{-1}] \mathbb{E} [\psi_{l,d,D_{l-1}}^{-1}] \right),$$

and consider the terms relevant to derive each $q(b_{l,d}, \mathbf{W}_{l,d})$ separately:

$$\begin{aligned} q(b_{l,d}, \mathbf{W}_{l,d}) &\propto \exp \left(-\frac{1}{2} \widetilde{\mathbf{W}}_{l,d} \mathbf{D}_{l,d}^{-1} \widetilde{\mathbf{W}}_{l,d}^T - \frac{1}{2T^2} \widetilde{\mathbf{W}}_{l,d} \left(\sum_n^N \mathbb{E} [\omega_{n,l,d}] \mathbb{E} [\widetilde{\mathbf{a}}_{n,l-1} \widetilde{\mathbf{a}}_{n,l-1}^T] \right) \widetilde{\mathbf{W}}_{l,d}^T \right. \\ &\quad \left. - \frac{1}{2} \mathbb{E} [(\eta_{l,d})^{-2}] \widetilde{\mathbf{W}}_{l,d} \left(\sum_n^N \mathbb{E} [\gamma_{n,l,d}^2] \mathbb{E} [\widetilde{\mathbf{a}}_{n,l-1} \widetilde{\mathbf{a}}_{n,l-1}^T] \right) \widetilde{\mathbf{W}}_{l,d}^T + \mathbb{E} [(\eta_{l,d})^{-2}] \widetilde{\mathbf{W}}_{l,d} \left(\sum_n^N \mathbb{E} [\gamma_{n,l,d}] \mathbb{E} [\mathbf{a}_{n,l,d} \mathbf{a}_{n,l-1}] \right) \right. \\ &\quad \left. + \frac{1}{T} \widetilde{\mathbf{W}}_{l,d} \left(\sum_n^N \mathbb{E} [\gamma_{n,l,d}] \mathbb{E} [\widetilde{\mathbf{a}}_{n,l-1}] \right) - \frac{1}{2T} \widetilde{\mathbf{W}}_{l,d} \left(\sum_n^N \mathbb{E} [\widetilde{\mathbf{a}}_{n,l-1}] \right) \right) \\ &\propto \exp \left(-\frac{1}{2} \left(\widetilde{\mathbf{W}}_{l,d} \mathbf{B}_{l,d}^{-1} \widetilde{\mathbf{W}}_{l,d}^T - 2 \widetilde{\mathbf{W}}_{l,d} \mathbf{B}_{l,d}^{-1} \mathbf{m}_{l,d}^T \right) \right), \end{aligned}$$

where

$$\begin{aligned}\mathbf{B}_{l,d}^{-1} &= \mathbf{D}_{l,d}^{-1} + \sum_n^N \left(\left(\frac{1}{T^2} \mathbb{E}[\omega_{n,l,d}] + \mathbb{E}[(\eta_{l,d})^{-2}] \mathbb{E}[\gamma_{n,l,d}] \right) \mathbb{E}[\tilde{\mathbf{a}}_{n,l-1} \tilde{\mathbf{a}}_{n,l-1}^T] \right), \\ \mathbf{m}_{l,d}^T &= \mathbf{B}_{l,d} \left(\sum_n^N \left(\mathbb{E}[(\eta_{l,d})^{-2}] \mathbb{E}[\gamma_{n,l,d}] \mathbb{E}[\mathbf{a}_{n,l,d} \tilde{\mathbf{a}}_{n,l-1}] + \frac{1}{T} \mathbb{E}[\tilde{\mathbf{a}}_{n,l-1}] \left(\mathbb{E}[\gamma_{n,l,d}] - \frac{1}{2} \right) \right) \right).\end{aligned}$$

Again, completing the square, we obtain the Gaussian variational posterior

$$q(b_{l,d}, \mathbf{W}_{l,d}) = \mathcal{N}((b_{l,d}, \mathbf{W}_{l,d}) \mid \mathbf{m}_{l,d}, \mathbf{B}_{l,d}).$$

The complexity of obtaining variational update for \mathbf{W}, \mathbf{b} is then $\mathcal{O}((L \max(D_{L+1}, D)(N \max(D, D_0)^2 + \max(D, D_0)^3))$. Assuming $\max(D, D_0) < N$, one gets the same complexity as when updating $\boldsymbol{\eta}$, i.e. $\mathcal{O}(LN \max(D, D_0)^2 \max(D_{L+1}, D))$.

Augmented variables. The variational posterior of the augmented variables is

$$\begin{aligned}q(\boldsymbol{\omega}) &\propto \exp \left(\mathbb{E} \left[\log \prod_n^N \prod_l^L \prod_d^{D_l} \exp \left(-\frac{\omega_{n,l,d} z_{n,l,d}^2}{2T^2} \right) p(\omega_{n,l,d}) \right] \right) \\ &\propto \prod_n^N \prod_l^L \prod_d^{D_l} \exp \left(\mathbb{E} \left[-\frac{\omega_{n,l,d} z_{n,l,d}^2}{2T^2} \right] \right) p(\omega_{n,l,d}).\end{aligned}$$

Thus, they are independent across width, depth, and observations, with

$$\begin{aligned}q(\omega_{n,l,d}) &= \text{PG}(\omega_{n,l,d} \mid 1, \frac{1}{T} \sqrt{\mathbb{E}[z_{n,l,d}^2]}) \\ &= \text{PG}(\omega_{n,l,d} \mid 1, A_{n,l,d}),\end{aligned}$$

where

$$A_{n,l,d} = \frac{1}{T} \sqrt{\left(\text{Tr} \left(\mathbb{E}[\tilde{\mathbf{W}}_{l,d}^T \tilde{\mathbf{W}}_{l,d}] \mathbb{E}[\tilde{\mathbf{a}}_{n,l-1} \tilde{\mathbf{a}}_{n,l-1}^T] \right) \right)}.$$

The complexity of obtaining variational update for $\boldsymbol{\omega}$ is then $\mathcal{O}(NLD \max(D, D_0)^2)$.

Binary activation. The variational posterior of the binary activations is:

$$\begin{aligned}q(\boldsymbol{\gamma}) &\propto \exp \left(\mathbb{E} \left[\log \prod_n^N \prod_l^L \prod_d^{D_l} \mathcal{N}(\mathbf{a}_{n,l} \mid \boldsymbol{\gamma}_{n,l} \odot \mathbf{z}_{n,l}, \boldsymbol{\Sigma}_l) + \log \left(\prod_n^N \prod_l^L \prod_d^{D_l} \exp \left(\frac{\gamma_{n,l,d} z_{n,l,d}}{T} \right) \right) \right] \right) \\ &\propto \prod_n^N \prod_l^L \prod_d^{D_l} \exp \left(-\frac{1}{2\eta_{l,d}^2} \mathbb{E}[(\mathbf{a}_{n,l,d} - \gamma_{n,l,d} (\mathbf{W}_{l,d} \mathbf{a}_{n,l-1} + b_{l,d}))^2] + \mathbb{E} \left[\frac{\gamma_{n,l,d} (\mathbf{W}_{l,d} \mathbf{a}_{n,l-1} + b_{l,d})}{T} \right] \right).\end{aligned}$$

Therefore, the variational posterior $q(\boldsymbol{\gamma})$ factories across observations $n = 1, \dots, N$, layers $l = 1, \dots, L$, and dimensions of the layer $d = 1, \dots, D_l$, with each factor $q(\gamma_{n,l,d})$ given by:

$$\begin{aligned}q(\gamma_{n,l,d}) &\propto \exp \left(-\frac{1}{2} \mathbb{E}[\eta_{l,d}^{-2}] \left(\gamma_{n,l,d}^2 \mathbb{E}[(\tilde{\mathbf{W}}_{l,d} \tilde{\mathbf{a}}_{n,l-1})^2] - 2\gamma_{n,l,d} \mathbb{E}[\mathbf{a}_{n,l,d} \tilde{\mathbf{W}}_{l,d} \tilde{\mathbf{a}}_{n,l-1}] \right) + \frac{1}{T} \gamma_{n,l,d} \mathbb{E}[\tilde{\mathbf{W}}_{l,d} \tilde{\mathbf{a}}_{n,l-1}] \right) \\ &\propto \exp \left(\gamma_{n,l,d} \left(-\frac{1}{2} \mathbb{E}[\eta_{l,d}^{-2}] \text{Tr} \left(\mathbb{E}[\tilde{\mathbf{W}}_{l,d}^T \tilde{\mathbf{W}}_{l,d}] \mathbb{E}[\tilde{\mathbf{a}}_{n,l-1} \tilde{\mathbf{a}}_{n,l-1}^T] \right) \right. \right. \\ &\quad \left. \left. + \mathbb{E}[\eta_{l,d}^{-2}] \mathbb{E}[\tilde{\mathbf{W}}_{l,d}] \mathbb{E}[\tilde{\mathbf{a}}_{n,l-1} \mathbf{a}_{n,l,d}] + \frac{1}{T} \mathbb{E}[\tilde{\mathbf{W}}_{l,d}] \mathbb{E}[\tilde{\mathbf{a}}_{n,l-1}] \right) \right)\end{aligned}$$

$$\propto \exp(\gamma_{n,l,d} \sigma^{-1}(\rho_{n,l,d})),$$

where σ is the logistic function and

$$\rho_{n,l,d} = \sigma \left(\mathbb{E} [\eta_{l,d}^{-2}] \left(-\frac{1}{2} \text{Tr} \left(\mathbb{E} [\widetilde{\mathbf{W}}_{l,d}^T \widetilde{\mathbf{W}}_{l,d}] \mathbb{E} [\widetilde{\mathbf{a}}_{n,l-1} \widetilde{\mathbf{a}}_{n,l-1}^T] \right) + \mathbb{E} [\widetilde{\mathbf{W}}_{l,d}] \mathbb{E} [\widetilde{\mathbf{a}}_{n,l-1} \mathbf{a}_{n,l,d}] \right) + \frac{1}{T} \mathbb{E} [\widetilde{\mathbf{W}}_{l,d}] \mathbb{E} [\widetilde{\mathbf{a}}_{n,l-1}] \right).$$

Then noticing that $\sigma^{-1}(\rho) = \log(\rho(1-\rho)^{-1})$ and combining separate factors of the variational posterior of the binary activations, we obtain:

$$\begin{aligned} q(\boldsymbol{\gamma}) &\propto \prod_n^N \prod_l^L \prod_d^{D_l} \rho_{n,l,d}^{\gamma_{n,l,d}} (1 - \rho_{n,l,d})^{1-\gamma_{n,l,d}} \\ &\propto \prod_n^N \prod_l^L \prod_d^{D_l} \text{Bern}(\gamma_{n,l,d} \mid \rho_{n,l,d}). \end{aligned}$$

The complexity of obtaining variational update for $\boldsymbol{\gamma}$ is then $\mathcal{O}(LND \max(D, D_0)^2)$.

Stochastic activation. The variational posterior of the stochastic activation is

$$\begin{aligned} q(\mathbf{a}) &\propto \exp \left(\mathbb{E} \left[\log \prod_n^N \text{N}(\mathbf{y}_n \mid \mathbf{z}_{n,L+1}, \boldsymbol{\eta}_{L+1}) + \log \prod_n^N \prod_l^L \text{N}(\mathbf{a}_{n,l} \mid \boldsymbol{\gamma}_{n,l} \odot \mathbf{z}_{n,l}, \boldsymbol{\eta}_l) \right. \right. \\ &\quad \left. \left. + \log \prod_n^N \prod_l^L \prod_d^{D_l} \exp\left(\frac{(\gamma_{n,l,d} - \frac{1}{2})z_{n,l,d}}{T}\right) \exp\left(-\frac{\omega_{n,l,d}z_{n,l,d}^2}{2T^2}\right) \right] \right) \\ &\propto \prod_n^N \exp \left(-\frac{1}{2} \sum_d^{D_{L+1}} \mathbb{E} \left[\frac{1}{\eta_{L+1,d}^2} \right] \mathbb{E} \left[(y_{n,d} - \mathbf{W}_{L+1,d} \mathbf{a}_{n,L} - b_{L+1,d})^2 \right] \right) \\ &\quad \times \prod_n^N \exp \left(-\frac{1}{2} \sum_l^L \sum_d^{D_l} \mathbb{E} \left[\frac{1}{\eta_{l,d}^2} \right] \mathbb{E} \left[(a_{n,l,d} - \gamma_{n,l,d} (\mathbf{W}_{l,d} \mathbf{a}_{n,l-1} + b_{l,d}))^2 \right] \right) \\ &\quad \times \prod_n^N \exp \left(\sum_l^L \sum_d^{D_l} \mathbb{E} \left[\frac{(\gamma_{n,l,d} - \frac{1}{2})z_{n,l,d}}{T} - \frac{\omega_{n,l,d}z_{n,l,d}^2}{2T^2} \right] \right). \end{aligned}$$

Therefore, the variational posterior of the stochastic activations factories across observations $n = 1, \dots, N$ and we derive $q(\mathbf{a}_n)$ separately. For each layer $l = 1, \dots, L$, we introduce the following diagonal matrix $\hat{\boldsymbol{\Sigma}}_l^{-1} = \text{diag}(\mathbb{E}[\eta_{l,1}^{-2}], \dots, \mathbb{E}[\eta_{l,D_l}^{-2}])$ and consider the relevant terms of the variational posterior:

$$\begin{aligned} q(\mathbf{a}_n) &\propto \exp \left(-\frac{1}{2} \mathbf{a}_{n,L}^T \left(\sum_d^{D_{L+1}} \mathbb{E} \left[\frac{1}{\eta_{L+1,d}^2} \right] \mathbb{E} [\mathbf{W}_{L+1,d}^T \mathbf{W}_{L+1,d}] \mathbf{a}_{n,L} \right) \right) \\ &\quad \times \exp \left(-\mathbf{a}_{n,L}^T \left(\sum_d^{D_{L+1}} \mathbb{E} \left[\frac{1}{\eta_{L+1,d}^2} \right] (\mathbb{E} [\mathbf{W}_{L+1,d}^T b_{L+1,d}] - \mathbb{E} [\mathbf{W}_{L+1,d}^T] y_{n,d}) \right) \right) \\ &\quad \times \exp \left(-\frac{1}{2} \left(\mathbf{a}_{n,L}^T \hat{\boldsymbol{\Sigma}}_L^{-1} \mathbf{a}_{n,L} - 2 \mathbf{a}_{n,L}^T \hat{\boldsymbol{\Sigma}}_L^{-1} \left((\mathbb{E} [\boldsymbol{\gamma}_{n,L}] \mathbf{1}_{D_{L-1}}^T \odot \mathbb{E} [\mathbf{W}_L]) \mathbf{a}_{n,L-1} + \mathbb{E} [\boldsymbol{\gamma}_{n,L}] \odot \mathbb{E} [\mathbf{b}_L] \right) \right) \right) \\ &\quad \times \prod_{l=1}^{L-1} \exp \left(-\frac{1}{2} \left(\mathbf{a}_{n,l}^T \hat{\boldsymbol{\Sigma}}_l^{-1} \mathbf{a}_{n,l} - 2 \mathbf{a}_{n,l}^T \hat{\boldsymbol{\Sigma}}_l^{-1} \left((\mathbb{E} [\boldsymbol{\gamma}_{n,l}] \mathbf{1}_{D_{l-1}}^T \odot \mathbb{E} [\mathbf{W}_l]) \mathbf{a}_{n,l-1} + \mathbb{E} [\boldsymbol{\gamma}_{n,l}] \odot \mathbb{E} [\mathbf{b}_l] \right) \right) \right) \\ &\quad \times \prod_{l=1}^L \exp \left(-\frac{1}{2} \left(\mathbf{a}_{n,l-1}^T \left(\sum_{d=1}^{D_l} \mathbb{E} \left[\frac{1}{\eta_{l,d}^2} \right] \mathbb{E} [\gamma_{n,l,d}] \mathbb{E} [\mathbf{W}_{l,d}^T \mathbf{W}_{l,d}] \mathbf{a}_{n,l-1} \right) \right) \right) \times \end{aligned}$$

$$\begin{aligned}
& \times \prod_{l=1}^L \exp \left(-\mathbf{a}_{n,l-1}^T \left(\sum_{d=1}^{D_l} \mathbb{E} \left[\frac{1}{\eta_{l,d}^2} \right] \mathbb{E} [\gamma_{n,l,d}] \mathbb{E} [\mathbf{W}_{l,d}^T \mathbf{b}_{l,d}] \right) \right) \\
& \times \prod_{l=1}^L \exp \left(-\frac{1}{2} \left(\mathbf{a}_{n,l-1}^T \left(\frac{1}{T^2} \sum_{d=1}^{D_l} \mathbb{E} [\omega_{n,l,d}] \mathbb{E} [\mathbf{W}_{l,d}^T \mathbf{W}_{l,d}] \right) \mathbf{a}_{n,l-1} \right) \right) \\
& \times \prod_{l=1}^L \exp \left(\mathbf{a}_{n,l-1}^T \left(\frac{1}{T} \sum_{d=1}^{D_l} \mathbb{E} [\mathbf{W}_{l,d}^T] \left(\mathbb{E} [\gamma_{n,l,d}] - \frac{1}{2} \right) - \frac{1}{T^2} \sum_{d=1}^{D_l} \mathbb{E} [\omega_{n,l,d}] \mathbb{E} [\mathbf{W}_{l,d}^T \mathbf{b}_{l,d}] \right) \right).
\end{aligned}$$

The variational posterior of the stochastic activations does not factories into independent blocks, however it does have a structured sequential factorization $q(\mathbf{a}_n) = \prod_{l=1}^L q(\mathbf{a}_{n,l} \mid \mathbf{a}_{n,l-1})$. And, we can derive the variational factor $q(\mathbf{a}_{n,L} \mid \mathbf{a}_{n,L-1})$ by only considering the terms with $\mathbf{a}_{n,L}$. First, introduce the matrices $\mathbf{S}_{n,L}$ and $\mathbf{M}_{n,L}$ and a vectors $\mathbf{t}_{n,L}$:

$$\begin{aligned}
\mathbf{S}_{n,L}^{-1} &= \hat{\Sigma}_L^{-1} + \sum_{d=1}^{D_{L+1}} \mathbb{E} \left[\frac{1}{\eta_{L+1,d}^2} \right] \mathbb{E} [\mathbf{W}_{L+1,d}^T \mathbf{W}_{L+1,d}], \\
\mathbf{t}_{n,L} &= \mathbf{S}_{n,L} \left(\left(\sum_{d=1}^{D_{L+1}} \mathbb{E} \left[\frac{1}{\eta_{L+1,d}^2} \right] (-\mathbb{E} [\mathbf{W}_{L+1,d}^T \mathbf{b}_{L+1,d}] + \mathbb{E} [\mathbf{W}_{L+1,d}^T] y_{n,d}) \right) + \hat{\Sigma}_L^{-1} \mathbb{E} [\gamma_{n,L}] \odot \mathbb{E} [\mathbf{b}_L] \right), \\
\mathbf{M}_{n,L} &= \mathbf{S}_{n,L} \hat{\Sigma}_L^{-1} \mathbb{E} [\gamma_{n,L}] \mathbf{1}_{D_{L-1}}^T \odot \mathbb{E} [\mathbf{W}_L].
\end{aligned}$$

Then we consider relevant terms of the variational posterior:

$$\begin{aligned}
q(\mathbf{a}_{n,L} \mid \mathbf{a}_{n,L-1}) &\propto \exp \left(-\frac{1}{2} \left(\mathbf{a}_{n,L}^T \mathbf{S}_{n,L}^{-1} \mathbf{a}_{n,L} - 2\mathbf{a}_{n,L}^T \mathbf{S}_{n,L}^{-1} (\mathbf{t}_{n,L} + \mathbf{M}_{n,L} \mathbf{a}_{n,L-1}) \right) \right) \\
&\propto \exp \left(-\frac{1}{2} (\mathbf{a}_{n,L} - (\mathbf{t}_{n,L} + \mathbf{M}_{n,L} \mathbf{a}_{n,L-1}))^T \mathbf{S}_{n,L}^{-1} (\mathbf{a}_{n,L} - (\mathbf{t}_{n,L} + \mathbf{M}_{n,L} \mathbf{a}_{n,L-1})) \right) \times \\
&\times \exp \left(\frac{1}{2} (\mathbf{t}_{n,L} + \mathbf{M}_{n,L} \mathbf{a}_{n,L-1})^T \mathbf{S}_{n,L}^{-1} (\mathbf{t}_{n,L} + \mathbf{M}_{n,L} \mathbf{a}_{n,L-1}) \right) \\
&\propto N(\mathbf{a}_{n,L} \mid \mathbf{t}_{n,L} + \mathbf{M}_{n,L} \mathbf{a}_{n,L-1}, \mathbf{S}_{n,L}) \times \exp \left(\frac{1}{2} (\mathbf{t}_{n,L} + \mathbf{M}_{n,L} \mathbf{a}_{n,L-1})^T \mathbf{S}_{n,L}^{-1} (\mathbf{t}_{n,L} + \mathbf{M}_{n,L} \mathbf{a}_{n,L-1}) \right),
\end{aligned}$$

where the first term in the equation above provides $q(\mathbf{a}_{n,L} \mid \mathbf{a}_{n,L-1})$ and the second terms is relevant for computing the subsequent $q(\mathbf{a}_{n,L-1} \mid \mathbf{a}_{n,L-2})$. Recursively repeating a similar procedure for $l = L-1, \dots, 1$, we are then able to obtain each of the variational posteriors $q(\mathbf{a}_{n,l} \mid \mathbf{a}_{n,l-1})$. Each time we define $\mathbf{S}_{n,l}$, $\mathbf{M}_{n,l}$ and $\mathbf{t}_{n,l}$ as follows:

$$\begin{aligned}
\mathbf{S}_{n,l}^{-1} &= \hat{\Sigma}_l^{-1} - \mathbf{M}_{n,l+1}^T \mathbf{S}_{n,l+1}^{-1} \hat{\mathbf{M}}_{n,l+1} + \sum_{d=1}^{D_{l+1}} \left(\mathbb{E} \left[\frac{1}{\eta_{l+1,d}^2} \right] \mathbb{E} [\gamma_{n,l+1,d}] + \frac{1}{T^2} \sum_{d=1}^{D_{l+1}} \mathbb{E} [\omega_{n,l+1,d}] \right) \mathbb{E} [\mathbf{W}_{l+1,d}^T \mathbf{W}_{l+1,d}] \\
\mathbf{t}_{n,l} &= \mathbf{S}_{n,l} \left(\mathbf{M}_{n,l+1}^T \mathbf{S}_{n,l+1}^{-1} \mathbf{t}_{n,l+1} + \hat{\Sigma}_l^{-1} \mathbb{E} [\gamma_{n,l}] \odot \mathbb{E} [\mathbf{b}_l] + \frac{1}{T} \sum_{d=1}^{D_{l+1}} \mathbb{E} [\mathbf{W}_{l+1,d}^T] \left(\mathbb{E} [\gamma_{n,l+1,d}] - \frac{1}{2} \right) \right. \\
&\quad \left. - \sum_{d=1}^{D_{l+1}} \left(\mathbb{E} \left[\frac{1}{\eta_{l+1,d}^2} \right] \mathbb{E} [\gamma_{n,l+1,d}] + \frac{1}{T^2} \mathbb{E} [\omega_{n,l+1,d}] \right) \mathbb{E} [\mathbf{W}_{l+1,d}^T \mathbf{b}_{l+1,d}] \right), \\
\mathbf{M}_{n,l} &= \mathbf{S}_{n,l} \hat{\Sigma}_l^{-1} \mathbb{E} [\gamma_{n,l}] \mathbf{1}_{D_{l-1}}^T \odot \mathbb{E} [\mathbf{W}_l].
\end{aligned}$$

Then substituting the above into the terms of the variational posterior containing $\mathbf{a}_{n,l}$:

$$q(\mathbf{a}_{n,l} \mid \mathbf{a}_{n,l-1}) \propto \exp \left(-\frac{1}{2} (\mathbf{a}_{n,l} - (\mathbf{t}_{n,l} + \mathbf{M}_{n,l} \mathbf{a}_{n,l-1}))^T \mathbf{S}_{n,l}^{-1} (\mathbf{a}_{n,l} - (\mathbf{t}_{n,l} + \mathbf{M}_{n,l} \mathbf{a}_{n,l-1})) \right)$$

$$\begin{aligned} & \times \exp \left(\frac{1}{2} (\mathbf{t}_{n,l} + \mathbf{M}_{n,l} \mathbf{a}_{n,l-1})^T \mathbf{S}_{n,l}^{-1} (\mathbf{t}_{n,l} + \mathbf{M}_{n,l} \mathbf{a}_{n,l-1}) \right) \\ & \propto \mathcal{N}(\mathbf{a}_{n,l} \mid \mathbf{t}_{n,l} + \mathbf{M}_{n,l} \mathbf{a}_{n,l-1}, \mathbf{S}_{n,l}) \times \exp \left(\frac{1}{2} (\mathbf{t}_{n,l} + \mathbf{M}_{n,l} \mathbf{a}_{n,l-1})^T \mathbf{S}_{n,l}^{-1} (\mathbf{t}_{n,l} + \mathbf{M}_{n,l} \mathbf{a}_{n,l-1}) \right). \end{aligned}$$

Finally, we combine the terms $q(\mathbf{a}_{n,l} \mid \mathbf{a}_{n,l-1})$ for $l = 1, \dots, L+1$ and get the variational posterior of the stochastic activation

$$q(\mathbf{a}) \propto \prod_{n=1}^N \prod_{l=1}^L \mathcal{N}(\mathbf{a}_{n,l} \mid \mathbf{t}_{n,l} + \mathbf{M}_{n,l} \mathbf{a}_{n,l-1}, \mathbf{S}_{n,l}).$$

B ELBO computation

B.1 ELBO for training

Recall that optimal variational parameters maximize the ELBO function of Equation (10), which for our model is:

$$\begin{aligned} \text{ELBO} = & \mathbb{E}[\log p(\mathbf{y}, \mathbf{a}, \boldsymbol{\gamma}, \boldsymbol{\omega} \mid \mathbf{W}, \mathbf{b}, \boldsymbol{\Sigma})] + \mathbb{E}[\log p(\mathbf{W} \mid \boldsymbol{\psi}, \boldsymbol{\tau})] + \mathbb{E}[\log p(\boldsymbol{\psi})] + \mathbb{E}[\log p(\boldsymbol{\tau})] + \mathbb{E}[\log p(\mathbf{b})] + \mathbb{E}[\log p(\boldsymbol{\Sigma})] \\ & - \mathbb{E}[\log q(\mathbf{a})] - \mathbb{E}[\log q(\boldsymbol{\gamma})] - \mathbb{E}[\log q(\boldsymbol{\omega})] - \mathbb{E}[\log q(\mathbf{W}, \mathbf{b})] - \mathbb{E}[\log q(\boldsymbol{\eta})] - \mathbb{E}[\log q(\boldsymbol{\psi})] - \mathbb{E}[\log q(\boldsymbol{\tau})]. \end{aligned}$$

Similar to the variational update, we compute the terms of the ELBO corresponding to different blocks of parameters separately.

ELBO of $\boldsymbol{\tau}$. First, consider the terms of the ELBO containing the global shrinkage parameters:

$$\begin{aligned} \mathbb{E}[\log p(\boldsymbol{\tau}) - \log q(\boldsymbol{\tau})] &= \sum_{l=1}^{L+1} \mathbb{E} \left[\log \text{GIG}(\tau_l \mid \nu_{\text{glob}}, \delta_{\text{glob}}, \lambda_{\text{glob}}) - \log \text{GIG}(\tau_l \mid \hat{\nu}_{\text{glob},l}, \hat{\delta}_{\text{glob},l}, \lambda_{\text{glob}}) \right] \\ &= C_{\tau} + \sum_{l=1}^{L+1} \mathbb{E} \left[\log \tau_l^{\nu_{\text{glob}}-1} \exp \left(-\frac{1}{2} \left(\frac{\delta_{\text{glob}}^2}{\tau_l} + \lambda_{\text{glob}}^2 \tau_l \right) \right) \right] - \sum_{l=1}^{L+1} \mathbb{E} \left[\log \left(\tau_l^{\hat{\nu}_{\text{glob},l}-1} \right) \exp \left(-\frac{1}{2} \left(\frac{\hat{\delta}_{\text{glob},l}^2}{\tau_l} + \lambda_{\text{glob}}^2 \tau_l \right) \right) \right] \\ &= C_{\tau} + \frac{1}{2} \sum_{l=1}^{L+1} D_l D_{l-1} \mathbb{E}[\log \tau_l] + \mathbb{E} \left[\frac{1}{\tau_l} (\hat{\delta}_{\text{glob},l}^2 - \delta_{\text{glob}}^2) \right], \end{aligned}$$

where the normalizing constant is

$$\begin{aligned} C_{\tau} &= \sum_{l=1}^{L+1} (\nu_{\text{glob}} - \hat{\nu}_{\text{glob},l}) \log(\lambda_{\text{glob}}) + \hat{\nu}_{\text{glob},l} \log(\hat{\delta}_{\text{glob},l}) - \nu_{\text{glob}} \log(\delta_{\text{glob}}) \\ &\quad + \sum_{l=1}^{L+1} \log(K_{\hat{\nu}_{\text{glob},l}}(\lambda_{\text{glob}} \hat{\delta}_{\text{glob},l})) - \log(K_{\nu_{\text{glob}}}(\lambda \delta_{\text{glob}})). \end{aligned}$$

ELBO of $\boldsymbol{\psi}$. Similarly, the terms of the ELBO containing the local shrinkage parameters are

$$\begin{aligned} \mathbb{E}[\log p(\boldsymbol{\psi}) - \log q(\boldsymbol{\psi})] &= C_{\psi} + \sum_{l=1}^{L+1} \sum_{d=1}^{D_l} \sum_{d'=1}^{D_{l-1}} \mathbb{E} \left[\log \text{GIG}(\psi_{l,d,d'} \mid \nu_{\text{loc},l}, \delta_{\text{loc},l}, \lambda_{\text{loc},l}) - \log \text{GIG}(\psi_{l,d,d'} \mid \hat{\nu}_{\text{loc},l,d,d'}, \hat{\delta}_{\text{loc},l,d,d'}, \lambda_{\text{loc},l}) \right] \\ &= C_{\psi} + \sum_{l=1}^{L+1} \sum_{d=1}^{D_l} \sum_{d'=1}^{D_{l-1}} \mathbb{E} \left[\log \psi_{l,d,d'}^{\nu_{\text{loc},l}-1} \exp \left(-\frac{1}{2} \left(\frac{\delta_{\text{loc},l}^2}{\psi_{l,d,d'}} + \lambda_{\text{loc},l}^2 \psi_{l,d,d'} \right) \right) \right] - \log \left(\psi_{l,d,d'}^{\hat{\nu}_{\text{loc},l,d,d'}-1} \right) \exp \left(-\frac{1}{2} \left(\frac{\hat{\delta}_{\text{loc},l,d,d'}^2}{\psi_{l,d,d'}} + \lambda_{\text{loc},l}^2 \psi_{l,d,d'} \right) \right) \\ &= C_{\psi} + \frac{1}{2} \sum_{l=1}^{L+1} \sum_{d=1}^{D_l} \sum_{d'=1}^{D_{l-1}} \mathbb{E}[\log \psi_{l,d,d'}] + \mathbb{E} \left[\frac{1}{\psi_{l,d,d'}} \right] (\hat{\delta}_{\text{loc},l,d,d'}^2 - \delta_{\text{loc},l}^2), \end{aligned}$$

where the normalizing constant is

$$\begin{aligned}
C_\psi &= \sum_{l=1}^{L+1} \sum_{d=1}^{D_l} \sum_{d'=1}^{D_{l-1}} (\nu_{\text{loc},l} - \hat{\nu}_{\text{loc},l,d,d'}) \log(\lambda_{\text{loc},l}) + \hat{\nu}_{\text{loc},l,d,d'} \log(\hat{\delta}_{\text{loc},l,d,d'}) - \nu_{\text{loc},l} \log(\delta_{\text{loc},l}) \\
&\quad + \sum_{l=1}^{L+1} \sum_{d=1}^{D_l} \sum_{d'=1}^{D_{l-1}} \log(K_{\hat{\nu}_{\text{loc},l,d,d'}}(\lambda_{\text{glob}} \hat{\delta}_{\text{loc},l,d,d'})) - \log(K_{\nu_{\text{loc},l}}(\lambda_{\text{loc},l} \delta_{\text{loc},l})).
\end{aligned}$$

ELBO of η . As before, the covariance matrix is assumed to be diagonal so that the relevant ELBO is:

$$\begin{aligned}
&\mathbb{E}[\log p(\Sigma) - \log q(\eta)] \\
&= C_\eta + \sum_{l=1}^L \sum_{d=1}^{D_l} \mathbb{E}[\log \text{IG}(\eta_{l,d}^2 | \alpha_0^h, \beta_0^h)] + \sum_{d=1}^{D_{L+1}} \mathbb{E}[\log \text{IG}(\eta_{L+1,d}^2 | \alpha_0, \beta_0)] - \sum_{l=1}^{L+1} \sum_d \mathbb{E}[\log \text{IG}(\eta_{l,d}^2 | \alpha_{l,d}, \beta_{l,d})] \\
&= C_\eta + \sum_{l=1}^L \sum_d (\alpha_{l,d} - \alpha_0^h) \mathbb{E}[\log \eta_{l,d}^2] + \sum_{d=1}^{D_{L+1}} (\alpha_{L+1,d} - \alpha_0) \mathbb{E}[\log \eta_{L+1,d}^2] \\
&\quad + \sum_{l=1}^L \sum_{d=1}^{D_l} (\beta_{l,d} - \beta_0^h) \mathbb{E}\left[\frac{1}{\eta_{l,d}^2}\right] + \sum_{d=1}^{D_{L+1}} (\beta_{L+1,d} - \beta_0) \mathbb{E}\left[\frac{1}{\eta_{L+1,d}^2}\right] \\
&= C_\eta + \frac{N}{2} \sum_{l=1}^{L+1} \sum_d \mathbb{E}[\log \eta_{l,d}^2] + \sum_{l=1}^L \sum_{d=1}^{D_l} (\beta_{l,d} - \beta_0^h) \mathbb{E}\left[\frac{1}{\eta_{l,d}^2}\right] + \sum_{d=1}^{D_{L+1}} (\beta_{L+1,d} - \beta_0) \mathbb{E}\left[\frac{1}{\eta_{L+1,d}^2}\right],
\end{aligned}$$

where the normalizing constant is

$$\begin{aligned}
C_\eta &= \sum_{l=1}^L \sum_{d=1}^{D_l} \alpha_0^h \log \beta_0^h - \alpha_{l,d} \log \beta_{l,d} + \log \Gamma(\alpha_{l,d}) - \log \Gamma(\alpha_0^h) \\
&\quad + \sum_{d=1}^{D_{L+1}} \alpha_0 \log \beta_0 - \alpha_{L+1,d} \log \beta_{L+1,d} + \log \Gamma(\alpha_{L+1,d}) - \log \Gamma(\alpha_0).
\end{aligned}$$

ELBO of (\mathbf{W}, \mathbf{b}) . Recall, previously introduced matrices $\mathbf{D}_{l,d} = \text{diag}(s_0^{-2}, \mathbb{E}[\tau_l^{-1}] \mathbb{E}[\psi_{l,d,1}^{-1}], \dots, \mathbb{E}[\tau_l^{-1}] \mathbb{E}[\psi_{l,d,D_{l-1}}^{-1}])$ and denote further $\mathbf{D}_{l,d}^0 = \text{diag}(s_0^2, \tau_l \psi_{l,d,1}, \dots, \tau_l \psi_{l,d,D_{l-1}})$. Then the ELBO of weights and biases is:

$$\begin{aligned}
&\mathbb{E}[\log p(\mathbf{W} | \psi, \tau)] + \mathbb{E}[\log p(\mathbf{b})] - \mathbb{E}[\log q(\mathbf{W}, \mathbf{b})] \\
&= \sum_{l=1}^{L+1} \sum_{d=1}^{D_l} \sum_{d'=1}^{D_{l-1}} \mathbb{E}[\log \text{N}(\widetilde{\mathbf{W}}_{l,d} | 0, \mathbf{D}_{l,d}^0)] - \sum_{l=1}^{L+1} \sum_d \mathbb{E}[\log \text{N}(\widetilde{\mathbf{W}}_{l,d} | \mathbf{m}_{l,d}, \mathbf{B}_{l,d})] \\
&= \sum_{l=1}^{L+1} \sum_{d=1}^{D_l} \mathbb{E}\left[\log(|\mathbf{D}_{l,d}|)^{-\frac{1}{2}} \exp\left(-\frac{1}{2} \widetilde{\mathbf{W}}_{l,d} (\mathbf{D}_{l,d}^0)^{-1} \widetilde{\mathbf{W}}_{l,d}^T\right)\right] \\
&\quad - \sum_{l=1}^{L+1} \sum_d \mathbb{E}\left[\log|\mathbf{B}_{l,d}|^{-\frac{1}{2}} \exp\left(-\frac{1}{2} (\widetilde{\mathbf{W}}_{l,d} - \mathbf{m}_{l,d}) \mathbf{B}_{l,d}^{-1} (\widetilde{\mathbf{W}}_{l,d} - \mathbf{m}_{l,d})^T\right)\right] \\
&= \frac{1}{2} \sum_{l=1}^{L+1} \sum_d \mathbb{E}[\log|\mathbf{B}_{l,d}|] - \mathbb{E}[\log(|\mathbf{D}_{l,d}^0|)] - \mathbb{E}\left[\widetilde{\mathbf{W}}_{l,d} (\mathbf{D}_{l,d}^0)^{-1} \widetilde{\mathbf{W}}_{l,d}^T\right] + \mathbb{E}\left[(\widetilde{\mathbf{W}}_{l,d} - \mathbf{m}_{l,d}) \mathbf{B}_{l,d}^{-1} (\widetilde{\mathbf{W}}_{l,d} - \mathbf{m}_{l,d})^T\right] \\
&= \frac{1}{2} \sum_{l=1}^{L+1} \sum_d \log|\mathbf{B}_{l,d}| - \mathbb{E}[\log(|\mathbf{D}_{l,d}^0|)] - \text{Tr}\left(\mathbb{E}\left[\widetilde{\mathbf{W}}_{l,d}^T \widetilde{\mathbf{W}}_{l,d}\right] \mathbb{E}[(\mathbf{D}_{l,d}^0)^{-1}]\right) + \sum_{l=1}^{L+1} \frac{D_l}{2} \\
&= \frac{1}{2} \sum_{l=1}^{L+1} \sum_d \left(\log|\mathbf{B}_{l,d}| - \text{Tr}\left(\mathbb{E}\left[\widetilde{\mathbf{W}}_{l,d}^T \widetilde{\mathbf{W}}_{l,d}\right] \mathbf{D}_{l,d}\right) - \sum_{d'=1}^{D_{l-1}} \mathbb{E}[\log \psi_{l,d,d'}]\right) - \frac{1}{2} \sum_{l=1}^{L+1} D_l (\log s_0^2 + D_{l-1} \mathbb{E}[\log \tau_l] - 1).
\end{aligned}$$

ELBO of \mathbf{a} , γ and ω . The remaining terms of the ELBO are the ones with stochastic and binary activations and additional augmented variables:

$$\begin{aligned}
& \mathbb{E} [\log p(\mathbf{y}, \mathbf{a}, \gamma, \omega | \mathbf{W}, \mathbf{b}, \boldsymbol{\Sigma})] - \mathbb{E} [\log q(\mathbf{a})] - \mathbb{E} [\log q(\gamma)] - \mathbb{E} [\log q(\omega)] \\
&= \sum_{n=1}^N \sum_{d=1}^{D_{L+1}} \mathbb{E} [\log N(y_{n,d} | \mathbf{z}_{n,L+1,d}, \boldsymbol{\Sigma}_{L+1,d})] + \sum_{n=1}^N \sum_{l=1}^L \sum_{d=1}^{D_l} \mathbb{E} [\log N(\mathbf{a}_{n,l,d} | \gamma_{n,l,d} \odot \mathbf{z}_{n,l,d}, \boldsymbol{\Sigma}_{l,d})] \\
&+ \sum_{n=1}^N \sum_{l=1}^L \sum_{d=1}^{D_l} \mathbb{E} \left[\log \left(\exp \left(\frac{\kappa_{n,l,d} z_{n,l,d}}{T} \right) \exp \left(-\frac{\omega_{n,l,d} z_{n,l,d}^2}{2T^2} \right) \text{PG}(\omega_{n,l,d} | 1, 0) \right) \right] \\
&- \sum_{n=1}^N \sum_{l=1}^L \mathbb{E} [\log N(\mathbf{a}_{n,l} | \mathbf{t}_{n,l} + \mathbf{M}_{n,l} \mathbf{a}_{n,l-1}, \mathbf{S}_{n,l})] - \sum_{n=1}^N \sum_{l=1}^L \sum_{d=1}^{D_l} \mathbb{E} [\log \text{Bern}(\gamma_{n,l,d} | \rho_{n,l,d})] + \mathbb{E} [\log \text{PG}(\omega_{n,l,d} | 1, A_{n,l,d})] \\
&= \sum_{n=1}^N \sum_{d=1}^{D_{L+1}} \mathbb{E} \left[\log(\eta_{L+1,d}^2)^{-1/2} \exp \left(-\frac{1}{2\eta_{L+1,d}^2} (y_{n,d} - \mathbf{W}_{L+1,d} \mathbf{a}_{n,L} - b_{L+1,d})^2 \right) \right] - \frac{ND_{L+1}}{2} \log(2\pi) \\
&+ \sum_{n=1}^N \sum_{l=1}^L \sum_{d=1}^{D_l} \mathbb{E} \left[\log(\eta_{l,d}^2)^{-1/2} \exp \left(-\frac{1}{2\eta_{l,d}^2} (\mathbf{a}_{n,l,d} - \gamma_{n,l,d} \odot (\mathbf{W}_{l,d} \mathbf{a}_{n,l-1} + b_{l,d}))^2 \right) \right] - N \sum_{l=1}^L D_l \log(2) \\
&+ \frac{1}{T} \sum_{n=1}^N \sum_{l=1}^L \sum_{d=1}^{D_l} \mathbb{E} \left[\left(\gamma_{n,l,d} - \frac{1}{2} \right) (\mathbf{W}_{l,d} \mathbf{a}_{n,l-1} + b_{l,d}) \right] - \frac{1}{2T^2} \sum_{n=1}^N \sum_{l=1}^L \sum_{d=1}^{D_l} \mathbb{E} [\omega_{n,l,d} (\mathbf{W}_{l,d} \mathbf{a}_{n,l-1} + b_{l,d})^2] \\
&- \sum_{n=1}^N \sum_{l=1}^L \mathbb{E} \left[\log |\mathbf{S}_{n,l}|^{-\frac{1}{2}} \exp \left(-\frac{1}{2} (\mathbf{a}_{n,l} - \mathbf{t}_{n,l} - \mathbf{M}_{n,l} \mathbf{a}_{n,l-1})^T \mathbf{S}_{n,l}^{-1} (\mathbf{a}_{n,l} - \mathbf{t}_{n,l} - \mathbf{M}_{n,l} \mathbf{a}_{n,l-1}) \right) \right] \\
&- \sum_{n=1}^N \sum_{l=1}^L \sum_{d=1}^{D_l} (\rho_{n,l,d} \log \rho_{n,l,d} + (1 - \rho_{n,l,d}) \log(1 - \rho_{n,l,d})) + \sum_{n=1}^N \sum_{l=1}^L \sum_{d=1}^{D_l} \mathbb{E} \left[\log \frac{\text{PG}(\omega_{n,l,d} | 1, 0)}{\text{PG}(\omega_{n,l,d} | 1, A_{n,l,d})} \right] \\
&= -\frac{1}{2} \sum_{n=1}^N \sum_{d=1}^{D_{L+1}} \mathbb{E} \left[\frac{1}{\eta_{L+1,d}^2} \right] \left(y_{n,d}^2 - 2y_{n,d} \mathbb{E} [\widetilde{\mathbf{W}}_{L+1,d}] \mathbb{E} [\widetilde{\mathbf{a}}_{n,L}] + \text{Tr} \left(\mathbb{E} [\widetilde{\mathbf{W}}_{L+1,d}^T \widetilde{\mathbf{W}}_{L+1,d}] \mathbb{E} [\widetilde{\mathbf{a}}_{n,L} \widetilde{\mathbf{a}}_{n,L}^T] \right) \right) \\
&- \frac{1}{2} \sum_{n=1}^N \sum_{l=1}^L \sum_{d=1}^{D_l} \mathbb{E} \left[\frac{1}{\eta_{l,d}^2} \right] \left(\mathbb{E} [\mathbf{a}_{n,l,d}^2] - 2\mathbb{E} [\gamma_{n,l,d}] \mathbb{E} [\widetilde{\mathbf{W}}_{l,d}] \mathbb{E} [\widetilde{\mathbf{a}}_{n,l-1} \mathbf{a}_{n,l,d}] \right) \\
&- \frac{1}{2} \sum_{n=1}^N \sum_{l=1}^L \sum_{d=1}^{D_l} \mathbb{E} \left[\frac{1}{\eta_{l,d}^2} \right] \mathbb{E} [\gamma_{n,l,d}^2] \text{Tr} \left(\mathbb{E} [\widetilde{\mathbf{W}}_{l,d}^T \widetilde{\mathbf{W}}_{l,d}] \mathbb{E} [\widetilde{\mathbf{a}}_{n,l-1} \widetilde{\mathbf{a}}_{n,l-1}^T] \right) \\
&- \frac{N}{2} \sum_{d=1}^{D_{L+1}} \mathbb{E} [\log \eta_{L+1,d}^2] - \frac{N}{2} \sum_{l=1}^L \sum_{d=1}^{D_l} \mathbb{E} [\log \eta_{l,d}^2] + \frac{1}{2} \sum_{n=1}^N \sum_{l=1}^L \log(|\mathbf{S}_{n,l}|) \\
&+ \sum_{n=1}^N \sum_{l=1}^L \sum_{d=1}^{D_l} \left(\frac{1}{T} \left(\rho_{n,l,d} - \frac{1}{2} \right) \mathbb{E} [\widetilde{\mathbf{W}}_{l,d}] \mathbb{E} [\widetilde{\mathbf{a}}_{n,l-1}] - \frac{1}{2T^2} \mathbb{E} [\omega_{n,l,d}] \left(\text{Tr} \left(\mathbb{E} [\widetilde{\mathbf{W}}_{l,d}^T \widetilde{\mathbf{W}}_{l,d}] \mathbb{E} [\widetilde{\mathbf{a}}_{n,l-1} \widetilde{\mathbf{a}}_{n,l-1}^T] \right) \right) \right) \\
&- \sum_{n=1}^N \sum_{l=1}^L \sum_{d=1}^{D_l} \left(\rho_{n,l,d} \log \rho_{n,l,d} + (1 - \rho_{n,l,d}) \log(1 - \rho_{n,l,d}) - \frac{A_{n,l,d}^2}{2} \mathbb{E} [\omega_{n,l,d}] + \log(\cosh(\frac{A_{n,l,d}}{2})) \right) + C_a,
\end{aligned}$$

where the normalizing constant is

$$C_a = -\frac{ND_{L+1}}{2} \log(2\pi) - N \sum_{l=1}^L D_l \log(2).$$

Total ELBO Then, we can sum the derived parts above to get the total ELBO of our model:

$$\text{ELBO} = \text{const.} + \sum_{l=1}^{L+1} \frac{1}{2} \mathbb{E} \left[\frac{1}{\tau_l} \right] \left(\hat{\delta}_{\text{glob},l}^2 - \delta_{\text{glob}}^2 \right) + (\hat{\nu}_{\text{glob},l} \log(\hat{\delta}_{\text{glob},l}) + \log(K_{\hat{\nu}_{\text{glob},l}}(\lambda_{\text{glob}} \hat{\delta}_{\text{glob},l})))$$

$$\begin{aligned}
& + \sum_{l=1}^{L+1} \sum_{d=1}^{D_l} \sum_{d'=1}^{D_{l-1}} \frac{1}{2} \mathbb{E} \left[\frac{1}{\psi_{l,d,d'}} \right] \left(\hat{\delta}_{\text{loc},l,d,d'}^2 - \delta_{\text{loc},l}^2 \right) + \hat{\nu}_{\text{loc},l,d,d'} \log(\hat{\delta}_{\text{loc},l,d,d'}) + \log(K \hat{\nu}_{\text{loc},l,d,d'} (\lambda_{\text{loc},l} \hat{\delta}_{\text{loc},l,d,d'})) \\
& + \sum_{l=1}^{L+1} \sum_{d=1}^{D_l} \mathbb{E} \left[\frac{1}{\eta_{l,d}^2} \right] \left(\beta_{l,d} - \beta_0^l \right) - \alpha_{l,d} \log \beta_{l,d} + \frac{1}{2} \log |\mathbf{B}_{l,d}| - \frac{1}{2} \left(\frac{1}{s_0^2} \mathbb{E}[b_{l,d}^2] + \sum_{d'=1}^{D_{l-1}} \mathbb{E} \left[\frac{1}{\tau_l} \right] \mathbb{E} \left[\frac{1}{\psi_{l,d,d'}} \right] \mathbb{E}[w_{l,d,d'}^2] \right) \\
& + \frac{1}{2} \sum_{n=1}^N \sum_{l=1}^L \log(\mathbf{S}_{n,l}) - \frac{1}{2} \sum_{d=1}^{D_y} \mathbb{E} \left[\frac{1}{\eta_{L+1,d}^2} \right] \left(\sum_{n=1}^N \mathbb{E} \left[\left(y_{n,d} - \mathbb{E}[\tilde{\mathbf{W}}_{L+1,d}] \mathbb{E}[\tilde{\mathbf{a}}_{n,L}] \right)^2 \right] \right) \\
& - \frac{1}{2} \sum_{d=1}^{D_y} \mathbb{E} \left[\frac{1}{\eta_{L+1,d}^2} \right] \left(\sum_{n=1}^N \text{Tr}((\mathbf{B}_{L+1,d} + \mathbf{m}_{L+1,d} \mathbf{m}_{L+1,d}^T) \mathbb{E}[\tilde{\mathbf{a}}_{n,L} \tilde{\mathbf{a}}_{n,L}^T]) - \text{Tr}(\mathbf{m}_{L+1,d} \mathbf{m}_{L+1,d}^T \mathbb{E}[\tilde{\mathbf{a}}_{n,L}] \mathbb{E}[\tilde{\mathbf{a}}_{n,L}^T]) \right) \\
& - \frac{1}{2} \sum_{l=1}^L \sum_{d=1}^{D_l} \mathbb{E} \left[\frac{1}{\eta_{l,d}^2} \right] \left(\sum_{n=1}^N \left(\rho_{n,l,d} \mathbb{E}[\tilde{\mathbf{W}}_{l,d}] \mathbb{E}[\tilde{\mathbf{a}}_{n,l-1}] - \mathbb{E}[\mathbf{a}_{n,l,d}] \right)^2 + \mathbb{E}[\mathbf{a}_{n,l,d}^2] - \mathbb{E}[\mathbf{a}_{n,l,d}]^2 \right) \\
& - \frac{1}{2} \sum_{l=1}^L \sum_{d=1}^{D_l} \mathbb{E} \left[\frac{1}{\eta_{l,d}^2} \right] \left(\sum_{n=1}^N \rho_{n,l,d} \text{Tr}((\mathbf{B}_{l,d} + \mathbf{m}_{l,d} \mathbf{m}_{l,d}^T) \mathbb{E}[\tilde{\mathbf{a}}_{n,l-1} \tilde{\mathbf{a}}_{n,l-1}^T]) - \rho_{n,l,d}^2 \text{Tr}(\mathbf{m}_{l,d} \mathbf{m}_{l,d}^T \mathbb{E}[\tilde{\mathbf{a}}_{n,l-1}] \mathbb{E}[\tilde{\mathbf{a}}_{n,l-1}^T]) \right) \\
& - \sum_{l=1}^L \sum_{d=1}^{D_l} \mathbb{E} \left[\frac{1}{\eta_{l,d}^2} \right] \left(\sum_{n=1}^N \rho_{n,l,d} \mathbb{E}[\tilde{\mathbf{W}}_{l,d}] (\mathbb{E}[\mathbf{a}_{n,l,d}] \mathbb{E}[\tilde{\mathbf{a}}_{n,l-1}] - \mathbb{E}[\mathbf{a}_{n,l,d} \tilde{\mathbf{a}}_{n,l-1}]) \right) \\
& + \sum_{n=1}^N \sum_{l=1}^L \sum_{d=1}^{D_l} \frac{1}{T} \left(\rho_{n,l,d} - \frac{1}{2} \right) \left(\mathbb{E}[\tilde{\mathbf{W}}_{l,d}] \mathbb{E}[\tilde{\mathbf{a}}_{n,l-1}] \right) - \frac{1}{2T^2} \mathbb{E}[\omega_{n,l,d}] \left(\text{Tr}((\mathbf{B}_{l,d} + \mathbf{m}_{l,d} \mathbf{m}_{l,d}^T) \mathbb{E}[\tilde{\mathbf{a}}_{n,l-1} \tilde{\mathbf{a}}_{n,l-1}^T]) \right) \\
& - \sum_{n=1}^N \sum_{l=1}^L \sum_{d=1}^{D_l} (\rho_{n,l,d} \log \rho_{n,l,d} + (1 - \rho_{n,l,d}) \log(1 - \rho_{n,l,d})) - \frac{A_{n,l,d}^2}{2} \mathbb{E}[\omega_{n,l,d}] + \log(\cosh(A_{n,l,d}/2)).
\end{aligned}$$

Note that when implementing VI with EM scheme, we adjust the formula above by adding the term which arises in the normalizing constant C_τ defined when computing the ELBO of global shrinkage parameters, specifically, we add

$$\begin{aligned}
\text{ELBO}_{EM} & = (L+1) (\nu_{\text{glob}} (\log(\lambda_{\text{glob}}) - \log(\delta_{\text{glob}})) - \log(K \nu_{\text{glob}} (\lambda_{\text{glob}} \delta_{\text{glob}}))) \\
& + \sum_{l=1}^{L+1} (\nu_{\text{glob}} - 1) \mathbb{E}[\log \tau_l] - \frac{1}{2} \lambda_{\text{glob}}^2 \mathbb{E}[\tau_l] - \nu_l \log(\lambda_{\text{glob}}).
\end{aligned}$$

B.2 ELBO for prediction

To obtain the posterior predictive distribution, we compute the approximate variational predictive distributions of \mathbf{a}_* , γ_* and ω_* with the objective function being the ELBO of Equation (10). Thus, in the predictive step of our algorithm, we monitor the convergence of the ELBO of \mathbf{a}_* , γ_* and ω_* , which we derive as follows:

$$\begin{aligned}
& \mathbb{E}[\log p(\mathbf{a}_*, \gamma_*, \omega_* | \mathbf{W}, \mathbf{b}, \boldsymbol{\Sigma})] - \mathbb{E}[\log q(\mathbf{a}_*)] - \mathbb{E}[\log q(\gamma_*)] - \mathbb{E}[\log q(\omega_*)] \\
& = \sum_{l=1}^L \sum_{d=1}^{D_l} \mathbb{E}[\log \text{N}(a_{*,l,d} | \gamma_{*,l,d} \odot \mathbf{z}_{*,l,d}, \boldsymbol{\Sigma}_{l,d})] + \mathbb{E} \left[\log \left(\exp \left(\frac{\kappa_{*,l,d} z_{*,l,d}}{T} \right) \exp \left(-\frac{\omega_{*,l,d} z_{*,l,d}^2}{2T^2} \right) \text{PG}(\omega_{n,l,d} | 1, 0) \right) \right] - \\
& - \sum_{l=1}^L \mathbb{E}[\log \text{N}(\mathbf{a}_{*,l} | \mathbf{t}_{*,l} + \mathbf{M}_{*,l} \mathbf{a}_{*,l-1}, \mathbf{S}_{*,l})] - \sum_{l=1}^L \sum_{d=1}^{D_l} (\mathbb{E}[\log \text{Bern}(\gamma_{*,l,d} | \rho_{*,l,d})] + \mathbb{E}[\log \text{PG}(\omega_{*,l,d} | 1, A_{*,l,d})]) \\
& = -\frac{1}{2} \sum_{l=1}^L \sum_{d=1}^{D_l} \mathbb{E} \left[\frac{1}{\eta_{l,d}^2} \right] \left(\mathbb{E}[a_{*,l,d}^2] - 2 \mathbb{E}[\gamma_{*,l,d}] \mathbb{E}[\tilde{\mathbf{W}}_{l,d}] \mathbb{E}[\tilde{\mathbf{a}}_{*,l-1} a_{*,l,d}] \right) \\
& - \frac{1}{2} \sum_{l=1}^L \sum_{d=1}^{D_l} \mathbb{E}[\log \eta_{l,d}^2] + \frac{1}{2} \sum_{l=1}^L \log(|\mathbf{S}_{*,l}|) + \frac{1}{T} \sum_{l=1}^L \sum_{d=1}^{D_l} \left(\rho_{*,l,d} - \frac{1}{2} \right) \mathbb{E}[\tilde{\mathbf{W}}_{l,d}] \mathbb{E}[\tilde{\mathbf{a}}_{*,l-1}]
\end{aligned}$$

$$\begin{aligned}
& -\frac{1}{2} \sum_{l=1}^L \sum_{d=1}^{D_l} \left(\mathbb{E} \left[\frac{1}{\eta_{l,d}^2} \right] \mathbb{E} [\gamma_{*,l,d}^2] + \frac{1}{T^2} \mathbb{E} [\omega_{*,l,d}] \right) \text{Tr} \left(\mathbb{E} [\tilde{\mathbf{W}}_{l,d}^T \tilde{\mathbf{W}}_{l,d}] \mathbb{E} [\tilde{\mathbf{a}}_{*,l-1} \tilde{\mathbf{a}}_{*,l-1}^T] \right) \\
& - \sum_{l=1}^L \sum_{d=1}^{D_l} (\rho_{*,l,d} \log \rho_{*,l,d} + (1 - \rho_{*,l,d}) \log(1 - \rho_{*,l,d})) \\
& + \sum_{l=1}^L \sum_{d=1}^{D_l} \frac{A_{*,l,d}^2}{2} \mathbb{E} [\omega_{*,l,d}] - \sum_{l=1}^L \sum_{d=1}^{D_l} \log(\cosh(\frac{A_{*,l,d}}{2})) + \text{const} \\
& = -\frac{1}{2} \sum_{l=1}^L \sum_{d=1}^{D_l} \mathbb{E} \left[\frac{1}{\eta_{l,d}^2} \right] \left(\left(\rho_{*,l,d} \mathbb{E} [\tilde{\mathbf{W}}_{l,d}] \mathbb{E} [\tilde{\mathbf{a}}_{*,l-1}] - \mathbb{E} [a_{*,l,d}] \right)^2 + \mathbb{E} [a_{*,l,d}^2] - \mathbb{E} [a_{*,l,d}]^2 \right) \\
& - \frac{1}{2} \sum_{l=1}^L \sum_{d=1}^{D_l} \mathbb{E} \left[\frac{1}{\eta_{l,d}^2} \right] \left(\rho_{*,l,d} \text{Tr} ((\mathbf{B}_{l,d} + \mathbf{m}_{l,d} \mathbf{m}_{l,d}^T) \mathbb{E} [\tilde{\mathbf{a}}_{*,l-1} \tilde{\mathbf{a}}_{*,l-1}^T]) - \rho_{*,l,d}^2 \text{Tr} (\mathbf{m}_{l,d} \mathbf{m}_{l,d}^T \mathbb{E} [\tilde{\mathbf{a}}_{*,l-1}] \mathbb{E} [\tilde{\mathbf{a}}_{*,l-1}^T]) \right) \\
& - \sum_{l=1}^L \sum_{d=1}^{D_l} \mathbb{E} \left[\frac{1}{\eta_{l,d}^2} \right] \left(\rho_{*,l,d} \mathbb{E} [\tilde{\mathbf{W}}_{l,d}] (\mathbb{E} [\mathbf{a}_{*,l,d}] \mathbb{E} [\tilde{\mathbf{a}}_{*,l-1}] - \mathbb{E} [a_{*,l,d} \tilde{\mathbf{a}}_{*,l-1}]) \right) + \frac{1}{2} \mathbb{E} [\log \eta_{l,d}^2] \\
& + \frac{1}{2} \sum_{l=1}^L \log(|\mathbf{S}_{*,l}|) + \sum_{l=1}^L \sum_{d=1}^{D_l} \frac{1}{T} \left(\rho_{*,l,d} - \frac{1}{2} \right) \mathbb{E} [\tilde{\mathbf{W}}_{l,d}] \mathbb{E} [\tilde{\mathbf{a}}_{*,l-1}] + \frac{1}{2T^2} (\mathbb{E} [\omega_{*,l,d}]) \text{Tr} (\mathbb{E} [\tilde{\mathbf{W}}_{l,d}^T \tilde{\mathbf{W}}_{l,d}] \mathbb{E} [\tilde{\mathbf{a}}_{*,l-1} \tilde{\mathbf{a}}_{*,l-1}^T]) \\
& - \sum_{l=1}^L \sum_{d=1}^{D_l} \left(\rho_{*,l,d} \log \rho_{*,l,d} + (1 - \rho_{*,l,d}) \log(1 - \rho_{*,l,d}) - \frac{A_{*,l,d}^2}{2} \mathbb{E} [\omega_{*,l,d}] + \log(\cosh(\frac{A_{*,l,d}}{2})) \right) + \text{const}.
\end{aligned}$$

The complexity of obtaining variational update for \mathbf{a} is then $\mathcal{O}(NLD^3)$.

C Supplementary details for the stochastic variational inference algorithm

Here we provide additional details on the SVI developed for the VBNN in [Section 3.3](#). During one iteration t of the algorithm, one proceeds as follows:

1. Sample indices S_t uniformly, without replacement.
2. For $t = 1$ initialize as in [Appendix D.1](#) (similarly to CAVI) but where the input of [Algorithm 3](#) is taken to be \mathbf{x}_n for $n \in S_t$. For $t > 1$ only initialize local parameters of \mathbf{a} and γ by setting $\mathbf{z}_{n,0} = \mathbf{x}_n$ and iterating for $l = 1, \dots, L$ and $n \in S_t$ through

$$\begin{aligned}
\rho_{n,l,d} &= \sigma \left(\frac{(m_{l,d}^b)^{(t)} + (\mathbf{m}_{l,d}^W)^{(t)} \mathbf{z}_{n,l-1}}{T} \right) \quad d = 1, \dots, D_l, \\
\mathbf{M}_{n,l} &= (\mathbf{m}_l^W)^{(t)} \odot \rho_{n,l} \mathbf{1}_{D_l}^T, \text{ where by } \mathbf{1} \text{ we denote a vector of ones,} \\
\mathbf{t}_{n,l} &= (m_l^b)^{(t)} \odot \rho_{n,l}, \\
\mathbf{z}_{n,l} &= \mathbf{M}_{n,l} \mathbf{z}_{n,l-1} + \mathbf{t}_{n,l}.
\end{aligned}$$

3. Set $\ell_t = (t+1)^{-k}$, $k \in (0.5, 1]$.
4. Update global shrinkage parameters of $\boldsymbol{\tau}$ as in CAVI, for $l = 1, \dots, L+1$,

$$\begin{aligned}
\nu_{\text{glob},l}^{(t)} &= \nu_{\text{glob}} - \frac{D_l D_{l-1}}{2}, \\
\delta_{\text{glob},l}^{(t)} &= \sqrt{\delta_{\text{glob}}^2 + \sum_d \sum_{d'} \mathbb{E} \left[\frac{1}{\psi_{l,d,d'}} \right] \mathbb{E} [W_{l,d,d'}^2]},
\end{aligned}$$

where $\nu_{\text{glob},l}$ is only updated in the first iteration of the algorithm.

5. Update local shrinkage parameters of ψ as in CAVI, for $l = 1, \dots, L+1$, $d = 1, \dots, D_l$, $d' = 1, \dots, D_{l-1}$,

$$\nu_{\text{loc},l,d,d'}^{(t)} = \nu_{\text{loc},l} - \frac{1}{2},$$

$$\delta_{\text{loc},l,d,d'}^{(t)} = \sqrt{\mathbb{E} \left[\frac{1}{\eta_l} \right] \mathbb{E} [W_{l,d,d'}^2] + \delta_{\text{loc},l}^2},$$

where $\nu_{\text{loc},l,d,d'}$ is only updated once.

6. Find optimal variational parameters of local variables ω , γ , \mathbf{a} , namely, update $A^{(t)}$, $\mathbf{S}^{(t)}$, $\mathbf{t}^{(t)}$, $\mathbf{M}^{(t)}$, $\rho^{(t)}$ in a coordinate ascent algorithm and monitor the local ELBO for convergence:

- For $n \in S$, $l = 1, \dots, L$, $d = 1, \dots, D_l$, update

$$\mathbf{a}_{n,l,d} = \frac{1}{T} \sqrt{\left(\text{Tr} \left(\mathbb{E} [\widetilde{\mathbf{W}}_{l,d}^T \widetilde{\mathbf{W}}_{l,d}] \mathbb{E} [\widetilde{\mathbf{a}}_{n,l-1} \widetilde{\mathbf{a}}_{n,l-1}^T] \right) \right)}.$$

- Starting from the final layer $l = L$, update for $n \in S$

$$\begin{aligned} \mathbf{S}_{n,L}^{-1} &= \hat{\mathbf{\Sigma}}_L^{-1} + \sum_{d=1}^{D_{L+1}} \mathbb{E} \left[\frac{1}{\eta_{L+1,d}^2} \right] \mathbb{E} [\mathbf{W}_{L+1,d}^T \mathbf{W}_{L+1,d}] \quad (\text{same for all } n), \\ \mathbf{t}_{n,L} &= \mathbf{S}_L \left(\hat{\mathbf{\Sigma}}_L^{-1} \mathbb{E} [\gamma_{n,L}] \odot \mathbb{E} [\mathbf{b}_L] \right. \\ &\quad \left. + \sum_{d=1}^{D_{L+1}} \mathbb{E} \left[\frac{1}{\eta_{L+1,d}^2} \right] (-\mathbb{E} [\mathbf{W}_{L+1,d}^T b_{L+1,d}] + \mathbb{E} [\mathbf{W}_{L+1,d}^T] y_{n,d}) \right), \\ \mathbf{M}_{n,L} &= \mathbf{S}_L \hat{\mathbf{\Sigma}}_L^{-1} \mathbb{E} [\gamma_{n,L}] \mathbf{1}_{D_{L-1}}^T \odot \mathbb{E} [\mathbf{W}_L], \\ \hat{\mathbf{\Sigma}}_L^{-1} &= \text{diag} \left(\mathbb{E} [\eta_{L,1}^{-2}], \dots, \mathbb{E} [\eta_{L,D_L}^{-2}] \right). \end{aligned}$$

Then, in reverse order, for $l = L-1, \dots, 1$ and for $n \in S$ update

$$\begin{aligned} \mathbf{S}_{n,l}^{-1} &= \hat{\mathbf{\Sigma}}_l^{-1} - \mathbf{M}_{n,l+1}^T \mathbf{S}_{n,l+1}^{-1} \mathbf{M}_{n,l+1} \\ &\quad + \sum_{d=1}^{D_{l+1}} \left(\mathbb{E} \left[\frac{1}{\eta_{l+1,d}^2} \right] \mathbb{E} [\gamma_{n,l+1,d}] + \frac{1}{T^2} \mathbb{E} [\omega_{n,l+1,d}] \right) \mathbb{E} [\mathbf{W}_{l+1,d}^T \mathbf{W}_{l+1,d}], \\ \mathbf{t}_{n,l} &= \mathbf{S}_{n,l} \left(\mathbf{M}_{n,l+1}^T \mathbf{S}_{n,l+1}^{-1} \mathbf{t}_{n,l+1} + \hat{\mathbf{\Sigma}}_l^{-1} \mathbb{E} [\gamma_{n,l}] \odot \mathbb{E} [\mathbf{b}_l] \right. \\ &\quad \left. + \frac{1}{T} \sum_{d=1}^{D_{l+1}} \mathbb{E} [\mathbf{W}_{l+1,d}^T] \left(\mathbb{E} [\gamma_{n,l+1,d}] - \frac{1}{2} \right) \right. \\ &\quad \left. - \sum_{d=1}^{D_{l+1}} \left(\mathbb{E} \left[\frac{1}{\eta_{l+1,d}^2} \right] \mathbb{E} [\gamma_{n,l+1,d}] + \frac{1}{T^2} \mathbb{E} [\omega_{n,l+1,d}] \right) \mathbb{E} [\mathbf{W}_{l+1,d} b_{l+1,d}] \right), \\ \mathbf{M}_{n,l} &= \mathbf{S}_{n,l} \hat{\mathbf{\Sigma}}_l^{-1} \mathbb{E} [\gamma_{n,l}] \mathbf{1}_{D_{l-1}}^T \odot \mathbb{E} [\mathbf{W}_l], \\ \hat{\mathbf{\Sigma}}_l^{-1} &= \text{diag} \left(\mathbb{E} [\eta_{l,1}^{-2}], \dots, \mathbb{E} [\eta_{l,D_l}^{-2}] \right). \end{aligned}$$

- For $n \in S$, $l = 1, \dots, L$, $d = 1, \dots, D_l$, update

$$\begin{aligned} \rho_{n,l,d} &= \sigma \left(-\frac{\mathbb{E} [\eta_{l,d}^{-2}]}{2} \text{Tr} \left(\mathbb{E} [\widetilde{\mathbf{W}}_{l,d}^T \widetilde{\mathbf{W}}_{l,d}] \mathbb{E} [\widetilde{\mathbf{a}}_{n,l-1} \widetilde{\mathbf{a}}_{n,l-1}^T] \right) \right. \\ &\quad \left. + \mathbb{E} [\eta_{l,d}^{-2}] \mathbb{E} [\widetilde{\mathbf{W}}_{l,d}] \mathbb{E} [\widetilde{\mathbf{a}}_{n,l-1} \mathbf{a}_{n,l,d}] + \frac{1}{T} \mathbb{E} [\widetilde{\mathbf{W}}_{l,d}] \mathbb{E} [\widetilde{\mathbf{a}}_{n,l-1}] \right). \end{aligned}$$

The local ELBO is given by

$$\begin{aligned}
& \mathbb{E} [\log p(\mathbf{y}, \mathbf{a}, \boldsymbol{\gamma}, \boldsymbol{\omega} | \mathbf{W}, \mathbf{b}, \boldsymbol{\Sigma})] - \mathbb{E} [\log q(\mathbf{a})] - \mathbb{E} [\log q(\boldsymbol{\gamma})] - \mathbb{E} [\log q(\boldsymbol{\omega})] \\
&= \frac{N}{|S|} \sum_{n \in S} \sum_{d=1}^{D_{L+1}} \mathbb{E} [\log N(y_{n,d} | \mathbf{z}_{n,L+1,d}, \boldsymbol{\Sigma}_{L+1,d})] \\
&+ \frac{N}{|S|} \sum_{n \in S} \sum_{l=1}^L \sum_{d=1}^{D_l} \mathbb{E} [\log N(\mathbf{a}_{n,l,d} | \boldsymbol{\gamma}_{n,l,d} \odot \mathbf{z}_{n,l,d}, \boldsymbol{\Sigma}_{l,d})] \\
&+ \frac{N}{|S|} \sum_{n \in S} \sum_{l=1}^L \sum_{d=1}^{D_l} \mathbb{E} \left[\log \left(\exp \left(\frac{\kappa_{n,l,d} z_{n,l,d}}{T} \right) \exp \left(-\frac{\omega_{n,l,d} z_{n,l,d}^2}{2T^2} \right) \text{PG}(\omega_{n,l,d} | 1, 0) \right) \right] \\
&- \frac{N}{|S|} \sum_{n \in S} \sum_{l=1}^L \mathbb{E} [\log N(\mathbf{a}_{n,l} | \mathbf{t}_{n,l} + \mathbf{M}_{n,l} \mathbf{a}_{n,l-1}, \mathbf{S}_{n,l})] \\
&- \frac{N}{|S|} \sum_{n \in S} \sum_{l=1}^L \sum_{d=1}^{D_l} \mathbb{E} [\log \text{Bern}(\gamma_{n,l,d} | \rho_{n,l,d})] + \mathbb{E} [\log \text{PG}(\omega_{n,l,d} | 1, \mathbf{a}_{n,l,d})] \\
&= \frac{N}{|S|} \sum_{n \in S} \sum_{d=1}^{D_{L+1}} \mathbb{E} \left[\log(\eta_{L+1,d}^2)^{-1/2} \exp \left(-\frac{1}{2\eta_{L+1,d}^2} (y_{n,d} - \mathbf{W}_{L+1,d} \mathbf{a}_{n,L} - b_{L+1,d})^2 \right) \right] \\
&+ \frac{N}{|S|} \sum_{n \in S} \sum_{l=1}^L \sum_{d=1}^{D_l} \mathbb{E} \left[\log(\eta_{l,d}^2)^{-1/2} \exp \left(-\frac{1}{2\eta_{l,d}^2} (\mathbf{a}_{n,l,d} - \gamma_{n,l,d} \odot (\mathbf{W}_{l,d} \mathbf{a}_{n,l-1} + b_{l,d}))^2 \right) \right] \\
&- N \sum_{l=1}^L D_l \log(2) - \frac{ND_{L+1}}{2} \log(2\pi) \\
&+ \frac{1}{T} \frac{N}{|S|} \sum_{n \in S} \sum_{l=1}^L \sum_{d=1}^{D_l} \mathbb{E} \left[\left(\gamma_{n,d} - \frac{1}{2} \right) (\mathbf{W}_{l,d} \mathbf{a}_{n,l-1} + b_{l,d}) \right] \\
&- \frac{1}{2T^2} \frac{N}{|S|} \sum_{n \in S} \sum_{l=1}^L \sum_{d=1}^{D_l} \mathbb{E} [\omega_{n,l,d} (\mathbf{W}_{l,d} \mathbf{a}_{n,l-1} + b_{l,d})^2] \\
&- \frac{N}{|S|} \sum_{n \in S} \sum_{l=1}^L \mathbb{E} [\log |\mathbf{S}_{n,l}|^{-\frac{1}{2}}] \\
&- \frac{N}{|S|} \sum_{n \in S} \sum_{l=1}^L \mathbb{E} \left[-\frac{1}{2} (\mathbf{a}_{n,l} - \mathbf{t}_{n,l} - \mathbf{M}_{n,l} \mathbf{a}_{n,l-1})^T \mathbf{S}_{n,l}^{-1} (\mathbf{a}_{n,l} - \mathbf{t}_{n,l} - \mathbf{M}_{n,l} \mathbf{a}_{n,l-1}) \right] \\
&- \frac{N}{|S|} \sum_{n \in S} \sum_{l=1}^L \sum_{d=1}^{D_l} (\rho_{n,l,d} \log \rho_{n,l,d} + (1 - \rho_{n,l,d}) \log(1 - \rho_{n,l,d})) \\
&+ \frac{N}{|S|} \sum_{n \in S} \sum_{l=1}^L \sum_{d=1}^{D_l} \mathbb{E} \left[\log \frac{\text{PG}(\omega_{n,l,d} | 1, 0)}{\text{PG}(\omega_{n,l,d} | 1, A_{n,d})} \right] \\
&= -\frac{1}{2} \frac{N}{|S|} \sum_{n \in S} \sum_{d=1}^{D_{L+1}} \mathbb{E} \left[\frac{1}{\eta_{L+1,d}^2} \right] (y_{n,d}^2 - 2y_{n,d} \mathbb{E} [\widetilde{\mathbf{W}}_{L+1,d}] \mathbb{E} [\tilde{\mathbf{a}}_{n,L}]) \\
&- \frac{1}{2} \frac{N}{|S|} \sum_{n \in S} \sum_{d=1}^{D_{L+1}} \mathbb{E} \left[\frac{1}{\eta_{L+1,d}^2} \right] (\text{Tr} (\mathbb{E} [\widetilde{\mathbf{W}}_{L+1,d}^T \widetilde{\mathbf{W}}_{L+1,d}] \mathbb{E} [\tilde{\mathbf{a}}_{n,L} \tilde{\mathbf{a}}_{n,L}^T])) \\
&- \frac{1}{2} \frac{N}{|S|} \sum_{n \in S} \sum_{l=1}^L \sum_{d=1}^{D_l} \mathbb{E} \left[\frac{1}{\eta_{l,d}^2} \right] (\mathbb{E} [\mathbf{a}_{n,l,d}^2] - 2\mathbb{E} [\gamma_{n,l,d}] \mathbb{E} [\widetilde{\mathbf{W}}_{l,d}] \mathbb{E} [\tilde{\mathbf{a}}_{n,l-1} \mathbf{a}_{n,l,d}]) \\
&- \frac{1}{2} \frac{N}{|S|} \sum_{n \in S} \sum_{l=1}^L \sum_{d=1}^{D_l} \mathbb{E} \left[\frac{1}{\eta_{l,d}^2} \right] \mathbb{E} [\gamma_{n,l,d}^2] \text{Tr} (\mathbb{E} [\widetilde{\mathbf{W}}_{l,d}^T \widetilde{\mathbf{W}}_{l,d}] \mathbb{E} [\tilde{\mathbf{a}}_{n,l-1} \tilde{\mathbf{a}}_{n,l-1}^T]) \\
&- \frac{N}{2} \sum_{d=1}^{D_{L+1}} \mathbb{E} [\log \eta_{L+1,d}^2] - \frac{N}{2} \sum_{l=1}^L \sum_{d=1}^{D_l} \mathbb{E} [\log \eta_{l,d}^2] + \frac{1}{2} \sum_{n=1}^N \sum_{l=1}^L \log(|\mathbf{S}_{n,l}|)
\end{aligned}$$

$$\begin{aligned}
& + \frac{N}{|S|} \sum_{n \in S} \sum_{l=1}^L \sum_{d=1}^{D_l} \frac{1}{T} \left(\rho_{n,l,d} - \frac{1}{2} \right) \mathbb{E} [\widetilde{\mathbf{W}}_{l,d}] \mathbb{E} [\widetilde{\mathbf{a}}_{n,l-1}] \\
& - \frac{1}{2T^2} \frac{N}{|S|} \sum_{n \in S} \sum_{l=1}^L \sum_{d=1}^{D_l} \mathbb{E} [\omega_{n,l,d}] \left(\text{Tr} \left(\mathbb{E} [\widetilde{\mathbf{W}}_{l,d}^T \widetilde{\mathbf{W}}_{l,d}] \mathbb{E} [\widetilde{\mathbf{a}}_{n,l-1} \widetilde{\mathbf{a}}_{n,l-1}^T] \right) \right) \\
& - \frac{N}{|S|} \sum_{n \in S} \sum_{l=1}^L \sum_{d=1}^{D_l} \rho_{n,l,d} \log \rho_{n,l,d} + (1 - \rho_{n,l,d}) \log(1 - \rho_{n,l,d}) \\
& + \frac{N}{|S|} \sum_{n \in S} \sum_{l=1}^L \sum_{d=1}^{D_l} \frac{\mathbf{a}_{n,l,d}^2}{2} \mathbb{E} [\omega_{n,l,d}] - \log(\cosh(\frac{\mathbf{a}_{n,l,d}}{2})) + C_a,
\end{aligned}$$

where the normalizing constant is

$$C_a = -\frac{ND_{L+1}}{2} \log(2\pi) - N \sum_{l=1}^L D_l \log(2).$$

7. Find global variational parameters for which we recall the vector of natural parameters for (\mathbf{W}, \mathbf{b}) is $(\mathbf{B}^{-1} \mathbf{m}^T, -\mathbf{B}^{-1}/2)$, and for $\boldsymbol{\eta}^2$ that is $(-\boldsymbol{\alpha} + \mathbf{1}, -\boldsymbol{\beta}^{-1})$. We are only updating the parameter $\boldsymbol{\alpha}$ in the first iteration of the algorithm as

$$\begin{aligned}
\alpha_{l,d} &= \alpha_0^h + \frac{N}{2}, \text{ for } l = 1, \dots, L, \ d = 1, \dots, D_l, \\
\alpha_{L+1,d} &= \alpha_0 + \frac{N}{2} \text{ for } d = 1, \dots, D_{L+1}.
\end{aligned}$$

We then find $\boldsymbol{\beta}$ via the intermediate variable $\hat{\beta}_{l,d}$:

8. For $l = 1, \dots, L, \ d = 1, \dots, D_l$ set

$$\begin{aligned}
\hat{\beta}_{l,d} &= \beta_0^h + \frac{1}{2} \frac{N}{|S|} \sum_{n \in S} \left(\mathbb{E} [\mathbf{a}_{n,l,d}] - \mathbb{E} [\gamma_{n,l,d}] \mathbb{E} [\widetilde{\mathbf{W}}_{l,d}] \mathbb{E} [\widetilde{\mathbf{a}}_{n,l-1}] \right)^2 \\
& + \frac{1}{2} \frac{N}{|S|} \sum_{n \in S} \mathbb{E} [\mathbf{a}_{n,l,d}^2] - \mathbb{E} [\mathbf{a}_{n,l,d}]^2 + \mathbb{E} [\gamma_{n,l,d}] \text{Tr} \left(\mathbb{E} [\widetilde{\mathbf{W}}_{l,d}^T \widetilde{\mathbf{W}}_{l,d}] \mathbb{E} [\widetilde{\mathbf{a}}_{n,l-1} \widetilde{\mathbf{a}}_{n,l-1}^T] \right) \\
& - \frac{1}{2} \frac{N}{|S|} \sum_{n \in S} \mathbb{E} [\gamma_{n,l,d}]^2 \text{Tr} \left(\mathbb{E} [\widetilde{\mathbf{W}}_{l,d}^T] \mathbb{E} [\widetilde{\mathbf{W}}_{l,d}] \mathbb{E} [\widetilde{\mathbf{a}}_{n,l-1}] \mathbb{E} [\widetilde{\mathbf{a}}_{n,l-1}^T] \right).
\end{aligned}$$

And for the final layer $l = L + 1$ and $d = 1, \dots, D_{L+1}$

$$\begin{aligned}
\hat{\beta}_{L+1,d} &= \beta_0 + \frac{1}{2} \frac{N}{|S|} \sum_{n \in S} \left(y_{n,d} - \mathbb{E} [\widetilde{\mathbf{W}}_{L+1,d}] \mathbb{E} [\widetilde{\mathbf{a}}_{n,L}] \right)^2 \\
& + \frac{1}{2} \frac{N}{|S|} \sum_{n \in S} \text{Tr} \left(\mathbb{E} [\widetilde{\mathbf{W}}_{L+1,d}^T \widetilde{\mathbf{W}}_{L+1,d}] \mathbb{E} [\widetilde{\mathbf{a}}_{n,L} \widetilde{\mathbf{a}}_{n,L}^T] \right) \\
& - \frac{1}{2} \frac{N}{|S|} \sum_{n \in S} \text{Tr} \left(\mathbb{E} [\widetilde{\mathbf{W}}_{L+1,d}]^T \mathbb{E} [\widetilde{\mathbf{W}}_{L+1,d}] \mathbb{E} [\widetilde{\mathbf{a}}_{n,L}] \mathbb{E} [\widetilde{\mathbf{a}}_{n,L}^T] \right).
\end{aligned}$$

The update for $l = 1, \dots, L + 1, \ d = 1, \dots, D_l$ is given by

$$\beta_{l,d}^{(t)} = \left((1 - \ell_t) \times (\beta_{l,d}^{(t-1)})^{-1} + \ell_t \times \hat{\beta}_{l,d}^{-1} \right)^{-1}.$$

Similarly, the variational parameters \mathbf{B}, \mathbf{m} of global variables (\mathbf{b}, \mathbf{W}) are obtained as a reparametrized linear combination of previous and intermediate updates. Specifically, for $l = 1, \dots, L, \ d = 1, \dots, D_l$ set

$$\hat{\mathbf{B}}_{l,d}^{-1} = \mathbf{D}_{l,d}^{-1} + \frac{N}{|S|} \sum_{n \in S} \left(\frac{1}{T^2} \mathbb{E} [\omega_{n,l,d}] + \mathbb{E} [\eta_{l,d}^{-2}] \mathbb{E} [\gamma_{n,l,d}] \right) \mathbb{E} [\widetilde{\mathbf{a}}_{n,l-1} \widetilde{\mathbf{a}}_{n,l-1}^T],$$

$$\hat{\mathbf{B}}_{l,d}^{-1} \hat{\mathbf{m}}_{l,d}^T = \frac{N}{|S|} \sum_{n \in S} \mathbb{E} [\eta_{l,d}^{-2}] \mathbb{E} [\gamma_{n,l,d}] \mathbb{E} [\mathbf{a}_{n,l,d} \tilde{\mathbf{a}}_{n,l-1}] + \frac{1}{T} \mathbb{E} [\tilde{\mathbf{a}}_{n,l-1}] \left(\mathbb{E} [\gamma_{n,l,d}] - \frac{1}{2} \right).$$

For the final layer $l = L + 1$ and $d = 1, \dots, D_{L+1}$ set

$$\begin{aligned} \hat{\mathbf{B}}_{L+1,d}^{-1} &= \mathbf{D}_{L+1,d}^{-1} + \mathbb{E} [\eta_{L+1,d}^{-2}] \frac{N}{|S|} \sum_{n \in S} \mathbb{E} [\tilde{\mathbf{a}}_{n,L+1} \tilde{\mathbf{a}}_{n,L+1}^T], \\ \hat{\mathbf{B}}_{L+1,d}^{-1} \hat{\mathbf{m}}_{L+1,d}^T &= \mathbb{E} [\eta_{L+1,d}^{-2}] \left(\frac{N}{|S|} \sum_{n \in S} y_n \mathbb{E} [\tilde{\mathbf{a}}_{n,L+1}] \right), \end{aligned}$$

where for $l = 1, \dots, L + 1$ and $d = 1, \dots, D_l$,

$$\mathbf{D}_{l,d}^{-1} = \text{diag} \left(s_0^{-2}, \mathbb{E} [\tau_l^{-1}] \mathbb{E} [\psi_{l,d,1}^{-1}], \dots, \mathbb{E} [\tau_l^{-1}] \mathbb{E} [\psi_{l,d,D_{l-1}}^{-1}] \right).$$

Then the updates $l = 1, \dots, L + 1$ and $d = 1, \dots, D_l$, are given by

$$\begin{aligned} \mathbf{B}_{l,d}^{(t)} &= \left((1 - \ell_t) \times (\mathbf{B}_{l,d}^{(t-1)})^{-1} + \ell_t \times \hat{\mathbf{B}}_{l,d}^{-1} \right)^{-1}, \\ \mathbf{m}_{l,d}^{(t)} &= ((1 - \ell_t) \mathbf{B}_{l,d}^{(t)} (\mathbf{B}_{l,d}^{(t-1)})^{-1} (\mathbf{m}_{l,d}^{(t-1)})^T + \ell_t \mathbf{B}_{l,d}^{(t)} \hat{\mathbf{B}}_{l,d}^{-1} \hat{\mathbf{m}}_{l,d}^T)^T. \end{aligned}$$

We monitor the noisy estimate of the ELBO which is computed as in [Appendix B](#) but with sums over $n = 1, \dots, N$ replaced with the scaled sums over $n \in S$.

D Experiments

D.1 Initialization schemes

Initialization plays an important role in the ability of Bayesian inference algorithms to effectively approximate the posterior. This is especially true in variational schemes for complex posteriors (such as for BNNs), which are only guaranteed to converge to local optimum. We design two possible variations of random yet effective initialization schemes. To simplify the exposition, we describe the procedure in the case of Inverse Gamma shrinkage priors, for which $\lambda = 0$ and the selection of the scale parameters δ determines the level of shrinkage. Note that during the training step, we employ the expectation-maximization algorithm to set an optimal δ_{glob} , whilst the value of $\delta_{\text{loc},l}$ remains fixed. To encourage more shrinkage for larger depth, we assume $\delta_{\text{glob}} \propto 1/\sqrt{L}$, and to encourage shrinkage for larger width set $\delta_{\text{loc},l} \propto 1/\sqrt{D_l}$. Given specified values of $\nu_{\text{loc}}, \nu_{\text{glob}}, \delta_{\text{loc}}, \delta_{\text{glob}}, \alpha_0^h, \alpha_0, \beta_0^h, \beta_0$, we first re-scale the shrinkage parameters to scale appropriately

$$\delta_{\text{glob}} = \frac{\delta_{\text{glob}}}{\sqrt{L}}, \delta_{\text{loc},l} = \frac{\delta_{\text{loc}}}{\sqrt{D_{l-1}}}, \nu_{\text{loc},l} = \nu_{\text{loc}},$$

and the initialization steps are:

1. Covariance for biases and weights: $\mathbf{B}_{l,d} = 0.01 \mathbf{I}_{D_{l-1}+1}$ for $l = 1, \dots, L + 1, d = 1, \dots, D_l$.
2. Covariance for stochastic activation: $\mathbf{S}_{n,l} = 0.01 \mathbf{I}_{D_l}$ for $n = 1, \dots, N, l = 1, \dots, L$.
3. Variational parameters for $\boldsymbol{\eta}$: Set $\alpha_{L+1,d} = \alpha_0, \alpha_{l,d} = \alpha_0^h$ and $\beta_{L+1,d} = \beta_0, \beta_{l,d} = \beta_0^h$.
4. Variational parameters for $\boldsymbol{\tau}, \boldsymbol{\psi}$:

$$\begin{aligned} \nu_{\text{loc},l,d,d'} &= \nu_{\text{loc},l}, \nu_{\text{glob},l} = \nu_{\text{glob}}, \\ \delta_{\text{glob},l} &\sim \sqrt{2(\nu_{\text{glob},l} - 1) \text{IG}(\nu_{\text{glob},l}, \delta_{\text{glob}})}, \\ \delta_{\text{loc},l,d,d'} &\sim \sqrt{2(\nu_{\text{loc},l,d,d'} - 1) \text{IG}(\nu_{\text{loc},l,d,d'}, \delta_{\text{loc},l})}. \end{aligned}$$

5. Use [Algorithm 3](#) to initialize the variational means of the weights and biases for all intermediate layers, and the variational means of the stochastic activations and the variational parameters of the binary activations.
6. Variational mean of the weights and biases for the last layer \mathbf{m}_{L+1} is obtained as a solution of fitting D_y ridge regressions with inputs \mathbf{z}_L and outputs \mathbf{y}_d .

Algorithm 3 Initialization

Require: Training inputs \mathbf{x}_n , $n = 1, \dots, N$; choice of mode *laplace* or *spike-slab*

$\mathbf{z}_{n,0} = \mathbf{x}_n$

for $l = 1 \dots L$, **do**

 set $\Delta = 0.05 * (\max(\mathbf{z}_{n,l-1}) - \min(\mathbf{z}_{n,l-1}))$

for $d = 1 \dots D_l$ **do**

if *laplace* **then**

$$m_{l,d,d'}^W \sim \text{Laplace} \left(0, \sqrt{\frac{2}{D_{l-1}}} \right),$$

end if.

if *spike-slab* **then**

$$m_{l,d,d'}^W \sim \pi \text{N} \left(0, \frac{2}{\sqrt{D_{l-1}}} \right) + (1 - \pi) \delta_0, \text{ where } \pi = \frac{1}{1 + \sqrt{D_{l-1}}},$$

end if.

$\mathbf{s} = (s_1, \dots, s_{D_{l-1}})$, where $s_{d'} \sim \text{Unif}([\min(\mathbf{z}_{n,l-1,d'}) - \Delta_{d'}, \max(\mathbf{z}_{n,l-1,d'}) + \Delta_{d'}])$,

$m_{l,d}^b = -\mathbf{m}_{l,d}^W \mathbf{s}$, $\mathbf{m}_{l,d} = (m_{l,d}^b, \mathbf{m}_{l,d}^W)$,

end for.

$$\rho_{n,l,d} = \sigma \left(\frac{m_{l,d}^b + \mathbf{m}_{l,d}^W \mathbf{z}_{n,l-1}}{T} \right) \quad d = 1, \dots, D_l,$$

$\mathbf{M}_{n,l} = \mathbf{m}_l^W \odot \rho_{n,l} \mathbf{1}_{D_l}^T$, where by $\mathbf{1}$ we denote a vector of ones,

$\mathbf{t}_{n,l} = m_l^b \odot \rho_{n,l}$,

$\mathbf{z}_{n,l} = \mathbf{M}_{n,l} \mathbf{z}_{n,l-1} + \mathbf{t}_{n,l}$,

end for.

Ensure: $\mathbf{M}_{n,l}, \mathbf{t}_{n,l}, \mathbf{m}_{l,d}$ for $l = 1, \dots, L, d = 1, \dots, D_l$ and \mathbf{z}_L .

D.2 Implementation details

When comparing the performance of our method to already existing ones we implement the following model in Numpyro:

$$\mathbf{y} \sim \text{N}(\mathbf{W}_{L+1} \text{ReLU}(\mathbf{z}_L) + \mathbf{b}_L, \mathbf{\Sigma}), \text{ where } \mathbf{\Sigma} \sim \text{IG}(2, \sigma_y) \mathbf{I}_{D_y},$$

$$\mathbf{z}_l = \mathbf{W}_l \text{ReLU}(\mathbf{z}_{l-1}) + \mathbf{b}_l, W_{l,d,d'} \sim \text{N} \left(0, \frac{\sigma_W^2 \gamma}{\sqrt{D_{l-1}}} \right), \quad b_{l,d} \sim \text{N}(0, \sigma_b^2 \gamma),$$

where $\mathbf{z}_{n,0} = \mathbf{x}_n$, $\gamma \sim \text{IG}(2, 1)$ and $l = 1, \dots, L$, $d = 1, \dots, D_l$, $d' = 1, \dots, D_{l-1}$. The choice of σ_y, σ_W and σ_b is made in accordance with α_0, s_0 and $\delta_{\text{loc},l}$, respectively. For experiments with mfVI we use Adam optimizer with learning rate set to 0.001 and maximum number of iterations varying from 5000 to 20000 depending on the dataset and depth of the network. Additionally, we consider the Bayes by Backprop model of (Blundell et al., 2015) and adapt its Pytorch implementation from the publicly available repository (Javier, 2019). For all experiments with BBB we set the learning rate to 0.01 and maximum number of epochs varies from 500 to 1000.

In all examples, we normalize the input but do not re-scale the output. Suppose that the data on which we evaluate the predictive performance consists of N points and the true target is \mathbf{y}^* , then recorded evaluation metrics are RMSE, NLL and EC and are computed as follows:

$$\begin{aligned} \text{RMSE} &= \sqrt{\frac{1}{N} \sum_n [(y_n^* - \mathbb{E}[y_n^o])^2]}, \\ \text{NLL} &= \frac{1}{N} \sum_n \log \text{N}(y_n^* \mid \mathbb{E}[y_n^o], \text{Var}(y_n^o)) \\ \text{EC} &= \frac{\#\{\mathbf{y}^* \in [q_{0.025}^o, q_{0.975}^o]\}}{N}. \end{aligned}$$

where the predicted observations are \mathbf{y}^o and the corresponding quantiles are denoted as q^o . When computing quantiles to obtain empirical coverage and illustrating the uncertainty in Section 4 and below in Appendix D.3, we rely on the Gaussian approximation.

D.3 Supplementary material to the diabetes example.

Figure 12 supplements Table 3 and the diabetes example in Section 4.2. Here, in the case of VBNN, BBB and mfVI models we provide the uncertainty of the observations and in the case of the LassoCV we provide residual standard deviation. Additionally, we illustrate the sparse prediction and the uncertainty obtained from sparse weights of the VBNN, which largely coincide with the original prediction and uncertainty estimates. Whilst the coverage estimates for observations of VBNN and BBB are comparable, the mfVI underestimates the uncertainty and provides a dramatically lower coverage for observations.

D.4 Supplementary information on the datasets

Boston housing (Harrison and Rubinfeld, 1978): $n = 506, p = 13$, the predictors are per capita crime rate by town, the proportion of residential land zoned for lots over 25,000 sq.ft., the proportion of non-retail business acres per town, Charles River dummy variable, nitrite oxides concentration, average number of rooms per dwelling, the proportion of owner-occupied, units built before 1940, weighted distances to five Boston employment centres, index of accessibility to radial highways, full-value property-tax rate, the pupil-teacher ratio by town, the quantitative measure of systemic racism as a factor in house pricing, lower status of the population; the response of interest is the median value of owner-occupied homes. The Boston housing dataset is among the most popular pip available datasets, and with respect to variable selection, it was considered in e.g. (Schäfer and Chopin, 2013).

Energy (Tsanas and Xifara, 2012): $n = 768, p = 8$, the predictors are relative compactness, surface area, wall area, roof area, overall height, orientation, glazing area, and glazing area distribution, and the task is to predict the heating load of residential buildings.

Yacht dynamics (J. et al., 2013): $n = 308, p = 6$, the predictors are long position, prismatic coefficient, length-displacement ratio, beam-draught ratio, length-beam ratio and froude number, and the task is to model the residuary resistance per unit weight of displacement for a yacht hull.

Concrete compressive strength (Yeh, 2007): $n = 1030, p = 8$, the predictors are cement, furnace slag, fly ash, water, superplasticizer, coarse aggregate, fine aggregate and the age of testing, and the response variable is the compressive strength of concrete. This is also considered from the variable selection perspective in several works, including (Schäfer and Chopin, 2013; Griffin, 2024).

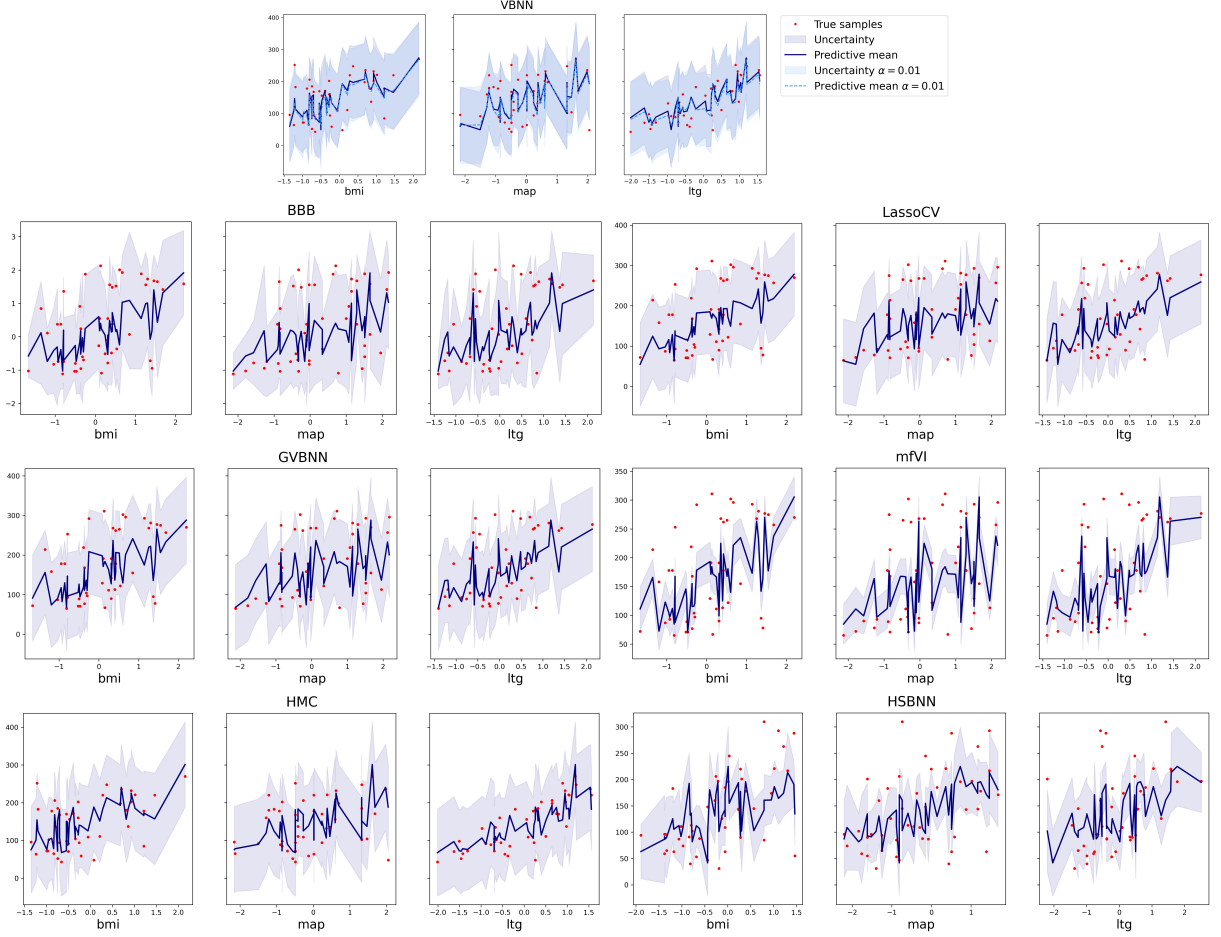


Figure 12: Predictive mean and the uncertainty estimates for the observations for three of the predictors with considerable contribution.

Concrete slump test (Yeh, 2009): $n = 103, p = 7$, the predictors are concrete ingredients, namely cement, furnace slag, fly ash, water, superplasticizer, coarse aggregate, and fine aggregate, and the task is to predict the slump of concrete.

D.5 Supplementary material to the UCI datasets experiments

Table 4 supplements Figure 10, Figure 11 and the experiments described in Section 4.3.

D.6 Supplementary material to the SVI experiments

We use a synthetic dataset generated in Section 4.1 to investigate the performance of VBNN trained with stochastic variational inference in comparison to VBNN trained with classical coordinate ascent. We consider a single-layer VBNN with the number of hidden units set to $D_H = 20$ and evaluate the performance of the SVI compared to CAVI for various step sizes (defined in Equation (21)) and mini-batch sizes. As before, we use 90% of the data to train the neural network and the rest is used for evaluation; when computing evaluation metrics, we average the results obtained in 10 different random runs. Similar to previous experiments, the recorded metrics are RMSE, NLL and the empirical coverage for the observations.

The computational gains obtained by utilising stochastic gradients and subsampling would motivate further research along the lines of model combination. Indeed, SVI makes ensembling techniques particularly appealing, in our experiment with a relatively small synthetic dataset, an ensemble of 5 SVI approximations

Table 4: RMSE, NLL and Coverage for UCI datasets.

Metric	Method	Dataset				
		Slump	Yacht	Boston	Energy	Concrete
RMSE	4SVIBNN	7.15 ± 1.5	$3.57 \pm .8$	$3.38 \pm .9$	$1.62 \pm .2$	$7.15 \pm .6$
	4VBNN	7.01 ± 1.2	$1.23 \pm .3$	$3.21 \pm .6$	$1.1 \pm .2$	$6.71 \pm .6$
	SVBNN	7.36 ± 1.62	5.57 ± 1.14	$3.76 \pm .92$	$2.41 \pm .49$	$8.43 \pm .75$
	VBNN	7.37 ± 1.4	2.47 ± 1.1	$3.47 \pm .8$	$1.37 \pm .3$	$7.67 \pm .9$
	GVBNN	7.64 ± 1.21	4.88 ± 2.66	$4.02 \pm .88$	$2.5 \pm .42$	$7.84 \pm .68$
	mfVI	7.9 ± 1.7	$1.61 \pm .36$	$3.29 \pm .6$	$2.27 \pm .25$	$6.11 \pm .5$
	BBB	7.33 ± 1.94	$1.45 \pm .6$	$3.46 \pm .96$	$2.65 \pm .26$	$6.48 \pm .61$
	HMC	$7. \pm 1.24$	$.56 \pm .13$	$2.42 \pm .47$	$.3 \pm .07$	$4.01 \pm .78$
	HSBNN	6.41 ± 1.28	$1.2 \pm .23$	$2.92 \pm .55$	$.6 \pm .09$	$5.21 \pm .56$
NLL	4SVBNN	3.42 ± 0.2	$2.74 \pm .2$	$2.61 \pm .2$	$1.94 \pm .1$	$3.38 \pm .07$
	4VBNN	$3.39 \pm .2$	$1.97 \pm .2$	$2.57 \pm .13$	$1.63 \pm .16$	$3.33 \pm .06$
	SVBNN	$3.47 \pm .29$	$3.13 \pm .27$	$2.78 \pm .31$	$2.31 \pm .22$	3.56 ± 0.11
	VBNN	3.46 ± 0.2	2.25 ± 0.4	$2.69 \pm .26$	$1.75 \pm .21$	$3.5 \pm .12$
	GVBNN	3.47 ± 0.17	$2.86 \pm .59$	$2.82 \pm .22$	$2.35 \pm .15$	$3.48 \pm .09$
	mfVI	$3.77 \pm .5$	$1.96 \pm .09$	$2.61 \pm .22$	$2.28 \pm .09$	$3.57 \pm .2$
	BBB	6.23 ± 2.76	$1.69 \pm .14$	$2.47 \pm .16$	$2.08 \pm .15$	3.21 ± 0.13
	HMC	$3.41 \pm .24$	$.87 \pm .1$	$2.28 \pm .18$	$.23 \pm .44$	$2.74 \pm .27$
	HSBNN	5.02 ± 1.79	$1.31 \pm .18$	5.01 ± 1.24	$1.08 \pm .2$	$4.32 \pm .69$
Coverage	4SVBNN	$.95 \pm .06$	$.98 \pm .03$	$.97 \pm .03$	$.98 \pm .01$	$.97 \pm .01$
	4VBNN	$.94 \pm .04$	$.99 \pm .02$	$.97 \pm .02$	$.99 \pm .0$	$.97 \pm .02$
	SVBNN	$.91 \pm .08$	$.93 \pm .02$	$.94 \pm .03$	$.91 \pm .04$	$.93 \pm .03$
	VBNN	$.92 \pm .06$	$.96 \pm .01$	$.95 \pm .03$	$.98 \pm .02$	$.94 \pm .02$
	GVBNN	$.96 \pm .04$	$.95 \pm .04$	$.96 \pm .02$	$.93 \pm .04$	$.95 \pm .02$
	mfVI	$.78 \pm .1$	$.96 \pm .03$	$.96 \pm .01$	$.95 \pm .03$	$.8 \pm .04$
	BBB	$.75 \pm .12$	$1. \pm 0$	$.97 \pm .02$	$.99 \pm .0$	$.97 \pm .02$
	HMC	$.9 \pm .08$	$.98 \pm .02$	$.96 \pm .02$	$.95 \pm .03$	$.94 \pm .03$
	HSBNN	$.67 \pm .14$	$.94 \pm .05$	$0.62 \pm .08$	$.89 \pm .04$	$.71 \pm .06$

with a mini-batch size of 10 performs comparable to CAVI while being more than 5 times faster than CAVI (see Figure 13 and Figure 14).

E Review of relevant distributions

E.1 Generalized Inverse Gaussian

The Generalized Inverse Gaussian has density:

$$p(x \mid \nu, \delta, \lambda) = \frac{(\lambda/\delta)^\nu}{2K_\nu(\lambda\delta)} x^{\nu-1} \exp\left(-\frac{1}{2}(\delta^2/x + \lambda^2 x)\right),$$

where $K_\nu()$ is the modified Bessel function of the second kind. The GIG prior requires $\nu > 0$ if $\delta = 0$ and $\nu < 0$ if $\lambda = 0$ for a proper prior. Then the expectations arising in computations throughout this paper are:

$$\begin{aligned} \mathbb{E}[x] &= \frac{\delta K_{\nu+1}(\lambda\delta)}{\lambda K_\nu(\lambda\delta)}, \\ \mathbb{E}\left[\frac{1}{x}\right] &= \frac{\lambda K_{\nu+1}(\lambda\delta)}{\delta K_\nu(\lambda\delta)} - \frac{2\nu}{\delta^2}. \end{aligned}$$

Often, it is sensible to consider special cases of the GIG, which include:

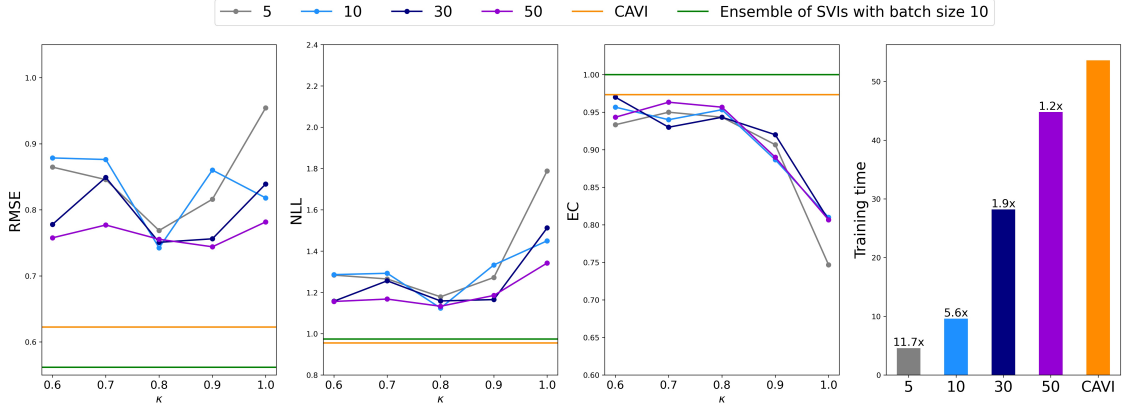


Figure 13: RMSE, NLL, EC of SVI compared to CAVI and plotted for various mini-batch sizes as a function of the forgetting rate k ; the most right plot compares training times, where bar labels indicate the scale of computational gains.

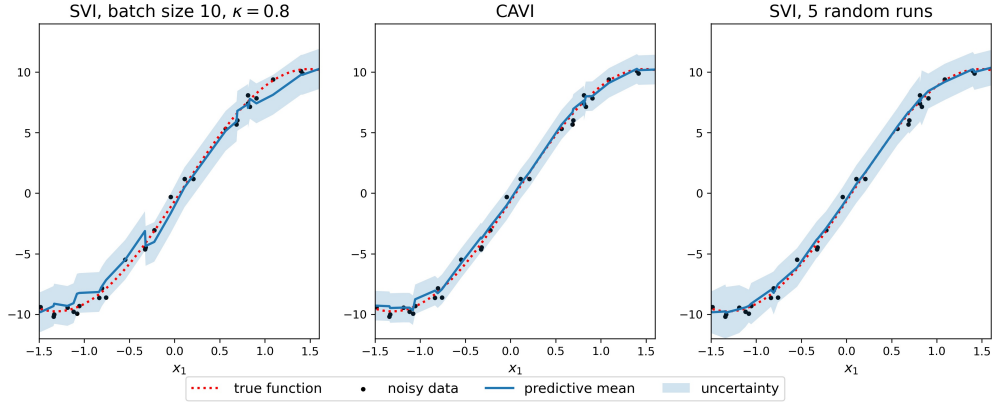


Figure 14: The predictive means and uncertainty estimate as a function of the first coordinate for SVI, CAVI and ensembles of SVI approximations.

1. Inverse Gamma: when $\lambda = 0$, the GIG reduces to the IG with density:

$$p(x \mid \nu, \delta) = \frac{2^\nu}{\delta^{2\nu} \Gamma(-\nu)} (1/x)^{-\nu+1} \exp\left(-\frac{\delta^2}{2x}\right),$$

where $\nu < 0$ and $\delta > 0$. This can also be rewritten in terms of the more standard parametrization of the IG:

$$p(x \mid \alpha, \beta) = \frac{\beta^\alpha}{\Gamma(\alpha)} (1/x)^{\alpha+1} \exp\left(-\frac{\beta}{x}\right),$$

where $\alpha = -\nu > 0$ and $\beta = \delta^2/2 > 0$. Note that if $w \sim N(0, \tau)$ and $\tau \sim \text{IG}(\alpha, \beta)$, this implies a marginal student t-prior on w with degrees of freedom $\text{dof} = 2\alpha = -2\nu$ and scale $s = \sqrt{\beta/\alpha} = \delta/\sqrt{-2\nu}$. For example, setting $\nu = -1.5$ would correspond to $\text{dof} = 3$ and $\nu = -2.5$ is equivalent to $\text{dof} = 5$.

The relevant expectations for the VI updates and ELBO computation include:

$$\begin{aligned} \mathbb{E}[x] &= \frac{\beta}{\alpha - 1} = \frac{-\delta^2}{2\nu + 2}, \\ \mathbb{E}\left[\frac{1}{x}\right] &= \frac{\alpha}{\beta} = \frac{-2\nu}{\delta^2}, \end{aligned}$$

where ψ is the logarithmic derivative of the gamma function (a.k.a. digamma function).

2. Gamma: when $\delta^2 = 0$, the GIG reduces to the Gamma with density:

$$p(x \mid \nu, \lambda) = \frac{\lambda^{2\nu}}{2^\nu \Gamma(\nu)} x^{\nu-1} \exp\left(-\frac{\lambda^2}{2}x\right),$$

where $\nu > 0$, rewriting in the standard parametrization with $\alpha = \nu$ and $\beta = \lambda^2/2$:

$$p(x \mid \alpha, \beta) = \beta^\alpha \frac{1}{\Gamma(\alpha)} x^{\alpha-1} \exp(-\beta x),$$

where $\alpha = \nu > 0$ and $\beta = \lambda^2/2 > 0$. Similarly, the relevant expectations are:

$$\begin{aligned} \mathbb{E}[x] &= \frac{\alpha}{\beta} = \frac{2\nu}{\lambda^2}, \\ \mathbb{E}\left[\frac{1}{x}\right] &= \frac{\beta}{\alpha-1} = \frac{\lambda^2}{2(\nu-1)}. \end{aligned}$$

Note that if $w \sim N(0, \tau)$ and $\tau \sim \text{Gam}(1, \beta)$, this implies a marginal Laplace prior on w (i.e. Bayesian Lasso ([Park and Casella, 2008](#))) with scale $s = 1/\sqrt{2\beta} = 1/\lambda$.

3. Inverse Gaussian (IGaus): when $\nu = -1/2$, the GIG reduces to the Inverse Gaussian with density:

$$p(x \mid \delta, \lambda) = \frac{\delta}{\sqrt{2\pi x^3}} \exp\left(-\frac{(\lambda x - \delta)^2}{2x}\right),$$

where setting $\alpha = \delta/\lambda > 0$ and $\beta = \delta^2 > 0$ we derive

$$p(x \mid \alpha, \beta) = \left(\frac{\beta}{2\pi x^3}\right)^{\frac{1}{2}} \exp\left(\frac{-\beta(x - \alpha)^2}{2\alpha^2 x}\right).$$

The relevant expectations for the VI updates and ELBO computation include:

$$\begin{aligned} \mathbb{E}[x] &= \alpha = \frac{\delta}{\lambda}, \\ \mathbb{E}\left[\frac{1}{x}\right] &= \frac{1}{\alpha} + \frac{1}{\beta} = \frac{\lambda}{\delta} + \frac{1}{\delta^2}. \end{aligned}$$

Note that if $w \sim N(0, \tau)$ and $\tau \sim \text{IGaus}(\alpha, \beta)$, the marginal distribution is of the form ([Caron and Doucet, 2008](#)):

$$\begin{aligned} p(w_k) &= \frac{1}{\pi\alpha} \left(\frac{\beta}{\beta + w_k^2}\right)^{\frac{1}{2}} \exp\left(\frac{\beta^{\frac{1}{2}}}{\alpha}\right) K_1\left(\frac{(\beta + w_k^2)^{\frac{1}{2}}}{\alpha}\right) \\ &= \frac{\lambda}{\pi} \exp(\lambda) (\delta^2 + w_k^2)^{-\frac{1}{2}} K_1\left(\frac{\lambda}{\delta} (\delta^2 + w_k^2)^{\frac{1}{2}}\right). \end{aligned}$$

E.2 EM update for different cases of global-local priors

As discussed above, the special cases of the GIG include Inverse Gamma, Gamma and Inverse Gaussian distributions, we derive the EM updates in each of the special cases of priors:

1. Inverse Gamma: when the global shrinkage parameter has an Inverse Gamma distribution, then

$$\begin{aligned} \delta_{\text{glob}} &= \arg \max \left(\delta_{\text{glob}}^2 \sum_{l=1}^{L+1} \frac{\nu_{\text{glob},l}}{\delta_{\text{glob},l}^2} - 2(L+1)\nu_{\text{glob}} \log(\delta_{\text{glob}}) \right), \\ \delta_{\text{glob}} &= ((L+1)\nu_{\text{glob}})^{\frac{1}{2}} \left(\sum_{l=1}^{L+1} \frac{\nu_{\text{glob},l}}{\delta_{\text{glob},l}^2} \right)^{-\frac{1}{2}}. \end{aligned}$$

2. Gamma: similarly, when global shrinkage parameter is Gamma:

$$\lambda_{\text{glob}} = \arg \max \left(4(L+1)\nu_{\text{glob}} \log(\lambda_{\text{glob}}) - \lambda_{\text{glob}}^2 \sum_{l=1}^{L+1} \frac{\delta_{\text{glob},l} K_{\nu_{\text{glob},l}+1}(\lambda_{\text{glob},l} \delta_{\text{glob},l})}{\lambda_{\text{glob},l} K_{\nu_{\text{glob},l}}(\lambda_{\text{glob},l} \delta_{\text{glob},l})} \right),$$

$$\lambda_{\text{glob}} = (2(L+1)\nu_{\text{glob}})^{\frac{1}{2}} \left(\sum_{l=1}^{L+1} \frac{\delta_{\text{glob},l} K_{\nu_{\text{glob},l}+1}(\lambda_{\text{glob},l} \delta_{\text{glob},l})}{\lambda_{\text{glob},l} K_{\nu_{\text{glob},l}}(\lambda_{\text{glob},l} \delta_{\text{glob},l})} \right)^{-\frac{1}{2}}.$$

3. Inverse Gaussian: if the global shrinkage parameter is Inverse Gaussian, then

$$\lambda_{\text{glob}} = \arg \max \left(2(L+1)\lambda_{\text{glob}}\delta_{\text{glob}} - \lambda_{\text{glob}}^2 \sum_{l=1}^{L+1} \frac{\delta_{\text{glob},l} K_{\nu_{\text{glob},l}+1}(\lambda_{\text{glob},l} \delta_{\text{glob},l})}{\nu_{\text{glob},l} K_{\nu_{\text{glob},l}}(\lambda_{\text{glob},l} \delta_{\text{glob},l})} \right),$$

$$\lambda_{\text{glob}} = 2(L+1)\delta_{\text{glob}} \left(\sum_{l=1}^{L+1} \frac{\delta_{\text{glob},l} K_{\nu_{\text{glob},l}+1}(\lambda_{\text{glob},l} \delta_{\text{glob},l})}{\nu_{\text{glob},l} K_{\nu_{\text{glob},l}}(\lambda_{\text{glob},l} \delta_{\text{glob},l})} \right)^{-1}.$$